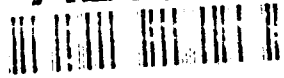


AD-A267 645



DTIC

S

AUG 4 1993

D

C

1489

FINAL REPORT

Investigation of the Optical,
Electronic, and Structural
Properties of Fiber Optic
Glasses

DISTRIBUTION STATEMENT A

100



Reproduced From
Best Available Copy

93-17272



93 8 3 003

FINAL REPORT

Investigation of the Optical, Electronic, and Structural Properties of Fiber Optic Glasses

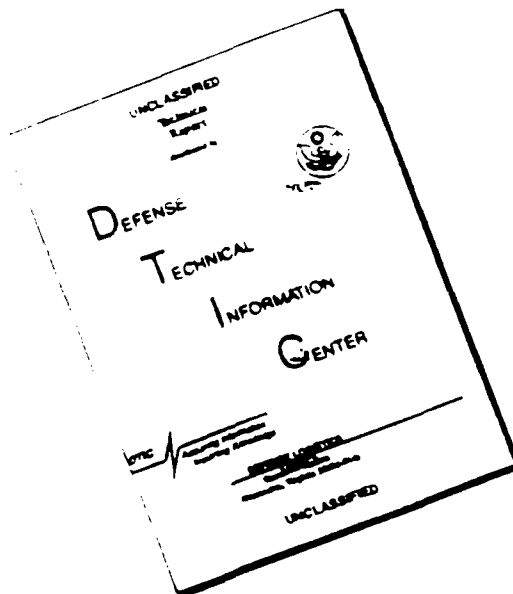
REPORT DOCUMENTATION PAGE

Form Approved
OMB No. 0704-0188

Public reporting burden for this collection of information is estimated to average 1 hour per response, including the time for reviewing instructions, searching existing data sources, gathering and maintaining data needed, and completing and reviewing the collection of information. Send comments regarding this burden estimate or any other aspect of this collection of information, including suggestions for reducing this burden to Washington Headquarters Services, Directorate for Information Operations and Reports, 1215 Jefferson Davis Highway, Suite 1204, Arlington, VA 22202-4302, and to the Office of Management and Budget, Paperwork Reduction Project (0704-0188), Washington, DC 20503.

| | | | |
|--|--|--|---|
| 1. AGENCY USE ONLY (Leave Blank) | 2. REPORT DATE June 1993 | 3. REPORT TYPE AND DATES COVERED Final Report 12/19/89 to 2/28/93 | |
| 4. TITLE AND SUBTITLE Investigation of the Optical, Electronic, and Structural Properties of Fiber Optic Glasses | | 5. FUNDING NUMBERS N00014-90-C-2020 | |
| 6. AUTHOR(S) J.A. Frietas, Jr. | | | |
| 7. PERFORMING ORGANIZATION NAME(S) AND ADDRESS(ES) SFA, Inc. 1401 McCormick Drive Landover, MD 20785 | | 8. PERFORMING ORGANIZATION REPORT NUMBER SFA--93/002 | |
| 9. SPONSORING/MONITORING AGENCY NAME(S) AND ADDRESS(ES) Naval Research Laboratory 4555 Overlook Ave., SW Washington, DC 20375-5000 | | 10. SPONSORING/MONITORING AGENCY REPORT NUMBER | |
| 11. SUPPLEMENTARY NOTES | | | |
| 12a. DISTRIBUTION/AVAILABILITY STATEMENT | | 12b. DISTRIBUTION CODE | |
| 13. ABSTRACT (Maximum 200 words) Under contract N00014-90-C-2020, SFA provided research support to the Naval Research Laboratory Electronic Materials Branch by conducting investigations on novel materials. These investigations ranged from using various techniques to characterize the optical, electronic, and structural properties of this semiconductor films to setting up a micro-Raman and microphotoluminescence laboratory to study microcrystalline films. The materials studied include heavy metal fluoride glasses, chalcogenide glasses, silicon carbide, diamond (chemical vapor deposition films, high-pressure, high-temperature synthetic and natural), and aluminum nitrides. These materials were investigated by such optical techniques as Raman scattering (RS), photoluminescence (PL), photoluminescence excitation, absorption, reflectivity, electron spin resonance (ESR), photo-induced ESR, optically detected magnetic response (ODMR), and Hall measurement. | | | |
| 14. SUBJECT TERMS | | 15. NUMBER OF PAGES 171 pages | |
| | | 16. PRICE CODE | |
| 17. SECURITY CLASSIFICATION OF REPORT Unclassified | 18. SECURITY CLASSIFICATION OF THIS PAGE Unclassified | 19. SECURITY CLASSIFICATION OF ABSTRACT Unclassified | 20. LIMITATION OF ABSTRACT Unlimited |

DISCLAIMER NOTICE



THIS DOCUMENT IS BEST QUALITY AVAILABLE. THE COPY FURNISHED TO DTIC CONTAINED A SIGNIFICANT NUMBER OF PAGES WHICH DO NOT REPRODUCE LEGIBLY.

SECURITY CLASSIFICATION: Unclassified

SFA--93/002

Investigation of the Optical, Electronic, and Structural Properties of Fiber Optic Glasses

Prepared by: J.A. Frietas, Jr.

SFA, Inc.
1401 McCormick Drive
Landover, Maryland 20785

Date: June 1993

Contract Number: N00014-90-C-2020

DTIC QUALITY INSPECTED 3

Prepared for: Naval Research Laboratory
4555 Overlook Avenue, SW
Washington, DC 20375-5000

| | |
|------------------------------|-------------------------------------|
| Accession For | |
| NTIS CRA&I | <input checked="" type="checkbox"/> |
| DTIC TAB | <input type="checkbox"/> |
| Unannounced Justification | <input type="checkbox"/> |
| By <i>Per H.C.</i> | |
| Distribution / | |
| Availability Codes | |
| Dist | Avail and/or Special |
| <i>A-1</i> | |

Under contract N00014-90-C-2020, SFA provided research support to the Naval Research Laboratory Electronic Materials Branch by conducting investigations on novel materials. These investigations ranged from using various techniques to characterize the optical, electronic, and structural properties of thin semiconductor films, to setting up a micro-Raman and microphotoluminescence laboratory to study microcrystalline films. The materials studied include heavy metal fluoride glasses, chalcogenide glasses, silicon carbide, diamond (chemical vapor deposition films, high-pressure, high-temperature synthetic and natural), and aluminum nitrides. These materials were investigated by such optical techniques as Raman scattering (RS), photoluminescence (PL), photoluminescence excitation, absorption, reflectivity, electron spin resonance (ESR), photo-induced ESR, optically detected magnetic response (ODMR), and Hall measurement. SFA personnel set up a micro-Raman and microphotoluminescence laboratory to study microcrystalline films.

Work on fluoride glasses concentrated on understanding the role of transition metal impurities in determining the optical and electronic properties of such glasses. One of the problems addressed in fluoride glass fibers was the absorption loss due to residual impurities. Because conventional techniques limit the impurity detection levels, PL—combined with ESR and absorption measurements—was used to measure very low concentrations of transition metal and rare earth impurities in bulk and fibers of fluoride glass. This work emphasized Nd^{3+} and Fe^{2+} , the most deleterious impurities for absorption loss in fluorozirconate glass fibers.

In order to make absolute measurements of Nd and Fe concentrations in fluoride glass, SFA used glass samples doped intentionally with Fe (Fe^{3+} concentration measured by electron paramagnetic resonance) and Nd (calibration curve using dope fractioning) as standards. The photoluminescent intensity of the ZrFe glasses was then compared with the photoluminescent intensity of the standards. These procedures allowed the measurement of concentrations as low as 0.05 ppb and 0.5 ppb for Nd^{3+} and Fe^{3+} respectively. These levels are below concentration levels which produce absorption losses equal to the theoretical intrinsic loss limit at the 2.5 to 3.5 micron low loss transmission window.

Time-resolved PL studies of Fe^{3+} -doped fluorozirconate glasses revealed evidence of the charge-transfer mechanism in the relaxation processes. Although the $\text{Fe}^{3+} \rightarrow \text{Fe}^{2+}$ charge-transfer process is one plausible possibility, the charge-transfer between iron and other impurities, like oxygen, cannot be ruled out. To verify this possibility, SFA conducted experiments in samples with different amounts of oxygen.

Preliminary optical studies of fluorozirconate glass fibers under tensile stress have shown that the fibers are permanently deformed if subjected to tensile stress above 70% of the tensile strength. This result suggests that further opto-mechanical experiments must be performed to evaluate how the optical properties of the fibers will be affected by mechanical property variations.

In bulk fluoride glasses, RS was used by SFA to identify crystalline inclusion and phase separation—common problems in multicomponent glasses. The PL background due to transition metal and rare earth impurities can be eliminated or reduced by using a convenient exciting light source, since a photoluminescent emission band has fixed energy shift from any exciting energy. The same approach may be used for fluoride glass fiber studies. Forward RS, in combination with PL measurements, was used to determine the concentration of rare earth and transition metals in glass fibers for levels below 1 ppt and 0.01 ppb respectively.

Room-temperature PL measurements conducted on fluorozirconate glasses (bulk and fibers) indicated that this technique could be conveniently used to identify and measure concentrations of transition metals and rare earths in these glasses. Room- and low-temperature PL measurements were used by SFA to verify the participation of impurities in the nucleation of crystallites in ZrF_4 -based glasses.

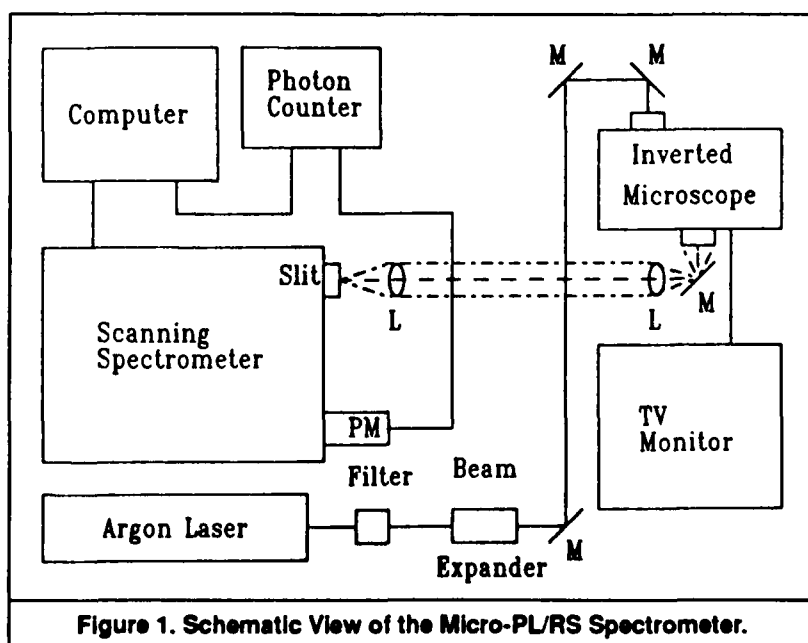
Room- and low-temperature electron paramagnetic resonance experiments carried out in ZrF_4 -based glasses identified and estimated the concentration of transition metals in unintentionally doped glasses. Electron paramagnetic resonance studies of intentionally Fe^{3+} -doped glasses prepared in different gas atmospheres revealed a variation of the Fe^{3+} concentration in fluoride glasses. SFA performed PL and electron paramagnetic resonance experiments to determine the efficiency of the oxidation/reduction process of iron in fluorozirconate glasses.

A novel micro-PL/RS spectrometer was set up to perform high spatial resolution measurements. This spectrometer features micron-sized spatial resolution of cryogenic temperatures, and is comprised of an argon ion laser, an inverse Carl Zeiss axiovert microscope (Model 408), and a double spectrometer (Spex Model 1401), fitted with a GaAs photomultiplier and a photon counter. The spatial resolution is about $\leq 1 \mu\text{m}$. Figure 1 shows the schematic view of the Micro-PL/RS spectrometer. Some accomplishments achieved with this spectrometer include:

- (1) Investigation of the spatial PL variations for polycrystalline diamond films deposited with an acetylene torch technique. Variations in the PL spectra were observed which could be qualitatively related to the variation with substrate temperature and possibly the flame species inhomogeneities.
- (2) Micro-Raman scattering to identify microcrystalline inclusions in the ZBLAN/HZBLAN glass system. The experimental results combined with EDAX data in the same crystallites and Raman scattering spectra of parent polycrystals reported in the literature suggest that the 'caterpillar' crystal is $\text{NaF} \cdot (2\text{ZrF}_4 \cdot \text{BaF}_2)$ and the 'notched rod' crystal is $\text{NaF} \cdot (\alpha\text{-HfF}_4 \cdot \text{ZrF}_4 \cdot \text{BaF}_4)$. SFA also identified a hexagonal micro-inclusion in a particular fiber core as a LaF_3 crystal by comparison with micro-Raman measurements of a LaF_3 single crystal. These latter results show that micro-Raman can unambiguously identify microcrystalline inclusions if high quality reference crystals are available for spectral comparison.
- (3) Cross-sectional microluminescence measurements for $1 \Omega \text{ cm}$ $70 \mu\text{m}$ porous silicon samples showing a continuous decrease of the photoluminescence band as a function of sample depth. No spectral shift was observed. For samples annealed at 390°C , in addition to spectral intensity reduction, the same redshift was observed in all luminescence spectra independent of depth. A study of this luminescence redshift as a function of annealing temperature revealed a striking similarity to results observed for optical band-gap shrinking of *a*-Si:H as a function of hydrogen loss during annealing.

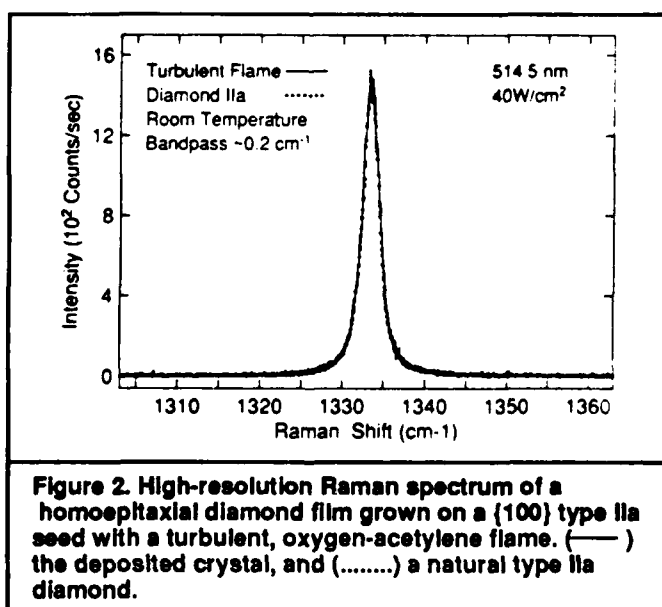
Other important results include:

- Homoepitaxial growth of high quality, faceted diamond crystals at rates exceeding 150 microns/hour was observed on millimeter sized {100} and {110} natural diamond seed crystals, using a laminar, pre-mixed oxygen-acetylene flame in air. The key element in achieving such high growth rates was a substrate temperature in the $1150\text{--}1400^\circ\text{C}$ range. Microscope and naked eye observations revealed the orig-

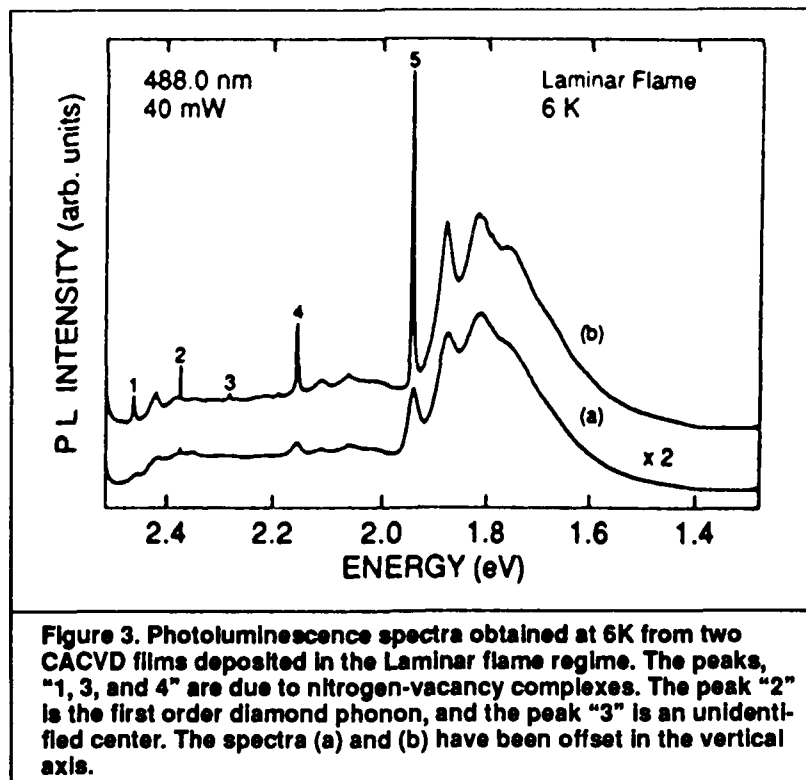


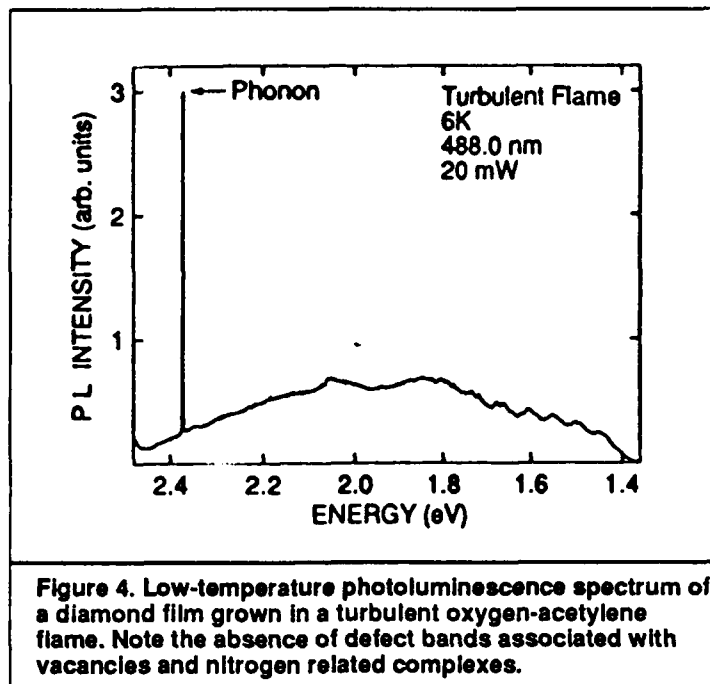
inal cylindrical-shaped seed crystals growing into polyhedral-shaped crystals with identifiable {100} and {111} faces. Examination under optical and scanning electron microscopes revealed terraces on the {100} faces. The deposited diamond was clear and exhibited Raman spectra almost identical to that of natural diamond. Laue X-ray diffraction analyses have confirmed the epitaxial nature of the growth. The deposition temperatures and growth rates reported were the highest ever observed for the homoepitaxial synthesis of diamond crystals at low pressures.

- High quality polycrystalline diamond were synthesized in a turbulent premixed, oxygen-acetylene flame, using a commercial brazing torch. The quality of the films was measured by high resolution RS, scanning and transmission electron microscopy, hemispherical transmittance measurements in the UV, visible and infrared, and PL spectroscopy. Turbulence was achieved by operating the torch with a sufficiently high Reynolds number. The presence of turbulence was confirmed by observations of changes in the flame shape, the characteristic sound of the flame, and calculation of the Reynolds number.
- Diamond has been grown epitaxially on 1.5 mm diameter, natural diamond seed crystals at temperatures of 1200–1300°C in a premixed, turbulent oxygen-acetylene flame. During a typical 1 h deposition, a polyhedral-shaped single crystal was observed to grow on top of a <100> oriented cylindrical seed crystal. The growth surface was composed of both {100} terraces and {100} ridges (See Figure 2), arranged into well-formed pyramidal shaped structures with very long range order. Raman analyses revealed a lack of non-diamond carbon and a 1332 cm⁻¹ peak which is indistinguishable from natural type IIa diamond. Low-temperature PL measurements indicated a greatly reduced level of localized radiative defects. Laue X-ray diffraction measurements confirmed the epitaxial nature of the deposit, and preliminary X-ray rocking curve analyses were presented. This was the first report of the high-temperature epitaxial growth of diamond in a turbulent flame.
- Polycrystalline diamond films were synthesized by using an open atmosphere combustion flame, and also using a combustion flame in an enclosed chamber. By operating the pre-mixed oxygen-acetylene torch in a chamber, SFA was able to vary the atmosphere around the flame in a controlled manner and study the effects on the diamond films. Varying the atmosphere around the flame was of interest to control the incorporation of unwanted gases, and to obtain finer control over the flame properties. SFA reported on the properties of films grown in the open atmosphere and in the chamber with oxygen and argon.



- Raman scattering and PL spectroscopies were used to characterize polycrystalline diamond films deposited on molybdenum substrates by laminar and turbulent premixed oxygen-acetylene flames in air. Samples deposited under laminar flame conditions were characterized by a high degree of incorporation of nitrogen-vacancy complexes. However, samples deposited with a turbulent flame indicated a significant decrease in the concentration of these defects and a reduction of the amorphous carbon film component (see Figures 3 and 4).
- The temperature and excitation intensity dependence of PL spectra were studied in thin films of SiC grown by chemical vapor deposition on Si (100) substrates. The low power PL spectra from all samples exhibited a DAP PL band which involved a previously undetected deep acceptor whose binding energy was approximately 470 meV. This deep acceptor was found in every sample studied independent of growth reactor, suggesting the possibility that this background acceptor is at least partially responsible for the high compensation observed in Hall effect studies of undoped films of cubic SiC.
- Two distinct spectra were reported from an optically detected magnetic resonance study of epitaxial films of cubic SiC. The first is a Lorentzian, single line with $g = 2.0065 \pm 0.0015$, which is strong in Al-doped SiC. This line is attributed to residual donors. The second spectrum, observed in both Al-doped and undoped samples, was dominated by a pair of exchange-split lines with $g = 2.0024$ and $a = 0.095 \text{ cm}^{-1}$. Although a definite assignment of this spectrum cannot be made, spectral dependence studies show it is associated with a defect-related luminescence band in the energy range from 1.6 to 1.9 eV.
- Cubic silicon carbide (β -SiC) films have been grown epitaxially on silicon-on-sapphire (SOS) substrates by CVD. A fresh layer of silicon was first deposited *in situ* on the SOS substrate at approximately 1050°C. The silicon layer was then carbonized while being heated to 1360°C. The β -SiC layer is grown





at 1360°C using silane and propane as sources. β -SiC films also can be grown directly on the SOS substrate without utilizing a fresh silicon layer. Deposition of β -SiC films on silicon-on-insulator (SOI) substrates also was accomplished with slight modification of the growth parameters described above.

- The β -SiC films were characterized by IR reflectance spectroscopy, optical microscopy, and electron microscopy. Typical films are 7 μm thick and have a specular surface with some physical features. Electrical transport properties as determined by the Van der Pauw Hall method show the β -SiC films to be p-type while those grown on SOI were n-type. X-ray rocking curve measurements were obtained to determine the crystalline quality of the films. In addition, preliminary optical characterization of the films was performed.
- Photoluminescence excitation spectroscopy was used to investigate the above gap and extrinsic optical absorption processes that excite the PL bands characterizing CVD films of cubic SiC grown on Si substrates. In undoped films, the PLE spectra provided a faithful representation of the indirect optical absorption edge which is consistent with the optical absorption spectrum reported previously for Lely-grown bulk crystals of cubic SiC. The undoped PLE spectra indicated no evidence of extrinsic (below gap) optical absorption. The PLE spectra of the N-Al DAP bands which dominated the PL spectra of Al-doped films of cubic SiC exhibited extrinsic absorption which is attributed to photoneutralization of compensated shallow donors. The extrinsic PLE spectra of the Al-doped samples contained peaks which corresponded to the ZPLs of the donor bound exciton PL bands observed in the undoped films, as well as onsets which could correspond to the thresholds for photoneutralization of the 54 meV N-donor and the unidentified 15–20 meV donor which are pervasive in CVD cubic SiC.

APPENDIX

Table of Contents

| Publication | Page |
|---|------|
| Micro-Raman studies of fluoride glass optical fibers. J.A. Freitas, Jr., P.C. Pureza, I.D. Aggarwal, and U. Strom. <i>Materials Science Forum</i> 67 & 68 (1991): 279 | 8 |
| Raman scattering studies of microcrystalline inclusions in fluoride glasses and fibers. J.A. Freitas, Jr., J.S. Sanghera, U. Strom, P.C. Pureza, and I.D. Aggarwal. <i>Journal of Non-Crystalline Solids</i> 140 (1992): 166 | 12 |
| Photoluminescence excitation spectroscopy of cubic SiC grown by chemical vapor deposition on Si substrates. J.A. Freitas, Jr., P.B. Klein, and S.G. Bishop. <i>Materials Science Forum</i> 83-87 (1992): 1195 | 18 |
| Chemical vapor deposition of B-SiC on silicon-on-sapphire and silicon-on-insulator substrates. J.C. Pazik, G. Kelner, N. Bottka, and J.A. Freitas, Jr. <i>Materials Science and Engineering</i> B11 (1992): 125 | 24 |
| A new deep acceptor in epitaxial cubic SiC. J.A. Freitas and S.G. Bishop. <i>Materials Research Society Symposium Proceedings</i> 162 (1990): 495 | 29 |
| Photoluminescence characterization of cubic SiC grown by chemical vapor deposition on Si substrates. S.G. Bishop and J.A. Freitas, Jr. <i>Journal of Crystal Growth</i> 106 (1990): 38 | 39 |
| Spectroscopic studies of donors in 3C-SiC films. J.A. Freitas, Jr., W.E. Carlos, and S.G. Bishop. <i>Springer Proceedings in Physics: Amorphous and Crystalline Silicon Carbide III</i> 56 (1992): 135 | 49 |
| Optically detected magnetic resonance of cubic SiC grown by chemical vapor deposition on Si. T.A. Kennedy, J.A. Freitas, Jr., and S.G. Bishop. <i>Journal of Applied Physics</i> 68 (1990): 6170 | 57 |
| Micro-photoluminescence studies of diamond films. J.A. Freitas, Jr., U. Strom, J.E. Butler, and K.A. Snail. <i>New Diamond Science and Technology</i> (1991): 723 | 65 |
| High-temperature epitaxy of diamond in a turbulent flame. K.A. Snail, C.L. Vold, C.M. Marks, and J.A. Freitas, Jr. <i>Diamond and Related Materials</i> 1 (1992): 180 | 71 |
| Optical studies of donors and acceptors in cubic SiC. J.A. Freitas, Jr., P.B. Klein, and S.G. Bishop. <i>Materials Science and Engineering</i> B11 (1992): 21 | 79 |
| Optical evidence of reduction of radiative defects in diamond films grown by acetylene-oxygen flames. J.A. Freitas, Jr., U. Strom, K. Doverspike, C.M. Marks, and K.A. Snail. <i>Materials Research Society Symposium Proceedings</i> 242 (1992): 139 | 85 |
| Growth of high quality diamond films in a turbulent flame. K.A. Snail, C.J. Craigie, R.G. Vardiman, C.M. Marks, and J.A. Freitas, Jr. <i>Proceedings of the Second International Symposium on Diamond Materials</i> (1991): 91 | 97 |
| High rate homoepitaxial synthesis of diamond in a flame. K.A. Snail, J.A. Freitas, C.L. Vold, and L.M. Hanssen. <i>Proceedings of the Second International Symposium on Diamond Materials</i> (1991): 81 | 113 |

| | |
|--|-----|
| Deposition of flame grown diamond films in a controlled atmosphere. K. Doverspike, J.E. Butler, and J.A. Freitas, Jr. <i>Materials Research Society Symposium Proceedings</i> 242 (1992): 37 | 133 |
| Microluminescence depth profiles and annealing effects in porous silicon. S.M. Prokes, J.A. Freitas, Jr., and P.C. Searson. <i>Applied Physics Letters</i> 60(26) (1992): 3295 | 145 |
| Photoluminescence studies of polycrystalline diamond films. J.A. Freitas, Jr., J.E. Butler, and U. Strom. <i>Journal of Materials Research</i> 5(11) (November 1990): 2502 . | 151 |
| Photoluminescence spectroscopy of diamond films. J.A. Freitas, Jr., J.E. Butler, S.G. Bishop, W.A. Carrington, and U. Strom. <i>Materials Research Society Symposium Proceedings</i> 162 (1990): 237 | 161 |

MICRO-RAMAN STUDIES OF FLUORIDE GLASS OPTICAL FIBERS

J.A. Freitas, Jr. (b), P.C. Pureza, I.D. Aggarwal and U. Strom (a)

(b) Naval Research Laboratory, Washington, DC 20375-5000, USA

(a) Sachs/Freeman Associates Inc., Landover, MD 20785-5396, USA

ABSTRACT

Micro-Raman scattering experiments were carried out in two types of crystalline phases observed in the ZBLAN/HZBLAN glass system used to make fiber preforms and fibers. Comparison of our results with Raman scattering spectra of the parent crystals, and with previously reported Raman, and chemical/structural investigations, suggests that the two types of crystalline phases are NaF·(α - or β -2ZrF₄·BaF₂) and NaF·(α - or β -HfF₄·ZrF₄·BaF₂).

INTRODUCTION

Extrinsic scattering centers in ZrF₄-based glass optical fibers have been recognized as one of the major causes of fiber losses that exceed the theoretical minimum loss value by several orders of magnitude [1]. Microcrystallites are one of these extrinsic centers. They are also one of the internal flaws that contribute significantly to the reduction in the strength of the optical fibers [2].

In order to understand the nucleation and growth mechanism of crystallites that appear during the different steps of fiber preparation, various authors [3-5] have used techniques such as differential thermal analysis (DTA) and/or differential scanning calorimetry (DSC) in combination with optical microscopy, scanning electron microscopy (SEM), X-ray diffraction, scanning transmission electron microscopy (STEM), selected area electron diffraction (SAED) and energy dispersive spectroscopy (EDS). Many different crystallizing phases have been reported in ZBLAN [3-5] and ZBLAL [3] glasses which have been subjected to different thermal treatments. The crystallites are made up of fluorozirconate-based crystals with and without Na, La, and Al, as well as simple fluorides such as LaF₃ and AlF₃ [5].

Despite the large volume of recent work reporting the investigation and identification of various crystalline phases present in HMF-based glasses, micro-Raman (MR) spectroscopy has only recently been used to identify ZrO₂ crystallites grown on the neck-down region during the fiber drawing process [6].

In the current paper we report preliminary results of MR investigations of microcrystals present in the bulk glass system ZBLAN/HZBLAN used to make fiber preforms, as well as in the fibers. The MR data are qualitatively compared with Raman scattering data of the parent

crystals to attempt identification of the crystalline composition .

EXPERIMENTAL

The composition of bulk glasses and fibers used in this investigation, as well as their preparation, are described elsewhere [3,7]. It is important to note that the studied materials have not been submitted to any kind of heat treatment to induce crystal nucleation and growth. The selection of the samples was done with a polarizing optical microscope.

The position of the crystallite inside the bulk glass was marked with a diamond scribe. The glass was then polished until the crystal was only few microns below the glass surface. This procedure was used to reduce the glass Raman scattering background. One crystal commonly found in our ZBLAN glasses is shown in Fig. 1. Lu et al [4] have named this a "caterpillar crystal", and their STEM and EDS experiments suggest that the caterpillar crystals are dominated by β -ZrF₄·BaF₂ and β -2ZrF₄·BaF₂ phases.

Another example of a crystal observed in our glasses is the "notched rod" present in the fiber cladding shown in Fig. 2. The fiber was aligned for polishing under the optical microscope in such a way that the crystal had its wide surface parallel to the polishing plane. The fiber was polished to bring the crystallite close to a flat surface, in order to reduce the background due to the scattered laser light and the glass Raman intensity (Fig. 2b). At this point, the voids are no longer observable in Fig. 2b, as the index matching oil filled the pierced bubbles.

The MR spectrometer used in this investigation comprises an argon ion laser, an Olympus model BH-2 optical microscope and a Spex Triplemate model 1877A with a 0.6 m triple spectrometer fitted with an EG&G model 1460 Optical Multichannel Analyzer (OMA). The laser light is focused on the sample by a 10x, 20x or 80x objective lens. The 80x objective gives a laser spot size of 1 μ m and a spatial resolution of approximately 1 μ m. An attenuated laser spot was used to aim the laser beam in selected areas of the crystal. The procedure was observed using a monitor screen via the vidicon camera or directly through the 10x eye piece. Polarization dependent measurements were carried out by changing the sample orientation under the microscope objective and by having an analyzer and a polarization scrambler in the spectrometer entrance slit. The 514.5 nm laser line was usually used and the power at the sample was typically 4 to 6 mW.

RESULTS and DISCUSSION

The unpolarized micro-Raman spectra of the caterpillar crystal are shown in Fig. 3. The spectrum 3a was measured with the incoming laser light electrical field (E_i) parallel to the length of the "dark leaf shape" located in the center of the crystal (i.e. E_i perpendicular to the crystal length). The spectrum 3b was acquired with E_i perpendicular to the length of the "dark leaf" (i.e. E_i parallel to the crystal length).

Despite the similarity of most features present in spectra 3a and 3b, there are some relative intensity variations between them. The peaks between 120 and 220 cm^{-1} are stronger in spectrum 3a than 3b. The feature at 284 cm^{-1} , which is only a shoulder in spectrum 3a, occurs as a sharp peak in spectrum 3b with about 1/2 of the intensity of the peak at 255 cm^{-1} . The most interesting feature in these spectra is the line shape of the dominant high frequency "broad peak" (symmetric stretching vibration modes, ν_s) around 600 cm^{-1} . An examination of this band, indicates line structures approximately at 564, 587, 610 and 645 cm^{-1} . The spectra in Fig. 3 are quite different from the Raman spectra of the crystalline α - and β -BaZrF₆ reported by Kawamoto et al [8]. However, they exhibit a very close resemblance to the Raman spectrum of a polycrystalline barium fluorozirconate sample with composition BaF₂/ZrF₄ = 33/67 (i.e.



Fig. 1. Optical micrograph of the caterpillar crystal, found in the ZBLAN bulk glass. The photograph was taken with a polarizing optical microscope.

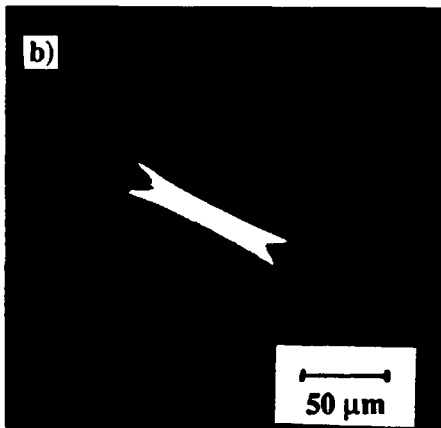
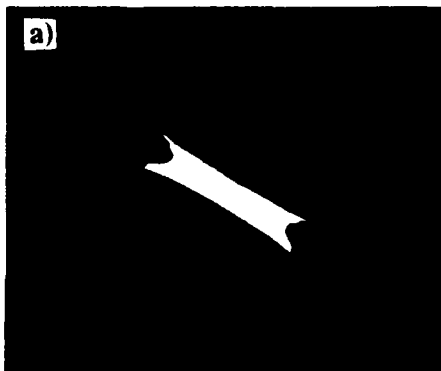


Fig. 2. Optical micrographs of the notched rod crystal present in the fiber cladding (HZBLAN glass). The photographs 2a and 2b were taken with a polarizing optical microscope, before and after the fiber polishing, respectively.

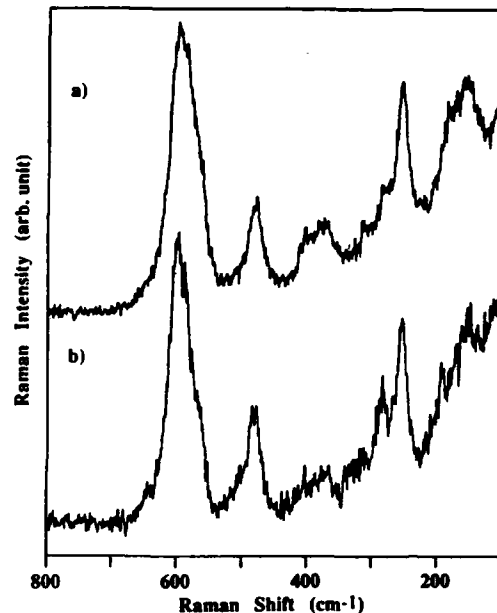


Fig. 3. Micro-Raman spectra of the caterpillar crystal. The spectra 3a and 3b was measured with E_i perpendicular and parallel to the length of the the crystal, respectively.

$2ZrF_4 \cdot BaF_2$ or 2ZB) reported by Kawamoto [9]. This suggests that the caterpillar crystal is a zirconium rich-fluorozirconate crystal phase.

Unfortunately, a more precise crystalline identification will not be possible based on the information available since we do not know the dominant crystalline phase, orientation of the polycrystalline barium fluorozirconate, and light polarization used in the Kawamoto investigation [9]. Besides, our glass (ZBLAN) has Na as a second modifier, thus one can expect the participation of this element in the crystalline structure. This may account for the extra features (the peaks at 255 cm^{-1} and 480 cm^{-1} , which are not observed in Ref. 9), energy shifts [8], and lineshape broadening observed in our spectra. We tentatively assign the spectra 3a and 3b as due to a $NaF \cdot (\alpha\text{- or } \beta\text{-}2ZrF_4 \cdot BaF_2)$ crystalline phase. This is based upon the similarity of our spectra with those in the Ref. 9 and upon the chemical/structural assignment of this type of crystallite made by Lu and Bradley [4]. Parker and co-workers have recently reported the observation of these crystalline phases in ZBLAN glasses [5].

Fig. 4 shows the unpolarized micro-Raman spectra of the notched rod crystal, observed in the fiber cladding (HZBLAN glass). The spectra 4a and 4b were obtained with E_i parallel and perpendicular to the crystal length, respectively.

The spectra 4a and 4b are quite similar, except for the sharp peak at 185 cm^{-1} and the intense peak at 266 cm^{-1} . These peaks are clear features in the lower frequency part of the spectrum 4a and are not observed in the spectrum 4b, thus indicating a strong orientational dependence not observed in the caterpillar crystal spectra (Fig. 4). Another interesting observation is that the strong peak at 616 cm^{-1} (ν_2) is much sharper than the "broad peak" at about 600 cm^{-1} observed in the caterpillar crystal (Fig. 4). A high frequency band with broad linewidth (multiple ν_3 peaks), as reported by Kawamoto [9], it is only observed in the zirconium-rich fluorozirconate crystalline phase, while high frequency sharp bands (single ν_3) are always detected in barium fluorozirconates with molar ratio of one ($BaF_2/ZrF_4=1$), i.e. α - and β - $ZrBaF_6$, as published by Kawamoto and Sakaguchi [8]. Therefore, the observation of a sharp band at 616 cm^{-1} suggests the absence of Zr-rich phase in the notched rod crystal.

Raman scattering studies of microcrystalline inclusions in fluoride glasses and fibers

J.A. Freitas Jr.^b, J.S. Sanghera^c, U. Strom^d, P.C. Pureza^a and I.D. Aggarwal^a

^a Naval Research Laboratory, Washington, DC 20375-5000, USA

^b Sachs / Freeman Associates, Inc., Landover, MD 20785-5396, USA

^c Geo-Center, Fort Washington, MD 20744, USA

Micro-Raman spectroscopy has been successfully used to identify crystalline inclusions in bulk fluoride glasses and optical fibers. The crystalline phases $\text{NaF} \cdot (2\text{ZrF}_4 \cdot \text{BaF}_2)$ and $\text{NaF} \cdot (\text{HfF}_4 \cdot \text{ZrF}_4 \cdot \text{BaF}_2)$ were identified in ZBLAN and HZBLAN glasses, respectively. Also, LaF_3 micro-crystallite inclusions were unambiguously identified in the core of a particular optical fiber.

1. Introduction

To date, the attenuation of ZrF_4 -based glass optical fibers still exceeds the theoretical minimum value by several orders of magnitude [1]. This is primarily due to extrinsic scattering centers which also contribute significantly to the reduction in the strength of the optical fibers [2].

Techniques such as differential thermal analysis (DTA) and/or differential scanning calorimetry (DSC) in combination with optical microscopy and/or tomography, scanning electron microscopy (SEM), X-ray diffraction, scanning transmission electron microscopy (STEM), selected area electron diffraction (SAED) and energy dispersive analysis of X-rays (EDAX) are commonly employed to characterize the glasses and identify micro-inclusions [3-6] which appear during the different steps of fiber fabrication. Recently Tick et al. [7] have used a hot stage optical microscope to study in situ nucleation and growth of crystallites in fluoride glass melts. Although many sub-micrometer and micrometer-sized particles and crystallites have been identified [3-6], many scattering centers still remain unresolved.

The use of Raman scattering, which is well established by its simplicity and generality as a spectroscopic technique, has been sparse. How-

ever micro-Raman scattering has been recently used to systematically identify micro-crystallites and bubbles in heavy-metal fluoride based bulk glasses and fibers [8,9].

In the present work, we report micro-Raman studies of microcrystalline inclusions observed in the ZBLAN/HZBLAN glass system used to make preforms and fibers. The Raman spectra of these inclusions are compared with Raman spectra of various parent fluoride crystals to identify their composition and structure. A comparison between Raman spectroscopy results and conventional SEM/EDAX analyses is presented in an attempt to obtain details on crystallite composition.

2. Experimental

The composition of the bulk glasses and fibers studied in the present work, as well as their preparation, are described in refs. [3] and [10]. One of the glasses was prepared with commercially available materials, without further purification procedure, and heat treated to induce crystallization. The crystallites were selected with a polarized optical microscope.

Although micro-Raman experiments can be performed in the sample without any special

preparation, the spectra quality can be improved considerably if one reduces the glass Raman scattering background. This can be achieved by reducing the thickness of the glass layer above the crystallite to be studied. In case of inclusions in the bulk glasses, the position of the crystallite was marked with a diamond scribe, and the glass was ground until the crystal was only a few micrometers below the glass surface. If the micro-crystal was present inside the fiber, the fiber was aligned under the microscope, keeping the crystallite largest lateral face parallel to the polarizing plane.

We have used two micro-Raman spectrometers in this investigation. The first one comprises an argon ion laser, an Olympus model BH-2 optical microscope and a Spex triplemate model 1877A with a 0.6 m triple spectrometer fitted with a EG&G model 1460 optical multichannel analyzer (OMA). In this case, a laser spot size of $1 \mu\text{m}$ and a spatial resolution of approximately $1 \mu\text{m}$ was achieved. The second micro-Raman spectrometer was constituted of an argon ion laser, a Zeiss Axiovert model 405 M inverted optical microscope, and a Spex 0.85 m scanning double spectrometer model 1404 fitted with a GaAs photomultiplier and a photon counter. For this system, the laser spot size was $\leq 3 \mu\text{m}$. The first system has the advantage of fast data acquisition, but lacks scanning capability and has a limited spectral resolution. The second spectrometer is characterized by its high resolution and scanning capability, which allows one to perform

photoluminescence experiments. However, the scanning feature slows down the data acquisition time significantly. In both systems, an attenuated laser spot was used to aim the laser beam in selected areas of the crystals. The procedure was observed using a monitor screen via the vidicon camera or directly through the eye piece. The partially polarized measurements were carried out by changing the sample orientation under the microscope objective and by having an analyzer and polarization scrambler in the spectrometer entrance slit. Polarization dependent spectral variations were used to identify different crystalline phases. The 514.5 nm laser line was usually used and the power at the sample was typically 4 to 8 mW. The Raman spectra of the micro-crystallites always showed the background Raman spectra due to the glass. This background was corrected by subtracting a normalized Raman spectrum from a nearby region without any crystallites. The normalization factor was such that the glass peak intensity at 580 cm^{-1} was minimized.

The EDAX spectra of the glasses and crystals were performed at MacCrone Associates, Inc. Typically, the crystals were isolated using an optical microscope and subsequently extracted from the glass by grinding the glass away. Sections $1\text{--}2 \mu\text{m}$ thick were mounted on Cu grids and then placed in the STEM. The samples were irradiated by high energy electrons and the X-ray energy emitted was analyzed. The X-ray energy is

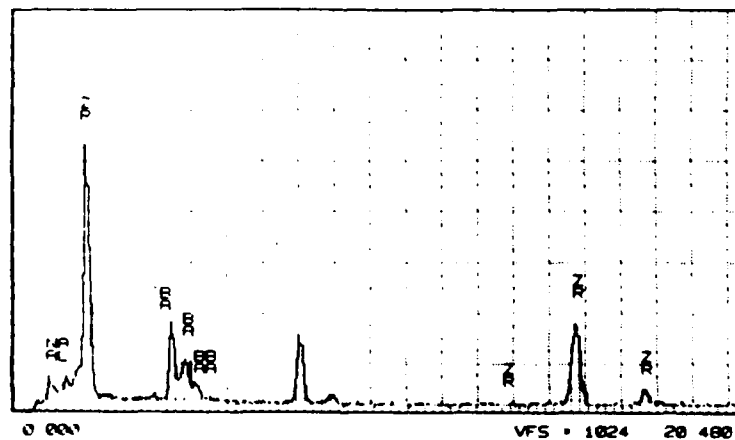


Fig. 1. EDAX spectrum of the 'caterpillar' micro-crystal.

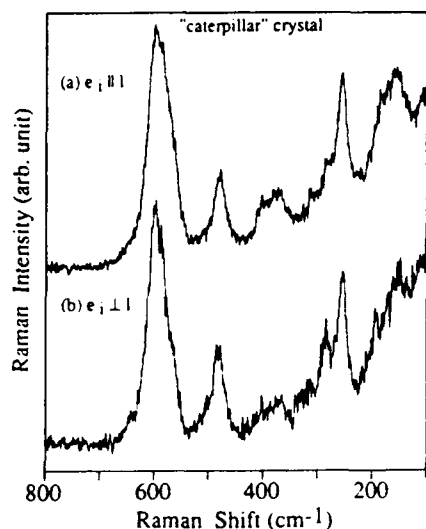


Fig. 2. Micro-Raman spectra of the 'caterpillar' crystallite. The spectra (a) and (b) were measured with the incoming laser polarization, e_1 , parallel and perpendicular to the crystal length, l , respectively.

characteristic of a given element. The sensitivity is approximately 0.5 wt%.

3. Results

Figure 1 shows the EDAX spectrum of the 'caterpillar' crystal described in ref. [8]. Note, the presence of Zr, Ba and traces of Na in the

spectrum of the crystal. The unlabeled peak is due to the copper grid. Therefore EDAX suggests that the crystal is made up of the following fluorides: Na, Zr, Ba. However, the actual crystallographic phase cannot be determined using this technique.

The micro-Raman spectra of the 'caterpillar' crystal is shown in fig. 2. The spectra (a) and (b) were measured with the incoming laser polarization perpendicular and parallel to the crystal length, respectively. The peaks observed between 120 and 220 cm^{-1} are stronger in spectra (a) than (b). The peak at 284 cm^{-1} , which is only a shoulder in spectrum (a), is observed in spectrum (b) with about $\frac{1}{2}$ of the 255 cm^{-1} peak intensity. Although the peaks around 400 cm^{-1} are present in both spectra, they are about twice as intense in spectrum (a). The dominant feature in both spectra is the stretching vibration modes around 600 cm^{-1} . A close look of this band suggested structures around 564, 587, 610 and 645 cm^{-1} .

Figure 3 shows the EDAX spectrum of the 'notched rod' crystal described in ref. [8], observed in the fiber cladding (HZBLAN glass). We observe the presence of Hf, Zr, Ba, and Na from the EDAX spectrum of the crystal. Hence, we conclude that the crystal must contain the following fluorides: Hf, Zr, Ba, Na. Again, the actual crystalline phase cannot be determined solely from EDAX spectra.

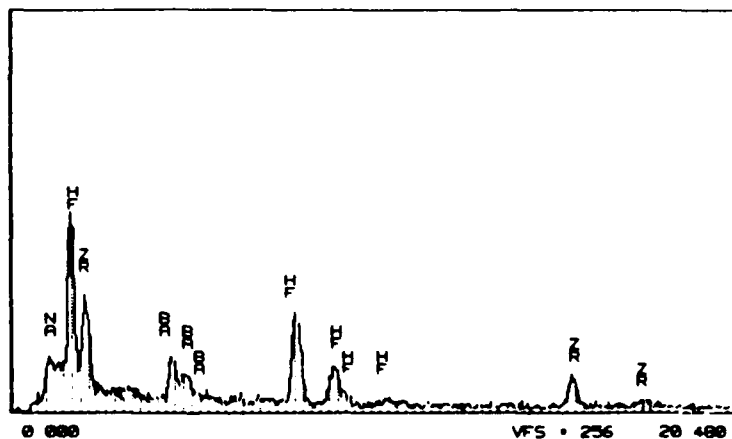


Fig. 3. EDAX spectrum of the 'notched rod' micro-crystal.

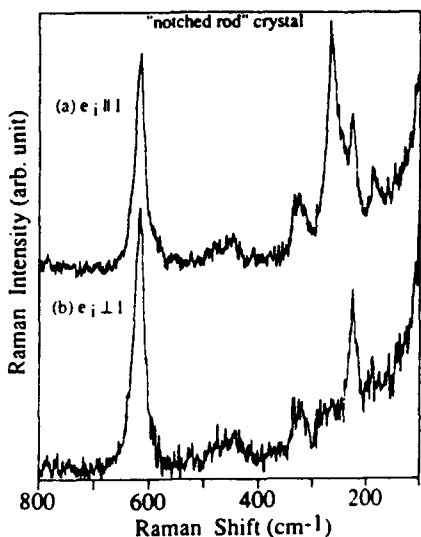


Fig. 4. Micro-Raman spectra of the 'notched rod' crystallite. The spectra (a) and (b) were obtained with the incoming laser polarization, e_i , parallel and perpendicular to the crystal length, l , respectively.

The micro-Raman spectra of the 'notched rod' micro-crystal is represented in fig. 4. The spectra (a) and (b) were obtained with the incoming laser polarization parallel and perpendicular to the crystal length, respectively. Except for the small peak at 185 cm^{-1} and the intense peak at 266 cm^{-1} , the spectra (a) and (b) are quite similar.

Glasses made with unpurified starting materials show a higher degree of nucleation. Submitting these glasses to heat treatment allows crystallites to grown as large as $400\text{ }\mu\text{m}$. Micro-Raman measurements performed on those crystallites under conditions described previously, show similar spectra to those represented in fig. 2. These suggest that the $2\text{ZrF}_4 \cdot \text{BaF}_2$ is the preferential crystallizing phase. Figure 5 shows the micro-Raman spectrum measured with the laser incident on the square cross-section of a micro-crystal in these glasses. Note the similarity of the Raman peak positions and lineshapes with the spectra in fig. 2. The difference in relative intensities is associated with the crystallite orientation in relation to the incoming laser beam polarization.

Figure 6 shows the micro-Raman measurements of (a) a hexagonal shaped micro-crystal inclusion in a fiber core and (b) a commercial

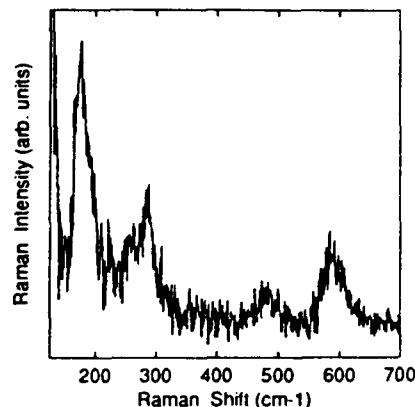


Fig. 5. Micro-Raman spectrum of a particular crystallite in the heat treated glass. The laser beam was incident on the square cross-section of the micro-crystal.

LaF_3 micro-crystal, respectively. The micro-crystal inclusion Raman spectrum was measured with the laser spot incident on the hexagonal crystal face. The micro-crystal LaF_3 Raman measurement was performed for different crystal orientations with respect to the incoming polarization laser beam. The excellent agreement between spectra (a) and (b) erase any doubt about the identification of the fiber micro-inclusion to be a LaF_3 crystal. This result shows that identification of any crystallite by Raman scattering will be

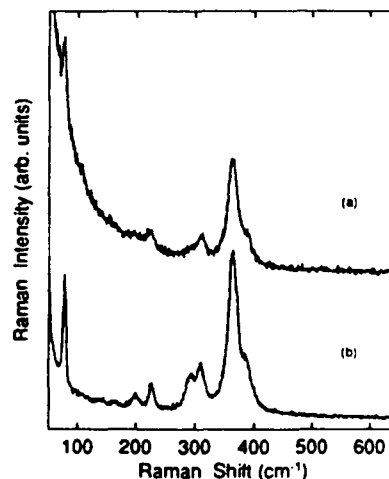


Fig. 6. Micro-Raman spectra of (a) a hexagonal shape micro-crystal in the fiber core and (b) a commercial LaF_3 crystal.

extremely precise if one has good quality reference crystals.

4. Discussion

The data shown in figs. 1–4 allow a tentative identification of the two distinctly shaped structural defects. The ‘caterpillar’ spectra shown in fig. 2 are dominated by the stretching vibration modes near 600 cm^{-1} and four sets of peaks in the range from 120 to 500 cm^{-1} . These spectra are different from spectra reported in the literature for α - and β - BaZrF_6 [11]. However, these spectra show many similarities to the spectrum of a polycrystalline barium fluorozirconate sample with composition $\text{BaF}_2/\text{ZrF}_4 = 33/67$ reported by Kawamoto [12]. This observation suggests that the caterpillar crystal is possibly the zirconium rich-fluorozirconate crystal phase $2\text{ZrF}_4 \cdot \text{BaF}_2$ (ZZB). Since this crystallite was observed in the glass which has Na(ZBLAN) as a second modifier, in addition to Ba, one can expect the participation of this element in the crystalline structure. This may account for the extra features (the peaks at 255 and 480 cm^{-1}), energy shifts and lineshape broadening observed in our spectra in comparison with reported data [11,12]. Note that this observation is in agreement with our EDAX measurements (fig. 1), which detect the presence of Na in this crystallite. A more precise crystalline structure and composition identification is not possible based on the limited information available, since we do not know the dominant crystallographic phase, orientation and light polarization in Kawamoto’s work [11,12].

The micro-Raman spectrum of the ‘notched’ crystal is shown in fig. 4. In this micro-crystal the stretching vibration mode is observed at 616 cm^{-1} . The linewidth of the 616 cm^{-1} band is much smaller than the linewidth of the 600 cm^{-1} band observed in the ‘caterpillar crystal’ (fig. 2). Broad high frequency bands, as discussed previously, are associated with the Zr-rich phase [12], while sharp high frequency bands are in general observed in barium fluorozirconates with molar ratio close to one ($\text{BaF}_2/\text{ZrF}_4 = 1$), i.e., α - and β - ZrBaF_6 , as reported in ref. [11]. Therefore, one can assume

that the ‘notched rod’ crystal is not associated with the Zr-rich phase (ZZB). Micro-Raman measurements carried out on commercially available polycrystalline HfF_4 and ZrF_4 show relative shifts of some vibrational bands towards lower frequency Raman shift. This behavior can be easily understood if we take into consideration the isomorphism between HfF_4 and ZrF_4 [13] and the large difference in mass. For crystallites grown in the HZBLAN glass host, one can expect that the Zr atoms may be partially replaced by the heavier Hf atoms, resulting in shifts of vibrational bands toward lower Raman shifts. This may explain the significant lack of intensity observed in the spectra (a) and (b) in the spectral range between 350 and 600 cm^{-1} in comparison with reported α - and β - ZrBaF_6 spectra [11]. The higher peak position observed in our measurements for the stretching mode may be also associated with the incorporation of Hf, which is expected to increase the degree of bridging of the $[\text{Hf-Zr}]F_8$ complex and/or change in nature of the complex [14]. Again, we point out that Na is a second modifier in our glass system, therefore peak positions and lineshape variations may be expected in comparison with non-Na-containing systems. Based on our EDAX results and the similarity of the micro-Raman spectra with the Raman spectrum reported by Kawamoto et al. [11], we suggest that the ‘notched rod’ crystal is the α - $\text{HfF}_4 \cdot \text{ZrF}_4 \cdot \text{BaF}_2$ phase.

5. Summary

We have used micro-Raman scattering to identify microcrystalline inclusions in the ZBLAN/HZBLAN glass system. Our experimental results combined with EDAX data in the same crystallites and Raman scattering spectra of parent polycrystals reported in the literature suggest that the ‘caterpillar’ crystal is $\text{NaF} \cdot (2\text{ZrF}_4 \cdot \text{BaF}_2)$ and the ‘notched rod’ crystal is $\text{NaF} \cdot (\alpha\text{-HfF}_4 \cdot \text{ZrF}_4 \cdot \text{BaF}_2)$. We have also identified a hexagonal micro-inclusion in a particular fiber core as a LaF_3 crystal by comparison with micro-Raman measurements of a LaF_3 single crystal. These latter results show that micro-Raman can unambigu-

ously identify microcrystalline inclusions if high quality reference crystals are available for spectral comparison.

References

- [1] T. Kanamori, H. Hattori, S. Sakagushi and Y. Ohishi, *Jpn. J. Appl. Phys.* 25 (1986) 1203.
- [2] G. Lu and I.D. Aggarwal, *Mater. Sci. Forum* 19&20 (1987) 375.
- [3] L.E. Busse, G. Lu, D.C. Tran and G.H. Sigel Jr., *Mater. Sci. Forum* 5 (1985) 219.
- [4] G. Lu and J.P. Bradley, *J. Am. Ceram. Soc.* 69 (1986) 585.
- [5] J.M. Parker, A.S. Seddon and A.G. Clare, *Phys. Chem. Glasses* 28 (1987) 4.
- [6] F. Gan, Q. Chen and R. Lee, *Mater. Sci. Forum* 32&33 (1988) 237.
- [7] P.A. Tick, K.E. Lu, S. Mitachi, T. Kanamori and S. Takahashi, these Proceedings, p. 275.
- [8] J.A. Freitas Jr., P.C. Pureza, I.D. Aggarwal and U. Strom, *Mater. Sci. Forum* 67&68 (1991) 279.
- [9] M. Bowden, N.M. Dixon, D.J. Gardiner and S.F. Carter, *J. Mater. Sci.: Mater. Elect.* 1 (1990) 34.
- [10] D.C. Tran, C.F. Fisher and G.H. Siegel, *Electron. Lett.* 17 (1982) 657.
- [11] Y. Kawamoto and F. Sakaguchi, *Bull. Chem. Soc. Jpn.* 56 (1982) 2138.
- [12] Y. Kawamoto, *Phys. Chem. Glasses*, 25 (1984) 88.
- [13] M. Goldstein, R.J. Hughes and W.D. Unsworth, *Spectrochim. Acta* 31A (1975) 621.
- [14] J.H.R. Clarke, P.J. Hartley and Y. Kuroda, *J. Phys. Chem.* 76 (1972) 1831.

PHOTOLUMINESCENCE EXCITATION SPECTROSCOPY OF CUBIC SiC GROWN BY CHEMICAL VAPOR DEPOSITION ON Si SUBSTRATES

J.A. FREITAS, Jr.¹, P.B. KLEIN², AND S.G. BISHOP³

¹Sachs-Freeman Associates, Landover, MD 20785, USA

²Naval Research Laboratory, Washington, DC 20375, USA

³Center for Compound Semiconductor Microelectronics, University of Illinois, Urbana, IL 61801, USA

ABSTRACT

Photoluminescence excitation (PLE) spectroscopy has been applied to the characterization of optical absorption processes in thin film samples of cubic (3C-) SiC grown by chemical vapor deposition (CVD) on Si substrates. Low temperature (6K) PLE spectra have been obtained using a double grating monochromator and a xenon lamp as a tunable source of excitation. For undoped, n-type films of cubic SiC, plots of the integrated PL intensity, in the range 2.4-1.5 eV, as a function of the wavelength of the exciting light are in excellent agreement with optical absorption spectra reported for bulk 3C-SiC. The observed shape of the absorption edge is characteristic of phonon assisted indirect transitions, and spectral features attributable to LA and TA phonons are discernible. No below-gap extrinsic absorption features are observed in the PLE spectra of the undoped films. These results demonstrate the use of the PLE technique for bandedge absorption measurements in thin semiconductor films for which transmission measurements may not be practical. The intense N-Al donor-acceptor pair (DAP) PL bands (2.2-1.5 eV) observed in Al-doped films provide much improved signal-to-noise ratios for the PLE spectra in these samples compared to those obtained in the undoped films. In addition to the characteristic above-gap indirect absorption edge spectrum, the PLE spectra for the Al-doped samples exhibit below-gap, extrinsic absorption features at photon energies corresponding to the nitrogen bound exciton peaks observed in the PL spectra. The extrinsic absorption process which contributes to the excitation of the N-Al DAP PL is apparently a photoneutralization of the compensated (positively charged) nitrogen donors.

1. Introduction

The successful epitaxial growth [1-4] of thin films of cubic SiC by chemical vapor deposition (CVD) on Si substrates has revived interest in this promising wide band-gap semiconductor. Photoluminescence (PL) spectroscopy has played an important role in the characterization [5-10] of both undoped and aluminum-doped thin film samples of CVD cubic SiC. The low temperature PL spectra of most films exhibit a rich variety of characteristic spectral features. However, only a few of these PL bands have been associated with identified impurities or with acceptors and donors of known binding energy. Specific observations include PL spectra attributable to excitons bound to 54 meV neutral nitrogen donors [5-9,11], free-to-bound PL transitions involving aluminum acceptors [8, 12-14], nitrogen-aluminum donor-acceptor pair recombination (N-Al DAP bands) [8,12-15] and a deep DAP band which reveals an unidentified 470 meV acceptor [10].

Photoluminescence excitation (PLE) spectroscopy provides valuable information concerning the optical absorption processes which lead to the excitation of recombination radiation. In PLE spectroscopy the intensity of a selected PL band is recorded as a function of the wavelength of the exciting light. Under some conditions the PLE spectrum constitutes an accurate representation of the absorption spectrum of the sample. (This is an important consideration when analyzing thin film samples for which absorption measurements by conventional optical transmission techniques are problematic.) However, the PLE spectrum incorporates an additional degree of specificity in that it provides a measure of the effectiveness of various absorption processes in the excitation of a particular PL band. This is particularly useful when extrinsic (below band gap) absorption processes excite the PL.

Both of these characteristics of PLE spectroscopy are pertinent to the investigation of CVD films of cubic SiC reported here. The PLE spectra obtained from undoped n-type samples provide the first detailed representation of the indirect optical absorption edge of thin film CVD SiC, which is found

to be in excellent agreement with the optical absorption spectra reported for bulk (Lely-grown) cubic SiC. In the case of Al-doped films, the PLE spectra exhibit extrinsic absorption features which are attributed to the photoneutralization of compensated donors.

2. Experimental

The thin film samples of cubic SiC, which were obtained from the Naval Research Laboratory, North Carolina State University, and the NASA Lewis Research Center, were all grown by CVD techniques [1,2,4] on Si substrates. Both undoped n-type and Al-doped films have been studied. In all cases the films were removed from their substrates to relieve the strain which results from the ~20% lattice mismatch between the SiC films and the Si substrates.

The PL and PLE spectra described here were obtained with the samples contained in a liquid helium cryostat which provided temperatures ranging from 2 to 300 K. Spectra were acquired in CW mode with excitation provided by an argon (476.5 nm) or krypton (476.2 nm) ion laser or light (460 nm) from a 150W xenon lamp dispersed through a double grating monochromator. The excited luminescence was analyzed by a grating monochromator and detected by a GaAs photomultiplier tube (PMT) which is sensitive to wavelengths shorter than about 900 nm. Appropriate glass filters were used to exclude exciting light from the analyzing monochromator.

The xenon lamp-double grating monochromator combination provided exciting light with wavelength tunable from about 400 to 1000 nm. For the PLE experiments, the luminescence excited by this system was focused onto the entrance slit of a 0.75 m focal length, single grating monochromator. PLE spectra were obtained with the detection monochromator serving as a band pass filter tuned to a particular PL wavelength, or with a mirror replacing the grating in the monochromator so that the integrated PL intensity was recorded. In the latter case, the wavelength limits of the detected PL band were determined by a longpass optical filter placed at the entrance slit and by the long wavelength limit of the GaAs PMT response (~900 nm). The PLE spectra were corrected for the wavelength dependence of the exciting light intensity.

The intensity of the exciting light for the PLE spectra was about $100 \mu\text{W}/\text{cm}^2$ at the peak of the spectral output for the lamp-monochromator system. PL spectra obtained under these excitation conditions first revealed the importance of recording PL spectra over a broad range excitation intensities. For example, nearly all PL spectra reported in the literature [5-10, 16] for n-type CVD cubic SiC are excited by relatively high power light ($>1 \text{ W}/\text{cm}^2$). They are dominated by the nitrogen bound exciton (NBE) spectrum (especially the phonon replicas) with its relatively short donor bound exciton radiative life time. In addition to the NBE spectrum, other characteristic features of these high power PL spectra include the 1.972 eV zero phonon line (ZPL) and 1 phonon replicas of the D1 defect band (which has been studied in detail in ion implanted Lely crystals [17] and CVD films [7,8] of cubic SiC), and a broad underlying PL band peaking near 1.8 eV. In contrast, the low power PL spectrum for such undoped samples, excited by light from the lamp and double monochromator system, exhibit only a weak vestige of the NBE spectrum. These spectra are dominated instead by a distant DAP band with peak at about 1.91 eV, the so-called G-band [9,10,18] which is attributed [10] to the pairing of the 54 meV nitrogen donors with an unidentified 470 meV acceptor.

Similarly, the two PL spectra shown in Fig.1 contrast the high- and low-power excitation conditions for an Al-doped sample of cubic SiC. The high power spectrum exhibits sharp line spectra at high energies due to close pair recombination. The low power spectrum is dominated by the long life time distant pair band peaking at about 2.12 eV. Note that the close pair spectra are not observed at low power and that the phonon replicas below the distant pair band exhibit sharper spectral details. It is important to remember that the PLE spectra presented here are obtained under conditions which produce the low power PL spectra of Fig.1. That is, they are dominated by deep PL bands with long lifetime recombination processes.

3. Results and Discussion

Figure 2 shows the 2.35 - 2.50 eV PLE spectrum from an undoped, n-type film of CVD cubic SiC, obtained at 5K under the integrated PL intensity conditions described above. The line shape or intensity distribution of this PLE spectrum exhibits a detailed similarity to the optical absorption spectrum reported by Choyke et al. [11] for bulk, Lely-grown cubic SiC. Note that PL intensity has been plotted on a square root scale in order to illustrate the indirect character of the absorption edge. Choyke et al. described the shape of the edge as characteristic of indirect transitions in which excitons are created. The onsets of optical absorption transitions assisted by the emission of TA, LA, TO, and LO phonons are indicated in Fig. 2. The phonon energies have been determined from the NBE PL spectra [11]. It follows that the exciton energy gap, $E_{Gx} = 2.390$ eV, is derived by subtracting the TA phonon energy from the observed onset of absorption.

The fact that the PLE spectrum scales closely with the absorption spectrum of Choyke et al. from the band edge up to energies in excess of 2.5 eV, indicates that the PLE spectrum provides a remarkably faithful representation of the interband optical absorption. Although the previously reported absorption measurements were performed on crystals with a light path of approximately 2 mm, Choyke et al. [11] noted that even larger crystals would be preferred for more accurate measurements. Thus the sensitivity of the PLE technique is apparent when one considers the fact that the light path for the thin film SiC samples is only about 10-15 μm .

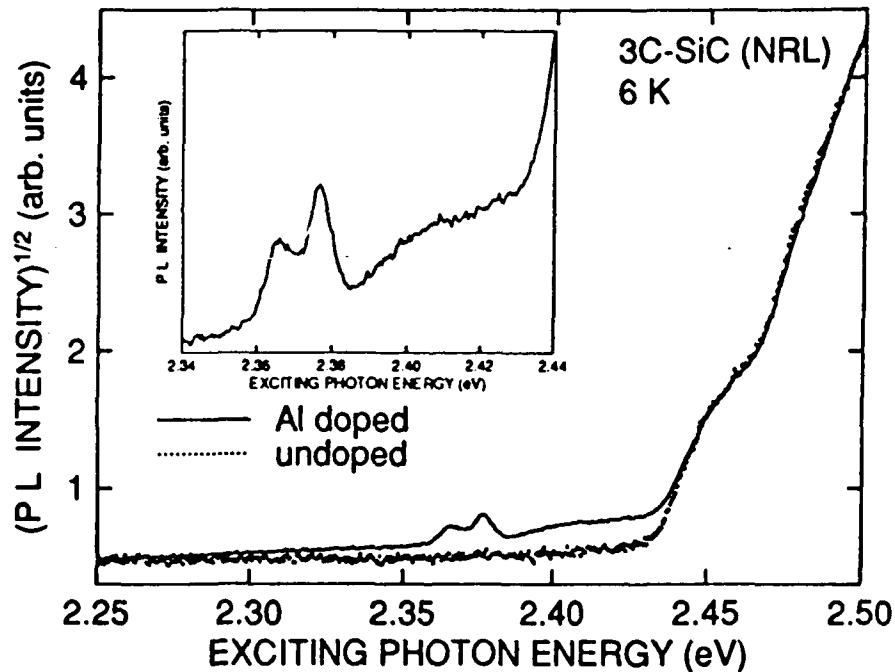


Fig. 3. Photoluminescence excitation spectra for an Al-doped (continuous line) and an undoped (dotted line) CVD 3C-SiC film. The square root of the integrated photoluminescence intensity (in the spectral range 1.4 - 2.3 eV) is plotted as a function of the photon energy of the exciting light. The undoped spectrum has been normalized to the Al-doped spectrum for the best spectral coincidence between 2.45 and 2.50 eV. The insert shows the extrinsic portion of the Al-doped PLE spectrum at high gain.

In Fig. 3 the PLE spectrum obtained from an Al-doped sample of cubic SiC is compared to that of the undoped sample presented in Fig. 2. The much greater integrated intensity of the N-Al DAP PL bands and phonon replicas in the Al-doped sample is apparent in the greater signal to noise ratio of its PLE spectrum relative to that of the undoped sample. Furthermore, the PLE spectrum of the Al-

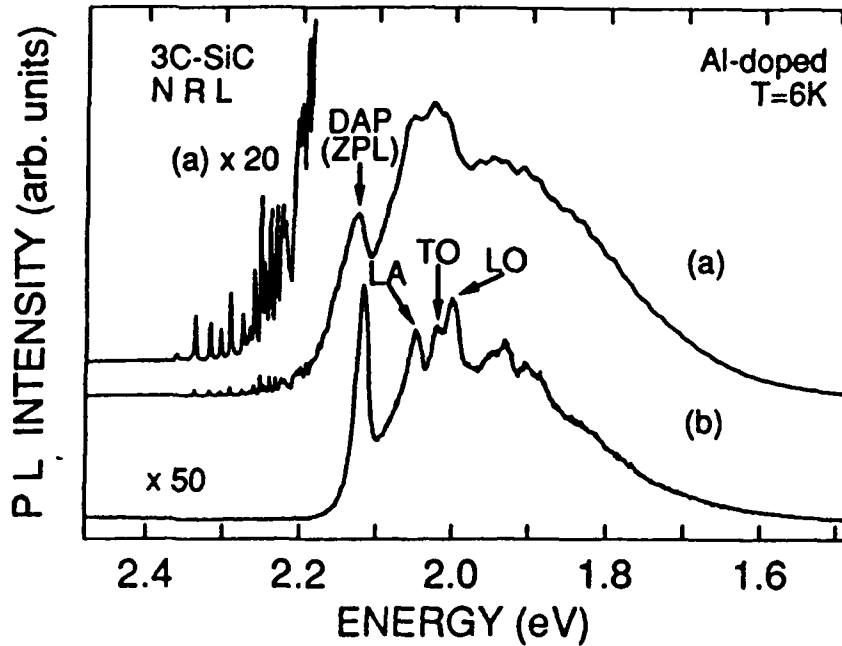


Fig. 1. Low temperature (6K) photoluminescence spectra from an Al-doped SiC film: (a) high power spectrum excited by an argon ion laser ($1\text{W}/\text{cm}^2$, 476.5 nm); X20 spectrum shows close donor-acceptor pair spectra; (b) low power spectrum excited by xenon lamp and 0.22 m monochromator ($0.1\text{mW}/\text{cm}^2$, 460 nm).

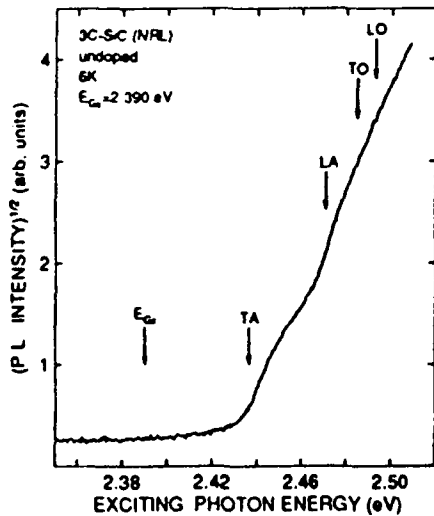


Fig. 2. Photoluminescence excitation spectrum for an un-doped CVD 3C-SiC film deposited with C/Si source gas ration of 2.4. The square root of the integrated photoluminescence intensity (in the spectral range 1.4 - 2.3 eV) is plotted as a function of the photon energy of the exciting light. The exciton energy gap, E_{GX} , and the emitted phonon energies are indicated in the figure.

doped sample exhibits extrinsic absorption features in the spectral range extending from the onset of interband absorption at about 2.436 eV down to about 2.349 eV.

The extrinsic portion of the Al-doped PLE spectrum is presented at higher gain and resolution, and on an expanded scale in the inset to Fig. 3. It is characterized by an onset at about 2.349 eV, although this is difficult to determine exactly, peaks at 2.367 and 2.377 eV, a dip or trough with minimum at about 2.385 eV, and a shoulder which rises to higher energy until it intersects the steeply rising interband PLE at about 2.436 eV.

There are two primary factors which enter into the interpretation of these extrinsic features in the PLE spectrum. First, they are observed only in relatively heavily Al-doped films, and second, the onset, peaks, and shoulder all occur in a spectral range which corresponds to the binding energies and PL bands associated with the known donors in cubic SiC. The first factor indicates that the absorption processes which give rise to these extrinsic PLE features require the presence of large concentrations of compensated (charged) donors. Undoped films are invariably n-type; they exhibit the NBE PL spectra which reveal the presence of the 54 meV donor identified as nitrogen [8,11,13,14,19], and temperature dependent Hall effect measurements which are interpreted in terms of a highly compensated 15-20 meV donor [13,20-23]. In heavily Al-doped samples these donors are compensated and extrinsic optical absorption transitions can photoneutralize the charged donors. The electrons on the resulting neutral donors can then undergo DAP radiative recombination with the holes on the neutral Al acceptors. Although no optical (PL) signature of the shallow (15-20 meV) donor has been identified to date, the N-Al DAP PL spectrum is well documented [8,13,14].

In considering the second factor, the most obvious correlation is between the 2.377 and 2.367 eV PLE peaks and the energies of the ZPL of the NBE bands and the low energy shoulder on the NBE band (believed to be a deeper donor bound exciton [5,8]), respectively, of the near-band edge PL spectrum observed in undoped n-type films [5-9]. Note that these energies are characteristic of the NBE PL spectra in the strained CVD films grown on Si (and subsequently removed from their substrates) which are slightly red-shifted (~1 meV) relative to the NBE spectra reported for bulk Lely crystals of cubic SiC. The obvious suggestion is that this portion of the extrinsic PLE involves the excitation of the nitrogen and unidentified deeper donor bound excitons. Far more speculative is the possible correlation between the approximate 2.349 eV low energy onset of the extrinsic PLE spectrum and the energy $2.349 \text{ meV} = E_{\text{gap}} - 54 \text{ meV}$ (the nitrogen donor binding energy), where the low temperature band gap of cubic SiC is taken to be 2.403 eV. This correlation suggests the hypothesis that 2.349 eV is the onset of extrinsic absorption transitions which photoneutralize the 54 meV nitrogen donors. However, the onset, whose position is highly uncertain, could also be explained as a low energy tail on the apparent donor bound exciton absorption band.

Even more interesting and speculative is the possibility that the absorption shoulder above the 2.385 eV trough might be associated with photoneutralization of compensated 15-20 meV donors. (The trough is positioned about 18 meV below the band gap.) If this hypothesis were correct, it would represent the first optical manifestation of the 15-20 meV shallow donor which appears to dominate the electrical properties of undoped CVD films of cubic SiC. However, it must be emphasized strongly that this is simply a conjecture and there are equally plausible alternative interpretations of this absorption shoulder.

4. Summary

Photoluminescence excitation spectroscopy has been used to investigate the above gap and extrinsic optical absorption processes which excite the PL bands that characterize CVD films of cubic SiC grown on Si substrates. In undoped films the PLE spectra provide a faithful representation of the indirect optical absorption edge which is consistent with the optical absorption spectrum reported previously for Lely-grown bulk crystals of cubic SiC. The undoped PLE spectra show no evidence of extrinsic (below gap) optical absorption. The PLE spectra of the N-Al DAP bands which dominate the PL spectra of Al-doped films of cubic SiC exhibit extrinsic absorption which is attributed to photoneutralization of compensated shallow donors. The extrinsic PLE spectra of the Al-doped samples contain peaks which correspond to the ZPLs of the donor bound exciton PL bands observed in the undoped films, as well as onsets which, it is speculated, could correspond to the

thresholds for photoneutralization of the 54 meV N donor and the unidentified 15-20 meV donor which are pervasive in CVD cubic SiC.

5. Acknowledgements

The authors wish to thank P.E.R. Nordquist, Jr. and M.L. Gipe of the Naval Research Laboratory, H.S. Kong and R.F. Davis of North Carolina State University, and J.A. Powell of the NASA Lewis Research Center for providing the samples which we have studied. This work was supported in part by the Office of Naval Research.

References

1. S. Nishino, J.A. Powell, and H. A. Will, *Appl. Phys. Lett.* **42**, 460 (1983).
2. A. Addamiano and P.H. Klein, *J. Cryst. Growth* **70**, 291 (1984).
3. K. Sasaki, E. Sukuma, S. Misawa, S. Yoshida, and S. Gonda, *Appl. Phys. Lett.* **45**, 72 (1984).
4. H.P. Liaw and R.F. Davis, *J. Electrochem. Soc.* **131**, 3014 (1984).
5. S.G. Bishop and J.A. Freitas, Jr., *J. Cryst. Growth* **106**, 38 (1990).
6. J.A. Freitas, Jr., S.G. Bishop, A. Addamiano, P.H. Klein, H.J. Kim, and R.F. Davis, *Mats. Res. Soc. Symp. Proc.*, **46**, 581, (1985).
7. J.A. Freitas, Jr., S.G. Bishop, J.A. Edmond, J. Ryu, and R.F. Davis, *J. Appl. Phys.* **61**, 2011 (1987).
8. J.A. Freitas, Jr., S.G. Bishop, P.E. R. Nordquist, Jr., and M.L. Gipe: *Appl. Phys. Lett.* **52**, 1695 (1988).
9. W.J. Choyke, Z.C. Feng, and J.A. Powell, *J. Appl. Phys.* **64**, 3163 (1988).
10. J.A. Freitas, Jr. and S.G. Bishop, *Appl. Phys. Lett.* **55**, 2757 (1989).
11. W.J. Choyke, D.R. Hamilton, and L. Patrick, *Phys. Rev.* **133**, A1163 (1964).
12. G. Zanmarchi, *J. Phys. Chem. Solids* **29** (1968) 1727.
13. W.E. Carlos, W.J. Moore, P.G. Siebenmann, J.A. Freitas, Jr., R. Kaplan, S.G. Bishop, P.E.R. Nordquist, Jr., M. Kong, and R.F. Davis, in *Proc. Mats. Res. Soc. Symp.* **27**, 253 (1987).
14. S.G. Bishop, J.A. Freitas, Jr., T.A. Kennedy, W.E. Carlos, W.J. Moore, P.E.R. Nordquist, Jr., and M.L. Gipe, in: *Amorphous and Crystalline Silicon Carbide*, Springer Proc. in Physics, Vol. 34, ed. G.L. Harris and C.Y.-W. Yang (Springer-Verlag, Berlin, Heidelberg, 1987), p. 90.
15. W.J. Choyke and L. Patrick, *Phys. Rev.* **B2**, 4959 (1970).
16. H. Okumura, M. Shinohara, E. Muncyama, H. Daimon, M. Yamanaka, E. Sakuma, S. Misawa, K. Endo, and S. Yoshida, *Japan. J. Appl. Phys.* **27**, L116 (1988).
17. W.J. Choyke and L. Patrick, *Phys. Rev.* **B4**, 6 (1971).
18. J.A. Freitas, Jr., S.G. Bishop, P.B. Klein, P.E. R. Nordquist, Jr., and M.L. Gipe, in: *Amorphous and Crystalline SiC II*, Springer Proc. in Physics, Vol. 43, eds. M.M. Rahman, C.Y.-W. Yang, and G.L. Harris (Springer-Verlag, Berlin, Heidelberg, 1988), p. 106.
19. J.A. Freitas, Jr., W.E. Carlos, and S.G. Bishop, in *Amorphous and Crystalline SiC III*, Howard University, Washington, DC, Apr 11-12, 1990, in press.
20. A. Suzuki, A. Uemoto, M. Shigeta, K. Furukawa, and S. Nakajima, *Appl. Phys. Lett.* **49**, 450 (1986).
21. B. Segall, S.A. Alterovitz, E.J. Haugland, and L.G. Matus, *Appl. Phys. Lett.* **49**, 584 (1986).
22. B. Segall, S.A. Alterovitz, E.J. Haugland, and L.G. Matus, *Appl. Phys. Lett.* **50**, 1533 (1987).
23. M. Shinohara, M. Yamanaka, H. Daimon, E. Sakuma, H. Okumura, S. Misawa, K. Endo, and S. Yoshida, *Japan J. of Appl. Phys.* **127**, L434 (1988).

Chemical vapor deposition of β -SiC on silicon-on-sapphire and silicon-on-insulator substrates

J. C. Pazik, G. Kelner and N. Bottka

Naval Research Laboratory, Washington, DC 20375-5000 (U.S.A.)

J. A. Freitas Jr.

Sachs-Freeman Associates, Landover, MD 20785-5396 (U.S.A.)

Abstract

Cubic silicon carbide (β -SiC) films have been grown epitaxially on silicon-on-sapphire (SOS) substrates by chemical vapor deposition. A fresh layer of silicon is first deposited *in situ* on the SOS substrate at approximately 1050°C. The silicon layer is then carbonized while being heated to 1360°C. The β -SiC layer is grown at 1360°C using silane and propane as sources. β -SiC films can also be grown directly on the SOS substrate without utilizing a fresh silicon layer. Deposition of β -SiC films on silicon-on-insulator (SOI) substrates has also been accomplished with slight modification of the growth parameters described above.

The β -SiC films have been characterized by IR reflectance spectroscopy, optical microscopy and electron microscopy. Typical films are 7 μm thick and have a specular surface with some physical features. Electrical transport properties as determined by the Van der Pauw Hall method show the β -SiC films to be p-type while those grown on SOI were n-type. X-ray rocking curve measurements were obtained to determine the crystalline quality of the films. In addition, preliminary optical characterization of the films has been performed.

1. Introduction

Advances in β -SiC device technology have been hampered by the limited quality of material available. Defect densities in β -SiC grown on Si(100) are high and carrier concentrations and Hall mobilities are typically much poorer than the theoretical limits. These problems are likely associated with the 20% lattice mismatch between silicon and β -SiC and an 8% difference in coefficients of thermal expansion. Furthermore, silicon substrates are not ideally suited for high temperature device applications and the reproducible growth of p-type β -SiC on silicon has been a persistent problem. The quality of β -SiC films has been improved by growth on substrates whose lattice parameters and coefficients of thermal expansion are more closely matched to those of β -SiC, such as α -SiC [1, 2] and TiC [3]. Unfortunately, the price, availability and quality of these substrates have limited their routine use. Silicon-on-sapphire (SOS) substrates provide an attractive alternative since they are readily avail-

able, low cost, able to withstand high temperatures and have been shown to be effective substrates for the heteroepitaxial growth of GaAs on silicon [4]. Perhaps more importantly, sapphire substrates have been shown to autodope the silicon epilayer with aluminum [5], a feature which could be exploited for the preparation of p-type β -SiC layers. In 1969, Khan [6] reported the "chemical conversion" of Si(100) on sapphire, at low pressure, to a β -SiC film. The films were characterized only by their electron diffraction pattern and little experimental detail was presented. We have succeeded in preparing the first example of epitaxial β -SiC grown on SOS substrates by chemical vapor deposition (CVD) [7]. In addition, we have begun investigations into the epitaxial growth of β -SiC on silicon-on-insulator (SOI) substrates by CVD.

2. Experimental details

A horizontal reactor with computer control of switching, flow and temperature was used to

produce β -SiC films on SOS and SOI substrates. Reactant gases were high purity propane (1% by volume in hydrogen) and silane (1% by volume in hydrogen). Purified hydrogen was used as the carrier gas. SOS substrates were produced in house by molecular beam epitaxy (MBE; 3 in diameter wafer with silicon thickness of $0.6 \mu\text{m}$ on 0.43 mm of Al_2O_3) or obtained from Union Carbide (4 in diameter wafers with silicon thickness of 0.3 , 0.55 or $1 \mu\text{m}$ on 0.55 mm of Al_2O_3). The wafers were cut into pieces of approximate dimensions $12 \times 15 \text{ mm}^2$. Substrates were degreased in organic solvents, etched by the RCA method [8] and then immediately transferred to the graphite susceptor in the horizontal reactor. The system was evacuated to 2 mTorr, backfilled and continuously flushed with high purity hydrogen. Under a $3.5 \text{ standard l min}^{-1}$ (slpm) flow of hydrogen the substrate was heated from ambient to 1150°C and held at this temperature for 5–10 min to remove any oxide coating. The temperature was then lowered to about 1050°C and a fresh layer of silicon ($0.7 \mu\text{m}$) was deposited on

the substrate using a silane flow of $100 \text{ standard cm}^3 \text{ min}^{-1}$ (sccm). After the growth of the fresh silicon layer the substrate was cooled to near room temperature and held there for 1 min. A buffer layer was grown by heating the substrate from near room temperature to 1360°C under a constant flow of 100 sccm of propane and 1 slpm of hydrogen. It is essential to begin carbonization at low temperature. Non-specular films were obtained if carbonization was initiated at 1050°C . This observation suggests a low temperature conversion of the silicon surface. After 1 min at 1360°C the propane flow was diverted to vent and the system purged with hydrogen for 1 min at a flow of 1.5 slpm. The epilayer was grown for 2 h in the temperature range 1340 – 1370°C using a C:Si ratio of 2.5. Alternatively, β -SiC was grown directly on SOS without first depositing a fresh silicon layer. The growth parameters were similar to those described above, except the growth of a silicon epilayer at 1050°C was eliminated.

SOI substrates were prepared in house and consisted of $3 \mu\text{m}$ of silicon on the surface and $1 \mu\text{m}$ of SiO_2 on a silicon substrate 0.55 mm thick. Substrate preparation and the growth profile are similar to those described above for β -SiC on SOS. No fresh layer of silicon was deposited.

3. Results and discussion

The β -SiC films prepared on SOS substrates both with and without the *in situ* silicon epilayer were specular with many physical features. Typically, the films have a translucent amber appearance in the center area of the substrate. Along the edges of the film an opaque gray area approximately 1 mm wide was observed. The Nomarsky optical micrograph of the β -SiC layer (Fig. 1(a)) depicts the overall surface morphology. Individual surface features were observed using a Cambridge scanning electron microscope. The photomicrograph in Fig. 1(b) reveals a textured surface along with columnar growth features and pits. Typically, the morphology of the β -SiC grown on SOS is poorer (many more growth features such as pits and columns) than that observed for β -SiC on silicon. The morphology of β -SiC grown on SOI was much better (few columns and pits) than that of β -SiC grown on SOS and was comparable to that observed for β -SiC films grown on silicon.

The most remarkable feature of β -SiC films

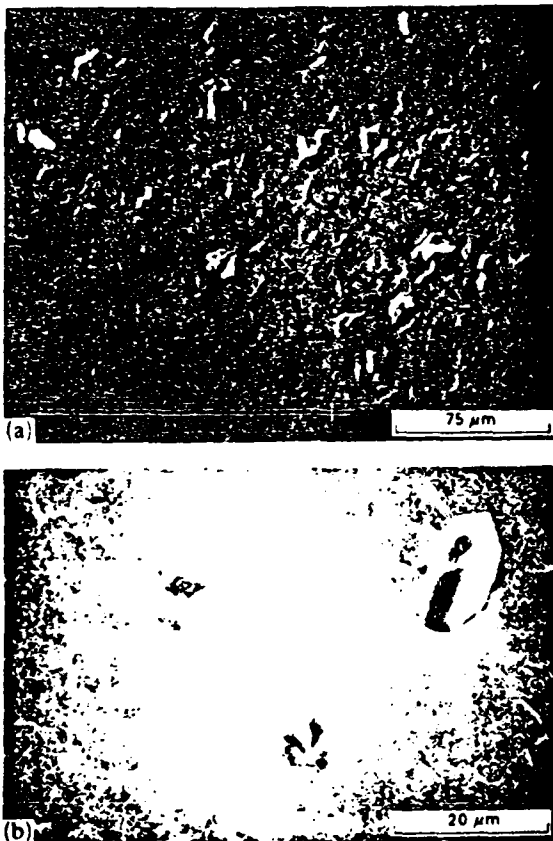


Fig. 1. (a) Optical and (b) scanning electron micrographs of β -SiC films grown on SOS

grown on SOS is their p-type nature. Grown layers were characterized by Hall measurements using the Van der Pauw technique. Samples 3 mm square were sawn with a diamond saw from the as-grown layers. Corner contacts of 700 Å of nickel deposited by thermal evaporation became ohmic after heat treatment at 1000 °C for 20 s, in an atmosphere of forming gas, using rapid thermal annealing. All measured samples were p-type with Hall mobilities and net hole concentrations ($N_a - N_d$) ranging from 7.9 to 51.7 cm² V⁻¹ s⁻¹ and 1.4×10^{20} to 5.6×10^{17} cm⁻³ respectively. Under identical growth conditions and using the same susceptor, β -SiC films grown at this laboratory on Si(100) are always n type with mobilities of 160–230 cm² V⁻¹ s⁻¹ and net electron concentrations ($N_d - N_a$) in the low 10¹⁷ cm⁻³ region. Autodoping of silicon with aluminum by sapphire is well documented [5] and is increased with higher growth temperatures [9]. Therefore at the high temperatures required for β -SiC growth it is likely that the SOS substrate is autodoping the β -SiC films with aluminum. This is also supported by the observation of donor-acceptor recombination pairs (DAPs) in the photoluminescence (PL) spectra of unintentionally doped β -SiC films grown on SOI using the same susceptor as that used for growth of β -SiC on SOS substrates. These same films have been shown to be n-type but highly compensated, again suggesting the presence of an acceptor. However, the possibility of doping due to defects cannot yet be fully ruled out.

The β -SiC grown on SOS appears to be highly stressed. In several instances the β -SiC films have been observed to shatter off the SOS substrate upon cooling to room temperature. In other instances the β -SiC films have shattered off SOS substrates when being cut for transport measurements. The scanning electron micrograph in Fig. 2 shows that the β -SiC film is cleanly removed from the SOS substrate and also shows a lifting of the remaining β -SiC from the substrate. Experiments to quantify the stress in these films are currently under way along with investigations into methods of reducing the stress, e.g. annealing. X-ray rocking curve (XRC) measurements were made on β -SiC films grown on silicon, SOS and SOI substrates to help quantify the β -SiC film quality. The β -SiC films grown on silicon and SOI exhibited the narrowest XRC halfwidths of 690–770 s. The XRC halfwidths of β -SiC films grown on SOS were much

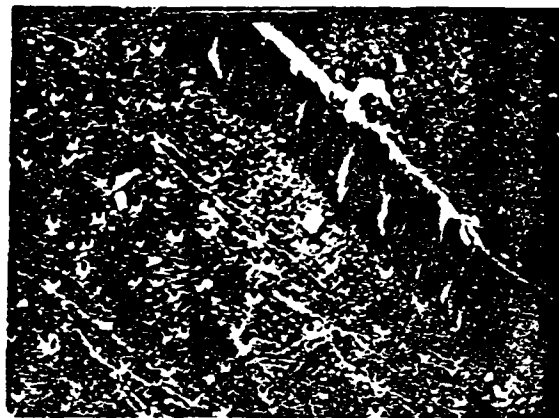


Fig. 2. Scanning electron micrograph of β -SiC and SOS surface after film has shattered off the substrate.

wider, ranging from 945 to 1620 s, with a typical value of approximately 1010 s. Neither the thickness of the sandwiched silicon layer nor the *in situ* deposition of a fresh silicon layer appears to significantly affect the XRC halfwidth.

Preliminary optical characterization of β -SiC on SOS and SOI substrates has also been accomplished. Micro-Raman spectroscopy has been performed to determine the film quality and the nature of the columnar growth features observed on the β -SiC surface. The micro-Raman spectra (Fig. 3) of β -SiC on SOS substrates exhibit the typical longitudinal optic (LO) and transverse optic (TO) phonon lines [10]. In Fig. 3 (a) for the β -SiC surface on SOS (inset is β -SiC on silicon), the TO phonon line is significantly lower in intensity than the LO phonon line. In addition, a weak feature is observed between 940 and 950 cm⁻¹. In the Raman spectrum of a columnar growth feature (Fig. 3(b)) the TO phonon line intensity is greatly enhanced relative to the LO line and the weak feature at 940–950 cm⁻¹ is not observed. No α -SiC phases were observed to be present in these samples. The increased intensity of the TO phonon line relative to the LO phonon line observed in the spectrum of the columnar growth features is the result of reduced stress [10] in the growth columns and/or a different orientation of the crystallites. However, the disappearance of the weak feature observed between 940 and 950 cm⁻¹ in the spectrum of the growth column suggests that increased TO phonon line intensity is a result of lower stress in the crystallite, since these weak features are only observed in spectra of films adhered to substrates and not in those of free-standing films [11]. Thus

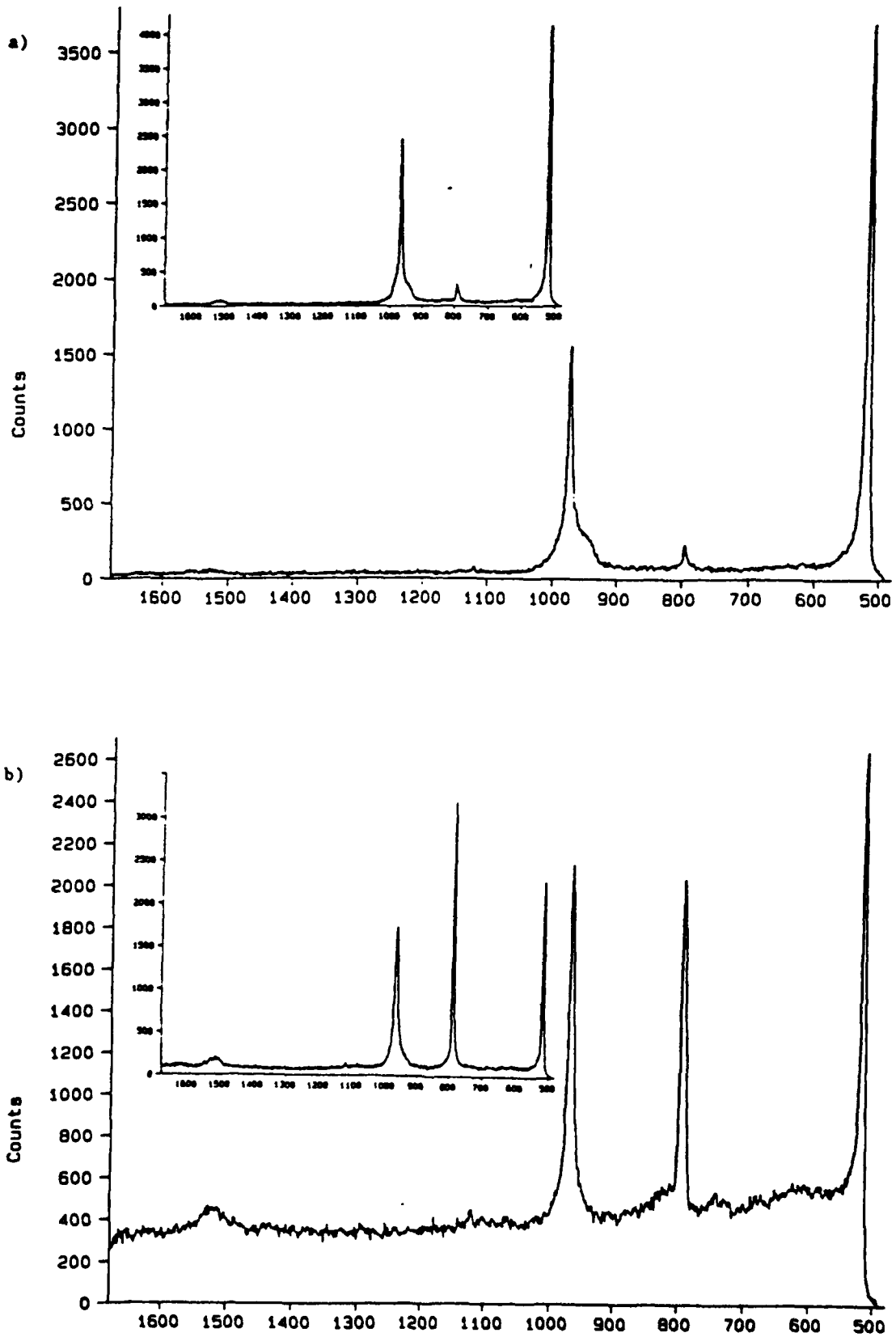


Fig. 3. Micro-Raman spectra of β -SiC films on SOS and silicon (inset): (a) surface and (b) columnar growth features.

the formation of these columnar features may provide a mechanism to relieve the stress in the β -SiC on SOS. The position of the TO and LO phonon lines is significantly different in β -SiC films grown on SOS vs. silicon. High resolution Raman spectroscopy must be performed to determine the contribution of stress and sample heating to the position of the TO and LO phonon lines. Photoluminescence experiments have been initiated on β -SiC grown on SOI and SOS substrates. Although the β -SiC film on SOI is n-type, a DAP band associated with nitrogen donors and aluminum acceptors [12] is observed in the PL spectra. The p-type dopant is possibly the result of aluminum contamination of the susceptor from previous growth using SOS substrates. Identification of the DAPs in β -SiC on SOS substrates is currently being pursued.

Acknowledgments

The authors wish to acknowledge L. Shirey and G. Stauf for technical assistance, B. Molnar for suggesting SOS as a potential substrate, P. E. R. Nordquist, R. S. Sillmon, D. K. Gaskill and P. H. Klein for helpful discussions, and G.

Campisi and Union Carbide for supplying the SOS substrates. This work is funded in part by a grant from the Office of Naval Research.

References

- 1 H. S. Kong, J. T. Glass and R. F. Davis, *J. Mater. Res.*, **4** (1989) 204.
- 2 J. A. Powell, D. J. Larkin, L. G. Matus, W. J. Choyke, J. L. Bradshaw, L. Henderson, M. Yoganathan, J. Yang and P. Pirouz, *Appl. Phys. Lett.*, **56** (1990) 1353.
- 3 J. D. Parsons, R. F. Bunshah and O. M. Stafsudd, *Solid State Technol.*, **28** (1985) 133.
- 4 J. B. Posthill, R. J. Markunas, T. P. Humphreys, R. J. Nemanich, K. Das, N. R. Parikh, P. L. Ross and C. J. Miner, *Appl. Phys. Lett.*, **55** (1989) 1756.
- 5 S. Cristoloveanu, *Rep. Prog. Phys.*, **50** (1987) 327.
- 6 I. H. Khan, *Mater. Res. Bull.*, **4** (1969) S285.
- 7 J. C. Pazik, G. Kelner, N. Bottka, *Appl. Phys. Lett.*, **58** (1991) 1419.
- 8 W. Kern and D. A. Puotinen, *RCA Rev.*, **31** (1970) 187.
- 9 D. Bhogswara Rao and K. T. Jacob, *J. Cryst. Growth*, **58** (1982) 79.
- 10 J. A. Freitas Jr., S. G. Bishop, A. Addamino and P. H. Klein, *MRS Symp. Proc.*, **45** (1985) 581.
- 11 Z. C. Feng, W. J. Choyke and J. A. Powell, *J. Appl. Phys.*, **64** (1988) 6827.
- 12 S. G. Bishop and J. A. Freitas Jr., *J. Cryst. Growth*, **106** (1990) 38.

A NEW DEEP ACCEPTOR IN EPITAXIAL CUBIC SiC

J.A. FREITAS, JR.* AND S.G. BISHOP**

Naval Research Laboratory, Washington, DC 20375-5000

*Sachs/Freeman Associates, Inc., Landover, MD 20785

** Present address: Dept. of Electrical and Computer Engineering and Center for Compound Semiconductor Microelectronics, University of Illinois at Urbana-Champaign, Urbana, IL 61801

ABSTRACT

The temperature and excitation intensity dependence of photoluminescence (PL) spectra have been studied in thin films of SiC grown by chemical vapor deposition on Si (100) substrates. The low power PL spectra from all samples exhibited a donor-acceptor pair PL band which involves a previously undetected deep acceptor whose binding energy is approximately 470 meV. This deep acceptor is found in every sample studied independent of growth reactor, suggesting the possibility that this background acceptor is at least partially responsible for the high compensation observed in Hall effect studies of undoped films of cubic SiC.

INTRODUCTION

Recently, we reported [1] evidence for the existence of a previously undetected deep acceptor (binding energy 470 meV) in thin films of cubic SiC grown by chemical vapor deposition (CVD) on Si substrates. An investigation [1-2] of the dependence of the photoluminescence spectra on excitation power and temperature revealed a deep donor-acceptor pair (DAP) band at about 1.91 eV which involves the recombination of electrons trapped at relatively shallow donors (probably 54 meV nitrogen donors) with the unidentified deep acceptor. This deep DAP PL band was observed in a variety of SiC films grown in several different reactors, and its pervasive character suggests the possibility that the associated deep acceptor is at least partially responsible for the high compensation observed [3-7] in undoped films of cubic SiC. In this paper we examine in detail the evidence for the DAP interpretation of this deep PL band, and some of the implications of the highly localized character of such a deep acceptor.

RESULTS AND DISCUSSION

Figure 1 compares low temperature PL spectra obtained at high and low excitation intensity from an undoped n-type film of cubic SiC grown at the Naval Research Laboratory. (The CVD growth [8, 9] and PL techniques [10] have been described in detail elsewhere). The high power spectrum, which was excited by 476.2 nm light from a krypton ion laser at a power density of 2 W/cm², is dominated by a sharp five-line spectrum between 2.23 and 2.39 eV which is attributed to the recombination of excitons bound to neutral nitrogen donors [11, 12] (the nitrogen bound exciton or NBE spectrum). This spectrum also exhibits two other characteristic but unidentified PL bands, the so-called W-bands [13] at 2.15 eV, and the D1 defect band [10, 14, 15] with zero phonon line (ZPL) at 1.972 eV. In the low power PL spectrum, excited from the same sample at a power density of 0.02 w/cm², the NBE spectrum is much weaker and the W and D1 bands are barely observable. The spectrum is dominated by the so-called G-band [1, 13] with ZPL at about 1.91 eV, and its apparent phonon replicas, labelled G1 and G2. These PL bands (G, G1, G2, and W) are present in the PL spectra of CVD SiC films reported by several different workers [2, 10, 13, 15, 16]. However, Choyke and co-workers assigned the alphabetical labels in ref. [13] in which they studied the dependence of these bands upon film thickness and excitation wavelength (penetration depth).

We now consider the evidence for the DAP interpretation of the G-band. The fact that the G-band dominates the low power PL spectra of every undoped SiC film we have studied, while the NBE, W, and D1 bands are either greatly diminished or unobservable, suggests that the G-

100 030

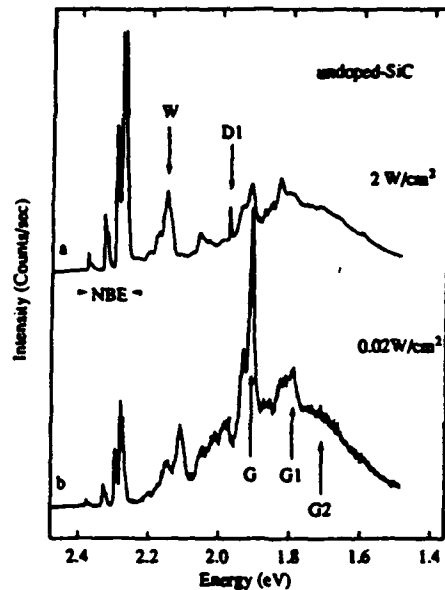


Fig. 1. Low temperature (6K) photoluminescence spectra obtained at high and low excitation intensity from an undoped n-type film of cubic SiC. The high power spectrum is dominated by the nitrogen bound exciton (NBE) bands and the low power spectrum by the G-band DAP feature and its phonon replicas G1 and G2.

band has a long radiative lifetime relative to those of the NBE, W, and D1 bands, and its intensity therefore saturates at high excitation intensity [1, 2]. Such a long PL lifetime is characteristic of radiative recombination at an extended defect such as a donor-acceptor pair [17]. We have found (in agreement with Choyke et al. [13], that the spectral position of the G-band varies by several meV from sample to sample. This is consistent with the behavior of a distant DAP PL band. The peak position of a distant DAP band is determined by the average interimpurity (DAP) separation, which can be expected to change from sample to sample if the concentrations of participating donors and acceptors vary significantly [17]. In addition, the G-band spectrum of the low power spectrum in Fig. 1 is resolved into two distinct features which we have identified [1] as a free-to-bound (FB) transition at 1.932 eV and a distant pair band about 20 meV lower in energy. The most obvious and important implication of these identifications is that there exists in these SiC films a deep defect (acceptor) level whose approximately 470 meV binding energy is given by the difference between the 2.403 eV low temperature band gap of cubic SiC and the 1.932 eV FB transition energy.

The FB and distant pair band identifications are based primarily on the temperature and power dependences of these spectral features [1]. Figure 2(a) shows the variations in the FB and DAP spectra over a three order of magnitude change in excitation intensity, and Fig. 3 shows the dependence of their peak positions over more than four orders of magnitude of change in exciting laser power. The lower energy feature (1.91 - 1.92 eV) identified as the DAP peak shifts to higher energy and broadens significantly with increasing excitation intensity as expected for a distant DAP band [17]. This shift arises because the more distant pairs, which give rise to the lower energy portion of the DAP band, have longer lifetimes and their emission is saturated at high power. Correspondingly, the higher energy side of the DAP band, which comprises transitions from closer pairs with shorter radiative lifetimes, is accentuated with increasing excitation intensity. On the other hand, the position and line width of the FB feature of the G-band spectrum (1.932 eV) are relatively insensitive to variations in the intensity of the exciting light. The FB band does broaden and shift slightly to higher energy as a consequence of optically induced carrier heating at the very highest excitation powers [18].

The temperature dependence of the low power G-band PL features is shown in Fig. 2b. As the temperature is increased from 6 to 100 K, the intensity of the 1.932 eV FB band increases at the expense of the distant DAP band at 1.912 eV. This behavior closely parallels the decrease

0000032

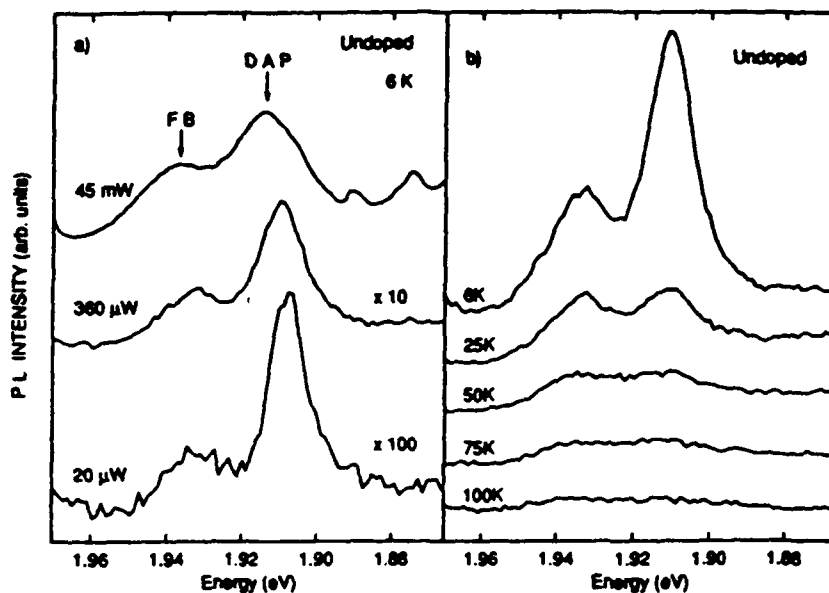


Fig. 2. Variations in the free-to-bound and donor-acceptor pair G-band PL spectra over a three order of magnitude change in excitation intensity at a temperature of 6K are shown in 2(a). The temperature dependence of the low power G-band PL features is shown in 2(b) in the temperature range 6 to 100K.

in the intensity of the N-AI distant DAP PL band and the commensurate increase in the AI acceptor FB band in this temperature range, which has been reported previously [19] for Al-doped films of cubic SiC. In the case of the N-AI DAP system, the observed behavior is attributable to the thermal ionization of the 54 meV N donors. The parallel behavior of the G-band DAP and FB bands in approximately the same temperature range suggests that an impurity of comparable depth (thermal ionization energy) is involved in the G-band DAP recombination process. The most likely candidate is the pervasive 54 meV N donor. This leads to the conclusion that the 470 meV deep defect is an acceptor, an interpretation which is consistent with the fact that the known acceptor impurities in SiC (Al, B) are observed to be much deeper than the donors [19-21].

Another measure of the smaller of the two binding energies participating in the DAP band is given by the energy separation of the FB and DAP bands. For pairs at infinite spatial separation, the energy difference would be just equal to the impurity binding energy, e.g., the 54 meV N binding energy for the N-AI DAP system. Obviously the actual position of the DAP peak is determined by the Coulomb interaction between the charged impurity final states for the finite pair separation which corresponds to the peak in the distribution of donor-acceptor pair separations [17]. The observed energy difference between the N-AI DAP and AI FB bands in Al-doped cubic SiC is usually [19-20] about 35 meV (it is a function of impurity concentration). Thus the 22 meV separation of the FB and DAP G-bands is consistent with the participation of a shallow donor in the G-band DAP recombination (e.g. the 54 meV N donor). The energy separation of the FB and distant DAP peaks will be significantly less for N donors coupled to the 470 meV deep acceptor than for N donors coupled to the 257 meV AI acceptor. This happens because the more highly localized hole wave function of the deeper acceptor enhances the contribution of closer pairs to the distant pair band thereby shifting its peak to higher energy (closer to the FB band).

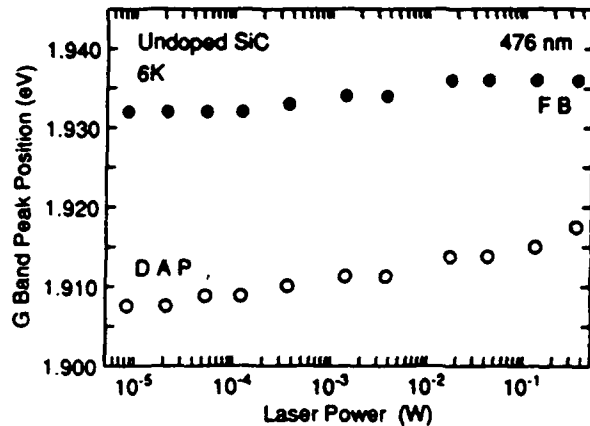


Fig. 3. The peak positions at 6K of the free-to-bound and donor-acceptor pair G-band PL features as a function of exciting light intensity.

The very fact that a FB transition can be observed for the G-band at low temperature and low excitation power is another consequence of the highly localized wave function of a hole trapped at a deep (470 meV) acceptor. For example, in the case of the N-Al DAP system in SiC, no FB transition is observed [12] below about 40K. In Al-doped material at low temperature the DAP transitions dominate because the greater spatial extent of the wave functions of holes trapped at 257 meV Al acceptors assures sufficient overlap with electrons trapped at neutral donors. Only at elevated temperatures which produce a significant number of ionized donors and a quasi-equilibrium population of free electrons in the conduction band does the FB recombination process become more favorable. In contrast, the highly localized wave functions of holes trapped at the 470 meV acceptors do not overlap as strongly with the neutral donors at low temperatures and a significant fraction of the trapped holes can recombine with photoexcited electrons in the conduction band.

CONCLUDING REMARKS

The pervasive character of the G-band and the fact that its intensity correlates with variations in the C/Si source gas ratio employed during growth [1] suggest the possibility that the deep acceptor is associated with a nonstoichiometric defect rather than a background impurity. However, the evidence is far from conclusive and the data could also be explained in terms of a background impurity whose incorporation is controlled by film stoichiometry.

ACKNOWLEDGEMENTS

The authors wish to thank P.E.R. Nordquist, Jr. and M.L. Gipe for providing the samples and P.B. Klein for valuable discussions. This work was supported in part by the Office of Naval Research.

References

1. J.A. Freitas, Jr. and S.G. Bishop, Appl. Phys. Lett., in press.

2. J.A. Freitas, Jr., S.G. Bishop, P.B. Klein, P.E.R. Nordquist, Jr., and M.L. Gipe, in: *Amorphous and Crystalline SiC II*, Springer Proc. in Physics, Vol. 43, eds. M.M. Rahman, C.Y.-W. Yang, and G.L. Harris (Springer-Verlag, Berlin, Heidelberg, 1988), p. 106.
3. A. Suzuki, A. Uemoto, M. Shigeta, K. Furukawa, and S. Nakajima, *Appl. Phys. Lett.* **49**, 450 (1986).
4. B. Segall, S.A. Alterovitz, E.J. Haugland, and L.G. Matus, *Appl. Phys. Lett.* **49**, 584 (1986).
5. B. Segall, S.A. Alterovitz, E.J. Haugland, and L.G. Matus, *Appl. Phys. Lett.* **50**, 1533 (1987).
6. W.E. Carlos, W.J. Moore, P.G. Siebenmann, J.A. Freitas, Jr., R. Kaplan, S.G. Bishop, P.E.R. Nordquist, Jr., M. Kong, and R.F. Davis, in *Proc. Mats. Res. Soc. Symp.* **92**, 253 (1987).
7. M. Shinohara, M. Yamanaka, H. Daimon, E. Sakuma, H. Okumura, S. Misawa, K. Endo, and S. Yoshida, *Japan J. of Appl. Phys.* **27**, L434 (1988).
8. S. Nishino, J.A. Powell, and H.A. Will, *Appl. Phys. Lett.* **42**, 460 (1983).
9. A. Addamiano and P.H. Klein, *J. Cryst. Growth* **70**, 291, (1984).
10. J.A. Freitas, Jr., S.G. Bishop, J.A. Edmond, J. Ryu, and R.F. Davis, *J. Appl. Phys.* **61**, 2011 (1987).
11. W.J. Choyke, D.R. Hamilton, and L. Patrick, *Phys. Rev.* **133**, A1163 (1964).
12. J.A. Freitas, Jr., S.G. Bishop, P.E.R. Nordquist, Jr., and M.L. Gipe, *Appl. Phys. Lett.* **52**, 1696 (1988).
13. W.J. Choyke, Z.C. Feng, and J.A. Powell, *J. Appl. Phys.* **64**, 3163 (1988).
14. W.J. Choyke and L. Patrick, *Phys. Rev.* **B4**, 6 (1971).
15. J.A. Freitas, Jr., S.G. Bishop, A. Addamiano, P.H. Klein, H.J. Kim, and R.F. Davis, *Mats. Res. Soc. Symp. Proc.*, **46**, 581, (1985).
16. S.G. Bishop and J.A. Freitas, Jr., *J. Crystal Growth*, in press.
17. P.J. Dean, in *Progress in Solid State Chemistry*, **8**, eds. J.O. McCaldin and Y.G. Somarjai (Pergamon, Oxford) 1973, p. 1.
18. K. Colbow and D.W. Nyberg, *Can. J. Phys.* **45**, 2833 (1967).
19. W.J. Choyke and L. Patrick, *Phys. Rev.* **B2**, 4959 (1970).
20. H. Kuwabara, S. Yamada, and S. Tsunekawa, *J. Lumin.* **12/13**, 531 (1976).

PHOTOLUMINESCENCE CHARACTERIZATION OF CUBIC SiC GROWN BY CHEMICAL VAPOR DEPOSITION ON Si SUBSTRATES

S.G. BISHOP *

Naval Research Laboratory, Washington, DC 20375, USA

and

J.A. FREITAS, Jr.

Sachs-Freeman Associates, Landover, Maryland 20785, USA

Photoluminescence (PL) spectroscopy has proven to be a powerful tool for the detection and identification of impurities and other defects in semiconductors. After a brief description of the phenomenology and experimental techniques, the application of PL to the characterization of thin films of cubic SiC grown on Si (100) substrates by chemical vapor deposition (CVD) will be discussed. Specific examples include the detection and/or identification of impurities and defects on the basis of PL spectra attributable to excitons bound to neutral impurities (nitrogen donor bound excitons), free carriers recombining with carriers bound at impurities (aluminum free-to-bound transitions), and donor-acceptor pair (DAP) recombination (N-Al DAP bands). The use of time decay characteristics and excitation power dependence to classify recombination processes on the basis of lifetimes, and the determination of impurity ionization energies from the temperature quenching of PL bands will be discussed.

1. Introduction

Characterization of semiconductors by PL spectroscopy involves the measurement and interpretation of the spectral distribution of recombination radiation emitted by the sample. Electrons and holes which are optically excited across the forbidden energy gap usually become localized or bound at an impurity or defect before recombining, and the identity of the localized center to which they are bound can often be determined from the PL spectrum. Relatively sharp-line, near-band edge spectra arise from the recombination of electron-hole pairs which form bound excitons [1] (BE) at impurity sites, or the free-to-bound (FB) transitions [2] which involve the recombination of free electrons (holes) with holes (electrons) bound at neutral acceptors (donors), while lower

energy and much broader PL bands arise from the recombination of carriers localized at deep traps. Qualitative information about crystal quality can be inferred from the efficiency and line widths of near band edge PL spectra, and impurities can sometimes be identified on the basis of the binding energies inferred from the spectral positions (energies) of BE or FB transitions.

Because PL has proven to be a convenient, sensitive, non-destructive technique for the characterization of semiconductor materials, it is now one of the most widely applied spectroscopic tools. The experimental technique is relatively inexpensive to implement, there are very few constraints on the materials to which it is applicable (e.g. carrier type or impurity and defect concentration), and a broad scope of phenomena such as excitations, defects, and recombination mechanisms can be investigated. Perhaps most important is the fact that PL spectroscopy is useful during all phases of the development of a new materials system or growth technique. Typically, broad PL spectra which convey only the most qualitative informa-

* Present address: Center for Compound Semiconductor Microelectronics and Department of Electrical and Computer Engineering, University of Illinois at Urbana-Champaign, Urbana, Illinois 61801, USA.

030 040

tion are obtained from poor quality semiconductors while sharper spectral features which provide more specific information will evolve as material quality improves. This has certainly been true of the PL characterization of thin film cubic SiC grown by chemical vapor deposition (CVD) on Si substrates, which we will briefly review in this paper.

2. Experimental technique

The PL spectra described here were obtained with the samples contained in a liquid helium cryostat which provided temperatures ranging from 1.5 to 330 K. Most spectra were obtained in CW mode with excitation provided by either an argon (476.5 nm) or krypton (476.2 nm) ion laser. These excitation photon energies are above the 2.4 eV indirect band gap of cubic SiC. Time decay studies of the PL spectra employed 10 nsec pulses of 355 nm excitation light which was obtained by tripling the photon energy of a pulsed 1065 nm Nd:YAG laser (peak power approximately 4 kW). For both the CW and pulsed experiments the excited luminescence was analyzed by a grating monochromator and detected by a GaAs photomultiplier tube (PMT). The GaAs PMT, which is sensitive to wavelengths shorter than about 900 nm, is operated in a photon counting mode for most experiments, which facilitates digital data acquisition and multiscan signal averaging.

The thin film samples of cubic SiC were grown by CVD techniques [4-7] on Si (100) substrates. Undoped n-type, al-doped, and a variety of ion-implanted samples have been studied. In some cases the films were studied on their Si substrates and the resulting red-shifted PL spectra [8] were used to assess the strain resulting from the 20% lattice mismatch between Si and cubic SiC. However, in most cases the films were removed from their substrates to relieve the strain, and some of the highest quality PL spectra have been obtained from such films which were subjected to high temperature annealing [9]. In addition, the effects of stoichiometry on film quality and defect content were investigated [10] by growing several SiC

samples with different values of C/Si source gas ratio.

3. Bound exciton emission

Twenty five years ago, Choyke, Hamilton and Patrick published a seminal paper [11] on the optical characterization of cubic SiC grown by the so-called Lely technique. With optical absorption spectroscopy they determined the indirect character of the band gap and obtained a measured value of 2.39 eV for the exciton band gap. In addition, they reported a five-line PL spectrum which included a 2.379 eV zero phonon line (ZPL) located just 10 meV below the exciton gap, and its TA, LA, TO, and LO phonon replicas. They attributed these spectral features to the recombination of excitons bound at neutral nitrogen donors on carbon sites (N_c). Subsequent work demonstrated that the donors giving rise to this spectrum are isolated point defects [12] and that the binding energy of the donor which traps the excitons is about 54 meV [13].

The far more recent studies of PL in CVD films of cubic SiC began by reproducing the spectra which Choyke et al. had obtained in Lely-grown crystals. Freitas et al. [8] reported the observation of the five-line nitrogen bound exciton (NBE) spectrum in as grown n-type films. Initially, these spectra were badly broadened and red-shifted by strain, but as the CVD material has improved, so has the quality of the NBE spectra [9,10,14] exhibited by the SiC films, an example of which is shown in fig. 1. However, the energy of the NBE ZPL is still slightly red-shifted (~ 1 meV) relative to its position in the Lely PL spectra, and the line widths of the NBE PL spectra in most films are ~ 2 meV. This is to be compared with exciton linewidths ~ 0.15 meV for spectra obtained [12] from Lely crystals. In addition, the intensity of the ZPL for the NBE spectrum in most CVD SiC films is much less than that of the phonon replicas (see fig. 1). These differences in the PL spectra are apparently caused by internal strain and high concentrations of charged centers in the CVD films. Very recently it has been reported [15] that CVD films of cubic SiC grown on alpha SiC substrates

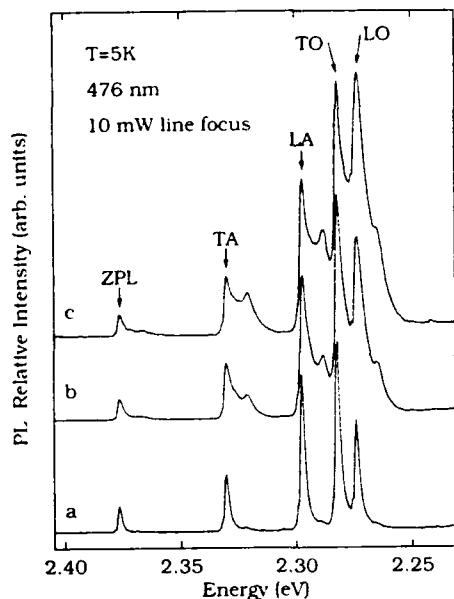


Fig. 1. Low-temperature nitrogen bound exciton photoluminescence spectra from three undoped SiC films grown with three different values of C/Si ratio: (a) 2.4, (b) 1.6, and (c) 1.2.

have exhibited NBE PL spectra whose quality is very close to Lely spectra in terms of energy position, spectral width, and ratio of ZPL and phonon replica intensities. It should be noted that all of these incremental advances in material quality have been detected and documented by PL spectroscopy.

The NBE PL spectra from CVD films of cubic SiC exhibit weak shoulders on the low-energy side of the ZPL and each of the well resolved phonon replicas (see fig. 1). Freitas and coworkers [10] have shown that the relative strengths of the NBE spectrum and these low-energy shoulders are a function of the C/Si source gas ratio. They found that the intensity of the shoulders is greatly enhanced for the lower C/Si ratios as shown in fig. 1, suggesting that the recombination centers responsible for these PL transitions might be attributable directly or indirectly to nonstoichiometric defects such as antisite defects, Si interstitials or C vacancies. Okumura et al. [16] have reported a similar enhancement of these shoulders on the NBE spectrum by N-doping during the CVD growth process, and have attributed the shoulders (rather than the primary five-line spectrum) to the

recombination of nitrogen bound excitons. However, we have found that Al-doping also enhances the intensity of the shoulders indicating that some indirect effect of significant concentrations of *any* dopant (such as the creation of attendant defects) leads to the enhancement.

Temperature dependence of the exciton PL spectra [10] yielded thermal quenching energies of 11 meV for the NBE spectrum and 17 meV for the shoulders, indicating that the shoulders originate from a separate defect and are not, for example, local phonon replicas of the NBE five-line spectrum. In addition, PL decay measurements [12,17] revealed that all of the PL features in the near-band edge spectra shown in fig 1 have lifetimes in the ~ 400 ns range expected for donor bound excitons (in indirect band gap materials) whose lifetimes are limited by Auger recombination processes. Excitons bound at isoelectronic defects (e.g. Si on a C site) are expected to have much longer decay times [18] ($\sim 10 \mu\text{s}$). It is therefore suggested that the most likely interpretation of the broad shoulders on the NBE PL spectrum is that they arise from recombination of excitons bound to donors which have a somewhat larger binding energy than the 54.5 meV donor (presumably nitrogen) which gives rise to the NBE spectrum. The broadened character of the shoulders indicates that they may arise from recombination centers which occur in very high concentrations or strained environments in inhomogeneities in the SiC films [10]. Our recent observation [19] of high contrast inhomogeneities in PL images of SiC films is consistent with this hypothesis.

4. Donor-acceptor pair spectra

In semiconductor materials containing substantial concentrations of both donors and acceptors the donor-acceptor pair (DAP) recombination process becomes a dominant contributor to the observed PL spectrum. In the DAP recombination mechanism [20,21], electrons bound at neutral donors recombine radiatively with holes bound at neutral acceptors. For a DAP with infinite separation, the energy of the PL transition would be equal to the band gap energy minus the sum of the

donor and acceptor binding energies. However, for finite separations the PL energy is shifted by interactions between the donor and acceptor, the most important of which is the Coulomb interaction between the charged (ionized) final states of the impurities (after recombination). The strength of the Coulomb interaction, and therefore the PL photon energy, is a function of the spatial separation of the DAP. For close pairs an array of discrete sharp line spectra occurs at high energy which gradually merges into a broad continuum at lower energy for increasingly larger separations [20,21].

The DAP spectrum obtained [10,22,23] at 6 K from an Al-doped CVD film of cubic SiC is shown in fig. 2. Aluminum doping was accomplished by introducing trimethyl aluminum with the source gases during growth. The sharp-line spectra between 2.20 and 2.35 eV correspond exactly to the DAP spectra obtained by Choyke and Patrick [21] in Al-doped Lely-grown crystals of

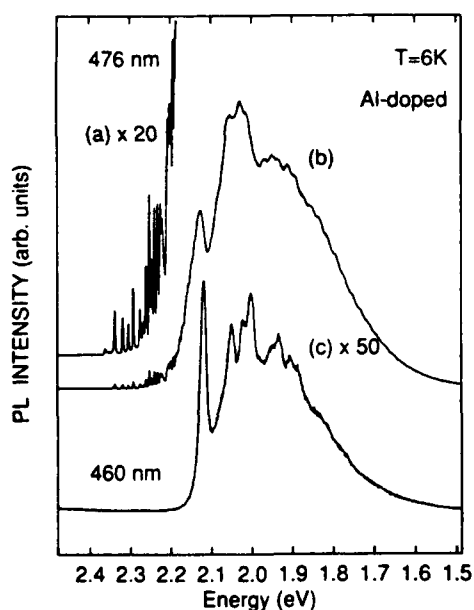


Fig. 2. The CW PL spectra excited by an argon laser (476.5 nm, 1 W/cm^2) from an Al-doped SiC film: (a) detail of sharp-line close pair spectra; (b) full spectrum showing close pair spectra, distant pair band at 2.12 eV, and its phonon replicas at lower energy. Spectrum (c) was excited by 0.1 mW/cm^2 of 460 nm light from a xenon lamp and a double monochromator.

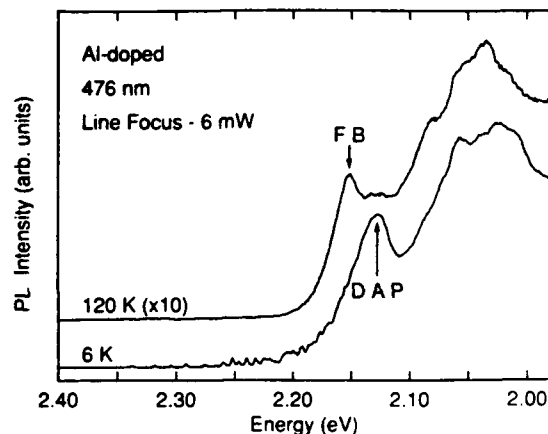


Fig. 3. The N-Al distant D-A pair band at 6 K and the Al free-to-bound (conduction band to acceptor) transition at 120 K.

cubic SiC which they attributed to radiative recombination at close N-Al pairs. We apply the same interpretation to the DAP spectra from our Al-doped film in which electron paramagnetic resonance (EPR) measurements [22,23] under optical illumination have detected the presence of residual nitrogen donors. Quantitative analysis of the energy positions of the sharp line spectra of fig. 2 provides a value of 310 meV for the sum of the nitrogen donor and aluminum acceptor binding energies [10,22]. At high temperatures, the nitrogen donors are thermally ionized and the DAP transitions are quenched. Under these conditions the PL spectrum [22] is dominated by the Al free-to-bound (FB) transition shown in fig. 3, i.e. electrons in the conduction band recombining with holes bound at neutral Al acceptors. The position of the Al FB transition and the temperature corrected value of the band gap then yield a value of 257 meV for the Al acceptor binding energy in CVD cubic SiC, which is in good agreement with that determined by Zanmarci [24] in Lely crystals. This value, in conjunction with the analysis of the close pair spectra, determines the 53 meV nitrogen donor binding energy [10].

Freitas et al. [10] have provided an independent measure of the nitrogen donor binding energy by studying the thermal quenching of one of the sharp close pair PL bands. Because the nitrogen donor binding energy is about one fifth that of the

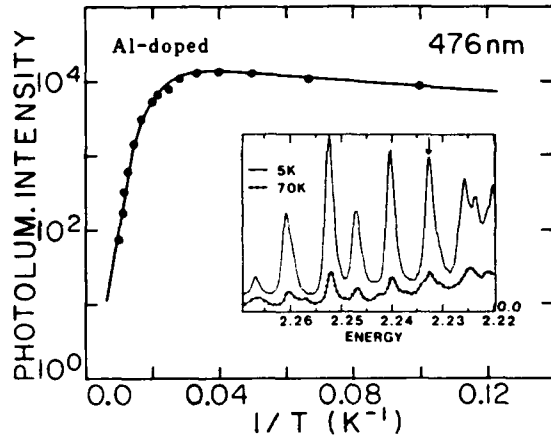


Fig. 4. Photoluminescence intensity as a function of reciprocal temperature for the 2.233 eV N-Al close DAP line in an Al-doped film of cubic SiC. The insert shows an expanded view of this portion of the spectrum for two different temperatures.

aluminum acceptor, the holes will remain bound to the aluminum acceptors over the temperature range of the donor ionization, and the PL quenching curve is characterized primarily by the donor binding energy [20]. The value of the donor binding energy determined from the slope of the exponential PL quenching curve shown in fig. 4 is 54 meV, which is in excellent agreement with the values determined from the spectral positions of the DAP spectra [10,21] and (in Lely material) from the two-electron satellites of the NBE spectrum [13].

Donor-acceptor pair PL spectra have also been observed [25] in boron-doped Lely crystals. A similar spectral analysis of the sharp line close pair spectra in the B-doped material provides values of 735 and 54 meV for the boron acceptors and the donors (presumably nitrogen), respectively. Clearly the same donor appears to be involved in the DAP spectra of both the Al-doped and B-doped SiC. However, the DAP spectra do differ in one fundamentally important aspect. The pattern of the close DAP PL lines in B-doped SiC are type I, meaning that the donors and acceptors are incorporated on the same sublattice [20]. In contrast, the DAP spectra in Al-doped SiC are type II, meaning that the donors and acceptors are on different sublattices [20]. The internally con-

sistent interpretation of all these facts places the N donor in both cases on the C sublattice, the B on the same (C) sublattice, and the Al on the opposite (Si) sublattice [23]. These assigned substitutions are also consistent with what would be expected on the basis of atomic sizes.

In addition to the sharp line close N-Al DAP spectra discussed above, the PL spectra shown in fig. 2 exhibit a broad distant N-Al pair band peaking at about 2.12 eV, its phonon replicas at lower energy, and a broad underlying band extending down to about 1.5 eV which might not be entirely attributable to N-Al pairs. In view of the fact that the low energy shoulders on the NBE PL spectrum have been interpreted in terms of a donor with binding energy larger than the 54 meV nitrogen donor, Freitas et al. [17] have looked for corroborating evidence for the existence of this deeper donor by studying the excitation intensity dependence and PL decay characteristics of the Al-doped films.

Just as the photon energies of the DAP transitions are a function of pair separation, so too are the radiative lifetimes. This is evident in the three DAP spectra shown in fig. 2 for different excitation intensities [17]. Spectrum c of fig. 2 was excited at 10^{-4} the power density used for spectra a and b. In the lower power spectrum (c), the distant pairs with their longer radiative lifetimes are accentuated, the sharp line close pair bands are not observed, and the distant pair band exhibits an expected shift [20] of about 10 meV to lower energy. In addition, the distant pair band is somewhat sharper and more intense in comparison to its phonon replicas, and the broad phonon replica band at lower energy exhibits more structure. However, there is nothing in the low energy portion of the broad underlying PL spectrum which can be attributed unambiguously to the presence of a deeper donor which is coupling to the Al acceptors.

The results of the pulsed excitation studies [17] of the DAP PL spectrum are highlighted in fig. 5. Decay curves for three different DAP PL wavelengths are shown. As expected, a range of decay times is observed because the decay of the close pair PL (2.213 eV) is more rapid than that of the more distant pairs whose PL occurs at lower en-

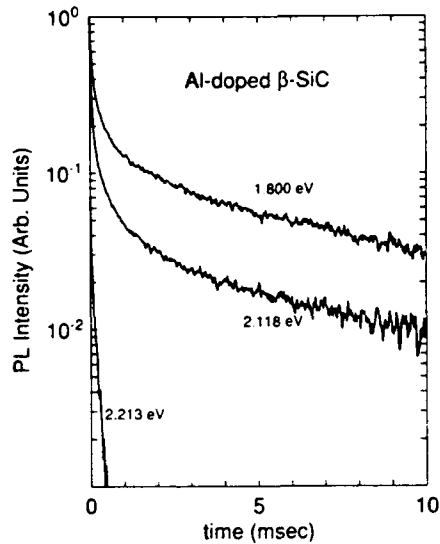


Fig. 5. The 0 to 10 ms PL decay curves for three different PL energies in the DAP PL spectrum shown in fig. 2. A range of decay times is observed because the decay of the close pair PL (2.213 eV) is more rapid than that of more distant pairs whose emission occurs at lower energies (2.118 and 1.800 eV).

ergies (2.118 and 1.800 eV in fig. 5). Decay curves taken at each photon energy cannot be characterized by a single exponential; they exhibit the range of decay times which are typical of DAP recombination radiation. Thus the decay curves can provide no definitive evidence for the existence of a second parallel DAP recombination channel involving a deeper donor, and no evidence for the existence of an underlying PL band which does not have DAP character.

5. Excitation intensity dependence

5.1. Detection of residual impurities

Surprisingly, Freitas et al. [17] found that pulsed PL studies of some of the *undoped*, n-type samples of CVD cubic SiC in the 1.8–2.2 eV range yielded PL decay curves which were virtually identical to those observed in the Al-doped samples. This observation is easily explained on the basis of the comparison of CW PL spectra obtained at high and low excitation intensity in the undoped, n-type sample shown in fig. 6. The high power spectrum

of fig. 6 is typical of nearly all PL spectra reported in the literature [8–10,14,16] for n-type CVD cubic SiC. It is dominated by the NBE spectrum (especially the phonon replicas) with its relatively short donor bound exciton radiative life time. In addition to the NBE spectrum, other characteristic features of the high power PL spectrum include the 1.972 eV ZPL and phonon replicas of the D1 defect band (which has been studied in detail in ion implanted Lely crystals [26] and CVD films [8,9] of cubic SiC), and a broad underlying PL band peaking near 1.8 eV. In contrast, the low power PL spectrum for this same sample exhibits only a weak vestige of the NBE spectrum. The PL spectrum is dominated by a distant DAP band with peak at about 2.113 eV, and the so-called G-band [14,17,27] at about 1.91 eV which will be discussed in the next section.

The most obvious explanation of the 2.113 eV band is that a very low concentration of residual Al acceptors in the nominally undoped sample interacts with the residual 54 meV donors (pre-

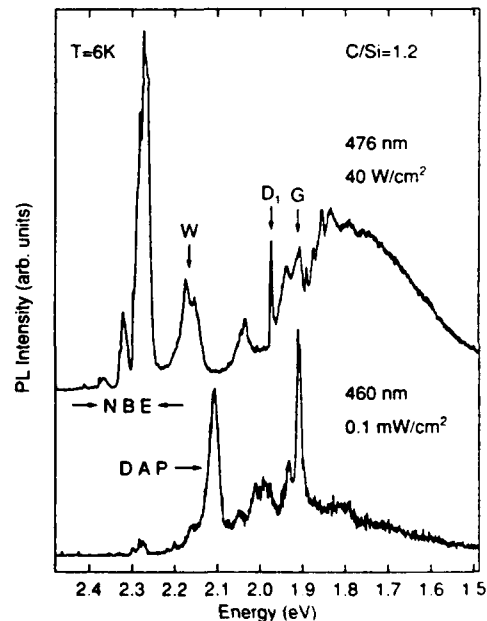


Fig. 6. The CW PL spectra from an undoped, n-type film of cubic SiC (C/Si ratio = 1.2). The top, high power spectrum was excited by an argon laser (476.5 nm, 40 W/cm²); the bottom, low power spectrum was excited by 0.1 mW/cm² of 460 nm light from a xenon lamp.

sumably N) to give rise to a distant DAP band. The low concentration of Al acceptors would dictate a large average pair separation which explains both the shift to lower energy and the fact that the band is easily saturated and therefore not observed at high excitation intensities [20]. The observation of this weak N-Al DAP spectrum in nominally undoped samples appears to be a manifestation of the so-called "memory" of dopants in CVD growth apparatus. Such weak DAP bands are observed only in undoped samples grown in the first few weeks subsequent to the growth of Al-doped films in the same reactor, in spite of efforts to clean the apparatus after the Al-doped growths. The intensity of the background DAP band diminishes with successive undoped growths and eventually disappears entirely. For present purposes, it is important to point out that this discussion of the low power PL spectra illustrates the sensitivity and versatility of the PL technique for the detection of very low concentrations of residual impurities.

5.2. Detection of a new deep acceptor in epitaxial cubic SiC

As pointed out in the previous section, the low power PL spectra of undoped, n-type films of cubic SiC are characterized by the presence of the so-called G-band [14,17,27]. This band may be observed weakly in high power spectra, but the low power spectra can be dominated by the ~ 1.91 eV ZPL of the G-band and its phonon replicas labelled G1 and G2, as shown in fig. 7. Very recently, Freitas and Bishop [27] have reported a detailed study of the power and temperature dependence of the G-band in several CVD samples from three different growth laboratories. On the basis of their experimental results they concluded that the G-band is a distant DAP band which involves the interaction of a deep acceptor (binding energy ~ 470 meV) with a donor or donors having much smaller binding energies.

In agreement with Choyke et al. [14], they found that the spectral position of the G-band varies by several meV from sample to sample as would be expected for a distant pair band when the concentrations of the participating donors and

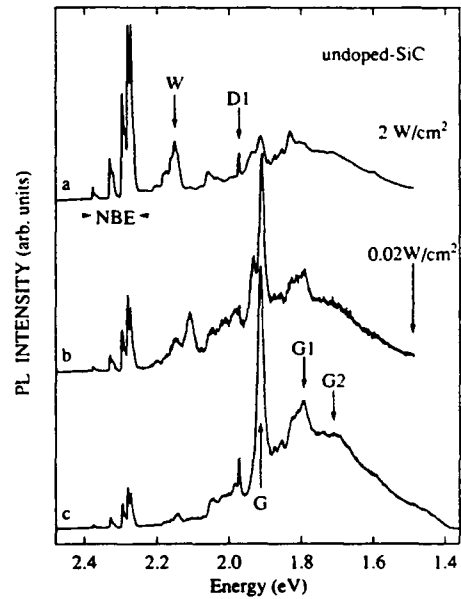


Fig. 7. Power dependence of PL spectra obtained from CVD films of cubic SiC. Spectrum (a) was obtained at high excitation power (2 W/cm^2) from an undoped n-type film grown at NRL. Spectrum (b) is from the same sample with low excitation power (0.02 W/cm^2); it is strikingly similar to the low power (0.02 W/cm^2) spectrum (c) which was observed in an undoped n-type film grown at the NASA Lewis Research Center. The symbols G, G₁, G₂ in spectrum (c) indicate the positions of the G-band ZPL and phonon replicas, respectively.

acceptors vary significantly from sample to sample. Furthermore, the low power spectra of some samples can be resolved into a FB transition at 1.932 eV and a distant pair band about 20 meV to lower energy. Coincidentally, this FB-distant DAP separation is certainly consistent with the participation of a relatively low binding energy donor such as the 54 meV nitrogen donor. In addition, both the power dependence and temperature dependence [27] of the 1.932 eV PL band and the accompanying band about 20 meV to lower energy were consistent with their interpretation as FB and distant DAP bands, respectively.

The ~ 470 meV binding energy of the deep acceptor which gives rise to the G-band is given by the difference between the 2.403 eV low temperature band gap of cubic SiC and the 1.932 eV acceptor FB transition energy. Although the iden-

tivity of this 470 meV acceptor remains uncertain, the observation of a background acceptor which is universally present in CVD films of cubic SiC is consistent with the reported electrical transport properties of these films. Currently accepted interpretations [22,28–31] of temperature dependent Hall effect measurements on CVD films of SiC indicate that the shallow background donors (15–20 meV binding energy) which appear to control the transport properties of all undoped, n-type films are about 95% compensated in all samples studied. This implies the existence of a substantial concentration of unidentified compensating acceptors. The results of Freitas and Bishop [27] appear to represent the first detection of a suitably pervasive deep background acceptor which could play the role of compensating the background donors.

6. Concluding remarks

It is hoped that the results outlined here will demonstrate the power, sensitivity, and versatility of PL techniques for the characterization of semiconductor materials. The use of CVD cubic SiC films as the vehicle demonstrate the application of the techniques has emphasized those aspects of the PL characterization which are appropriate to the investigation of a relatively immature materials system. However, the reader who is interested in greater detail or in the application of PL to the characterization of other semiconductor materials will find ample instruction and guidance in the generic PL references which we have cited.

Acknowledgements

The authors wish to thank E.R. Nordquist, Jr. and M.L. Gipe of the Naval Research Laboratory, H.S. Kong and R.F. Davis of North Carolina State University, and J.A. Powell of the NASA Lewis Research Center for providing the samples which we have studied, and P.B. Klein and W.J. Choyke for valuable discussions. This work was supported in part by the Office of Naval Research.

References

- [1] P.J. Dean and P.C. Herbert, in: *Excitons*, Solid State Sciences, Vol. 14, Ed. K. Cho (Springer, Berlin, 1979) p. 55.
- [2] D.J. Ashen, P.J. Dean, D.T.J. Hurlé, J.B. Mullin and A.M. White, *J. Phys. Chem. Solids* 36 (1975) 1041.
- [3] E.W. Williams and H. Bebb, in: *Semiconductors and Semimetals*, Vol. 8, Eds. R.K. Willardson and A.C. Beer (Academic Press, New York, 1972) p. 321.
- [4] S. Nishino, J.A. Powell and H.A. Will, *Appl. Phys. Letters* 42 (1983) 460.
- [5] A. Addamiano and P.H. Klein, *J. Crystal Growth* 70 (1984) 291.
- [6] K. Sasaki, E. Sukuma, S. Misawa, S. Yoshida and S. Gonda, *Appl. Phys. Letters* 45 (1984) 72.
- [7] H.P. Liaw and R.F. Davis, *J. Electrochem. Soc.* 131 (1984) 3014.
- [8] J.A. Freitas, Jr., S.G. Bishop, A. Addamiano, P.H. Klein, H.J. Kim and R.F. Davis, *Mater. Res. Soc. Symp. Proc.* 46 (1985) 581.
- [9] J.A. Freitas, Jr., S.G. Bishop, J.A. Edmond, J. Ryu and R.F. Davis, *J. Appl. Phys.* 61 (1987) 2011.
- [10] J.A. Freitas, Jr., S.G. Bishop, P.E.R. Nordquist, Jr. and M.L. Gipe, *Appl. Phys. Letters* 52 (1988) 1696.
- [11] W.J. Choyke, D.R. Hamilton and L. Patrick, *Phys. Rev.* 133 A1163 (1964).
- [12] R.L. Hartman and P.J. Dean, *Phys. Rev. B2* (1970) 951.
- [13] P.J. Dean, W.J. Choyke and L. Patrick, *Luminescence* 15 (1977) 299.
- [14] W.J. Choyke, Z.G. Feng and J.A. Powell, *J. Appl. Phys.* 63 (1988) 3163.
- [15] W.J. Choyke and J.A. Powell, private communication.
- [16] H. Okumura, M. Shinohara, E. Muncyama, H. Daimon, M. Yamanaka, E. Sakuma, S. Misawa, K. Endo and S. Yoshida, *Japan. J. Appl. Phys.* 27 (1988) L116.
- [17] J.A. Freitas, Jr., S.G. Bishop, P.B. Klein, P.E.R. Nordquist, Jr. and M.L. Gipe, in: *Amorphous and Crystalline SiC II*, Springer Proceedings in Physics, Vol. 43, Eds. M.M. Rahman, G.Y.-W. Yang and G.L. Harris (Springer, Berlin, 1988) p. 106.
- [18] J.P. Cuthbert and D.G. Thomas, *Phys. Rev.* 154 (1967) 763.
- [19] S.G. Bishop, J.A. Freitas, Jr., P.E.R. Nordquist, Jr. and M.L. Gipe, in: *Amorphous and Crystalline SiC II*, Springer Proceedings in Physics, Vol. 43, Eds. M.M. Rahman, C.Y.-W. Yang and G.L. Harris (Springer, Berlin, 1988) p. 112.
- [20] P.J. Dean, in: *Progress in Solid State Chemistry*, Vol. 8, Eds. J.O. McCaldin and Y.G. Somarjai (Pergamon, Oxford) 1973 p. 1.
- [21] W.J. Choyke and L. Patrick, *Phys. Rev. B2* (1970) 4959.
- [22] W.E. Carlos, W.J. Moore, P.G. Siebenmann, J.A. Freitas, Jr., R. Kaplan, S.G. Bishop, P.E.R. Nordquist, Jr., M. Kong and R.F. Davis, *Mater. Res. Soc. Symp. Proc.* 97 (1987) 253.
- [23] S.G. Bishop, J.A. Freitas, Jr., T.A. Kennedy, W.E. Carlos,

- W.J. Moore, P.E.R. Nordquist, Jr. and M.L. Gipe, in: *Amorphous and Crystalline Silicon Carbide, Springer Proceedings in Physics, Vol. 34*, Eds. G.L. Harris and C.Y.-W. Yang (Springer, Berlin, 1987) p. 90.
- [24] G. Zanmarchi, *J. Phys. Chem. Solids* 29 (1968) 1727.
- [25] H. Kuwabara, S. Yamada and S. Tsunekawa, *J. Luminescence* 12/13 (1976) 531.
- [26] W.J. Choyke and L. Patrick, *Phys. Rev. B* 4 (1971) 6.
- [27] J.A. Freitas, Jr. and S.G. Bishop, *Appl. Phys. Letters* 55 (1989) 2757.
- [28] A. Suzuki, A. Uemoto, M. Shigeta, K. Furukawa and S. Nakajima, *Appl. Phys. Letters* 49 (1986) 450.
- [29] B. Segall, S.A. Alterovitz, E.J. Haugland and L.G. Matus, *Appl. Phys. Letters* 49 (1986) 584.
- [30] B. Segall, S.A. Alterovitz, E.J. Haugland and L.G. Matus, *Appl. Phys. Letters* 50 (1987) 1533.
- [31] M. Shinohara, M. Yamanaka, H. Daimon, E. Sakuma, H. Okumura, S. Misawa, K. Endo and S. Yoshida, *Japan J. Appl. Phys.* 127 (1988) L434.

Spectroscopic Studies of Donors in 3C-SiC Films

J.A. Freitas, Jr.¹, W.E. Carlos², and S.G. Bishop³

¹Sachs-Freeman Associates, Landover, MD 20785, USA

²Naval Research Laboratory, Washington, DC 20375, USA

³Center for Compound Semiconductor Microelectronics and
Department of Electrical and Computer Engineering, University of Illinois,
Urbana, IL 61821, USA

The evidence from photoluminescence spectroscopy for the existence of a 54 meV donor in both undoped n-type and Al-doped cubic SiC is reviewed along with investigations of the three-line electron paramagnetic resonance spectra which reveal the presence of nitrogen donors in the same material. The basis for identifying isolated, substitutional nitrogen as the 54 meV donor in cubic SiC is then discussed.

1. Introduction

The development of chemical vapor deposition techniques [1-4] for the growth of thin films of cubic (3C) SiC has triggered a resurgent interest in the potential application of this semiconductor in a variety of electronic and optoelectronic devices. However, realization of the full device performance potential of CVD cubic SiC will require the identification, control, and/or elimination of the defect levels which dominate the electrical properties of the thin heteroepitaxial films of this material.

In a previous paper [5], we reviewed in detail the optical and magnetic resonance spectroscopy studies of both Lely-grown crystals and CVD films of cubic SiC and their application to the identification of background donors. In this paper, we focus on spectroscopic studies of CVD cubic SiC alone and attempt to resolve some of the controversy surrounding the interpretation of the photoluminescence (PL) [6-12] and electron paramagnetic resonance (EPR) [13-15] spectra. Of particular interest is the apparent contradiction between the 54 meV donor which manifests itself in the PL spectra of both undoped and Al-doped cubic SiC, and the 15-20 meV donor which is detected in temperature dependent Hall effect measurements [16-19] on as-grown n-type films of CVD cubic SiC. We relieve some of the confusion by initially separating the discussion of the determination of donor binding energies from the issue of donor identification. After reviewing the unequivocal optical evidence for the existence of a 54 meV donor in cubic SiC, and the three-line EPR spectra which reveal the presence of neutral nitrogen donors in the same material, we outline the basis for identifying isolated, substitutional nitrogen as the 54 meV donor.

2. Photoluminescence Spectroscopy of CVD Cubic SiC

2.1 Bound Exciton Spectra

Several workers [6-11] have reported the observation at liquid helium temperature of a characteristic five-line near-band edge (~ 2.38 eV) PL spectrum in undoped films of CVD-grown cubic SiC. Examples of such spectra obtained by FREITAS et al. [8] are shown in Fig. 1. They are basically equivalent to the five-line PL spectra first observed by CHOYKE et al. [20] in Lely-grown crystals of cubic SiC. HARTMAN and DEAN [21] studied the Zeeman (magnetic field) and uniaxial stress splitting of this spectrum in Lely crystals and concluded that the luminescence spectrum is attributable to the recombination of excitons bound to neutral donors, and that the donors are isolated point defects, not complexes. In 1977, DEAN et al. [22] studied the two electron satellite transitions associated with the five-line donor-bound exciton spectrum and inferred a highly accurate value of 53.6 ± 0.5 meV for the donor.

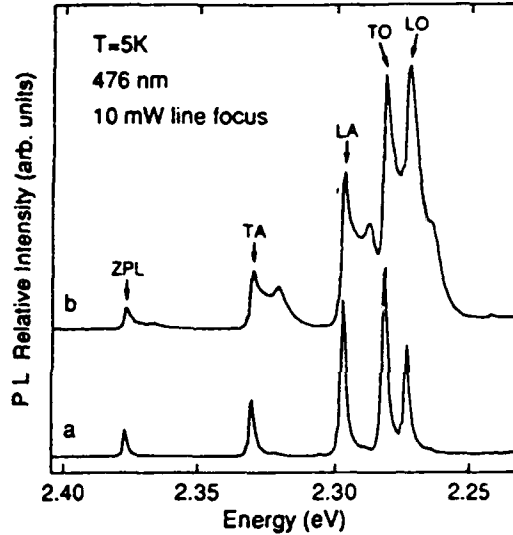


Fig. 1 The 54 meV donor bound exciton PL spectra measured at 5K in two undoped 3C-SiC films grown with two different values of C/Si source gas ratio: a) 2.4; b) 1.2. The zero phonon line (ZPL) and phonon replicas (TA, LA, TO, and LO) are indicated in the spectrum b.

As the quality of CVD films of cubic (3C) SiC has improved, the spectral quality and detail of the five-line bound exciton PL spectra obtained from the films has approached that of the spectra from Lely-grown crystals. Recently, POWELL et al.[11] reported the observation of low temperature bound exciton PL spectra in CVD films of 3C-SiC grown on 6H-SiC crystals which exhibited no strain induced red-shifts or spectral broadening relative to corresponding PL spectra from Lely crystals. The exact equivalence of the five-line bound exciton PL spectra in CVD films and Lely crystals of cubic SiC having been established, it follows that the observation of this characteristic PL spectrum in all of the undoped films which have been studied constitutes strong evidence for the pervasive presence of the ~54 meV donor in these films of cubic SiC.

The bound exciton PL spectra from CVD films of cubic SiC exhibit shoulders on the low-energy side of each of the five lines including the zero phonon line (ZPL) and the four well-resolved phonon replicas (Fig. 1). FREITAS and coworkers [8] have shown that the strength of these shoulders is enhanced with decreasing C/Si source gas ratio, suggesting that the recombination centers responsible for these PL transitions might be associated with nonstoichiometric defects. On the basis of the spectral position of these shoulders, their measured thermal quenching energy [8], and lifetime studies [23], it has been suggested [8,23,24] that the shoulders arise from recombination of excitons bound to donors having a somewhat larger binding energy than the pervasive ~54 meV donor which gives rise to the principal five line bound exciton spectrum. In contrast, there is no evidence in the near-band edge PL spectra for the recombination of excitons bound to a shallower donor.

2.2 Donor-Acceptor Pair Spectra

Evidence for the presence of a 54 meV donor in the CVD films of cubic SiC has also been inferred from donor-acceptor pair (DAP) PL spectra observed in Al-doped films. Figure 2 shows DAP PL spectra obtained by FREITAS et al.[8] from films which were heavily doped with Al by introducing trimethyl aluminum with the source gases during growth. In the DAP recombination process [25], electrons bound at neutral donors recombine radiatively with holes

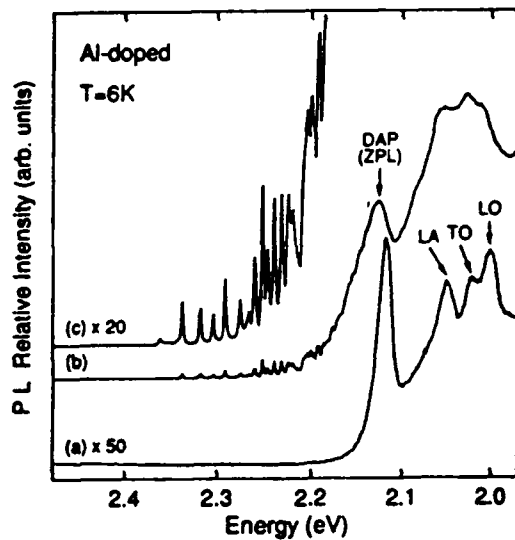


Fig. 2 Low temperature PL spectra of an Al-Doped 3C-SiC film: a) low excitation power ($\sim 10^{-4}$ W/cm²) spectrum showing the DAP and associated phonon replicas; b) high excitation power (1 W/cm²) spectrum with close and distant pair bands; c) detail of sharp-line close pairs spectrum.

bound at neutral acceptors. The emitted photon energy is a function of the spatial separation of the donor and acceptor atoms involved in the recombination. The closest pairs give rise to the discrete, sharp line spectra between 2.38 and 2.2 eV in Fig. 2, while more distant pairs give rise to the broad peak at about 2.12 eV.

These DAP PL spectra provide two independent measurements of the binding energy of the donor participating in the recombination process. First, quantitative analysis of the spectral energies of the sharp-line close pair spectra provides a value of 310 meV for the sum of the aluminum acceptor and unspecified donor binding energies. The binding energy of the deeper Al acceptor can be determined from PL spectra obtained at higher temperatures (>120 K) for which all of the shallow donors are ionized and an Al acceptor free-to-bound PL transition is observed [8,24,27], whose energy is approximately equal to the band gap minus the acceptor binding energy. Having thus measured a 257 meV Al acceptor binding energy, subtraction from 310 meV yields a donor binding energy of 53 meV. These values of the binding energies determined by FREITAS et al. [8] in Al-doped films of CVD SiC are in exact agreement with those measured by CHOYKE et al. [26] from DAP spectra in Al-doped Lely-grown crystals of cubic SiC. In addition, Kuwabara et al. [28] reported DAP PL spectra in boron-doped cubic SiC from which they inferred a value of 735 meV for the boron acceptor binding energy and 54 meV for the binding energy of the background donor which paired with the boron acceptors. Clearly, the same background donor seems to be involved in the DAP spectra of both the Al-doped and B-doped SiC.

A second, independent measure of the donor binding energy in Al-doped films of CVD cubic SiC was obtained by FREITAS et al. [8] who studied the thermal quenching of the sharp close DAP bands. Because the donor binding energy is about one fifth that of the 257 meV Al acceptor, the holes remain bound over the temperature range of donor ionization (≤ 25 K) and the PL quenching curve (Arrhenius plot) is characterized primarily by the donor binding energy [25]. The value of the donor binding energy inferred from the slope of the exponential DAP PL quenching curve was 54 meV [8].

We conclude this brief review of the PL studies of cubic SiC by emphasizing the following points: There is conclusive evidence in the PL spectra for the pervasive existence of a ~54 meV donor in undoped and Al-doped films of cubic SiC films grown by CVD techniques and in Lely-grown crystals of cubic SiC. The sharp, five-line bound exciton PL spectrum which appears in all undoped films and crystals of cubic SiC is an unambiguous, unmistakable signature of this 54 meV donor.

3. Electron Paramagnetic Resonance Spectra

The EPR spectrum exhibited by the unpaired spins of electrons bound to donors can provide an identification of the donor species through the interaction of the paramagnetic electrons with the nuclear magnetic moments of the donor atoms. This central hyperfine interaction splits the EPR spectrum into $2I+1$ lines, where I is the nuclear spin, providing in many cases an identification of the donor. In a previous paper [5], we have reviewed the published results of EPR spectroscopy as applied to both Lely crystals and CVD films of cubic SiC. From the perspective of the present discussion, the most important result of these studies is that a three-line EPR spectrum has been observed which is attributed to the hyperfine interaction of the paramagnetic electron with the magnetic moment of the ^{14}N nucleus (nuclear spin $I = 1$). This three-line EPR spectrum has been established as an unambiguous signature for the presence of neutral nitrogen donors and, under the proper experimental conditions, its intensity can provide a measure of the concentration of neutral nitrogen donors.

Examples of low-temperature EPR spectra obtained by CARLOS and coworkers [13] from undoped CVD films of cubic SiC are shown in Fig. 3. The small, isotropic hyperfine interaction which they observed ($A = 1.2\text{G}$) is consistent with expectations for a hydrogenic donor and is in excellent agreement with that reported by ALTAISKII et al. [29] for Lely grown cubic SiC and also by other workers [14-15] in CVD films. CARLOS et al. found that the ability to obtain well-resolved three-line spectra is apparently strongly dependent upon donor concentration in undoped films. At higher concentrations ($\gg 10^{17}\text{ cm}^{-3}$) broadening due to exchange interactions could obscure the relatively small hyperfine splitting [13]. However, studies of films prepared with a variety of growth parameters (e.g. C/Si source gas ratio) have shown that it is also possible that the loss of the hyperfine structure in the EPR spectra of higher concentration samples is caused by the superposition of a broad, structureless spectrum which arises from a second, distinct neutral donor [15,23,24].

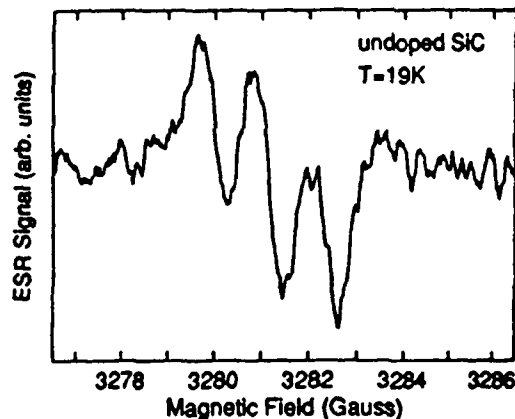


Fig. 3 EPR spectrum of the undoped 3C-SiC CVD film grown with C/Si source gas ratio of 2.4 (PL spectrum shown in Fig. 1a). The microwave power level was ~ 2 microwatts.

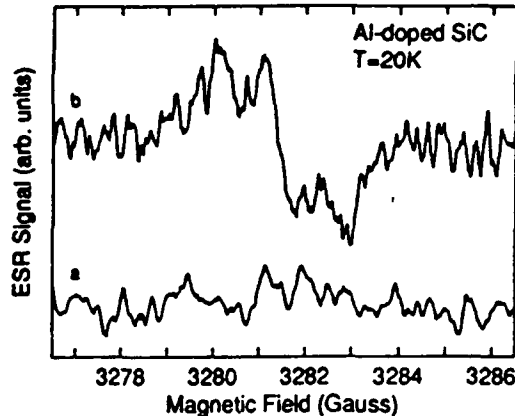


Fig. 4 Low temperature EPR spectra obtained at 9GHz from the Al-doped film (PL spectrum shown in Fig. 2) under two different conditions: a) unilluminated (dark); b) illuminated with 457.9 μm argon laser line with power density of $\sim 10^{-4}$ W/cm²

The photoinduced EPR spectrum (b) of Fig. 4 indicates that nitrogen donors can also be observed in Al-doped CVD films (FREITAS AND CARLOS, to be published [30]). In the dark (unilluminated) EPR spectrum (a) of Fig. 4, no EPR signal is observed in the spectral range of the donor lines, as might be expected for an Al-doped sample in which most if not all of the donors are compensated by the Al acceptors. Compensated (charged) donors have no bound electrons with unpaired spins and are not paramagnetic centers. However, when an Al-doped, compensated sample is illuminated with above-gap light, a quasi-equilibrium population of photoinduced neutral donors is generated and the three-line neutral nitrogen donor EPR spectrum appears as shown in the illuminated or photoinduced EPR spectrum of Fig. 4.

4. Discussion

Just as the PL results established the existence of a pervasive background donor with a 54 meV binding energy in CVD films of cubic SiC, the EPR spectra demonstrate that nitrogen is a pervasive background donor in these SiC films. In what follows we present the evidence and reasoning which support an association of the ubiquitous 54 meV donor in cubic SiC with isolated nitrogen donors.

The observation of sharp-line donor bound exciton and sharp close DAP PL spectra indicates that the donors participating in these radiative recombination processes are located on lattice sites of high crystalline quality. Optical (PL) spectra associated with donors which are located in highly strained material or in proximity with high concentrations of structural defects would be severely broadened and perhaps be unobservable. The same can be said for donors which give rise to EPR spectra with well resolved hyperfine splitting, such as the three-line ¹⁴N EPR spectrum observed in the CVD films of cubic SiC. In addition, studies of the magnetic field orientation dependence of both the five-line donor bound exciton PL spectrum [21] and the three-line ¹⁴N EPR spectrum [29] gave no evidence of anisotropy. This means that both the 54 meV donor giving rise to the donor bound exciton PL spectrum and the neutral ¹⁴N donor responsible for the three-line EPR spectrum are isolated, point defects.

Measurement of the binding energy of the nitrogen donor which exhibits the three-line EPR spectrum presents an obvious means of resolving the question of the possible connection between the 54 meV donor and the nitrogen donor. CARLOS et al.[13] attempted to accomplish this by measuring the thermal quenching of the ¹⁴N EPR spectrum in an undoped

n-type film of cubic SiC. However, an exact measure of the thermal quenching (ionization) energy of the neutral nitrogen donors was thwarted in these experiments by broadening of the three-line EPR spectrum and interference of an underlying broad resonance spectrum with increasing temperature. Recently, Nashiyama and coworkers [31] have successfully completed such a temperature dependence study in which they observed a close correspondence between the slope of the thermal quenching curve for the ^{14}N EPR spectrum and that of the close DAP PL spectrum reported previously by FREITAS et al.[8]. These results [31] indicate that the neutral nitrogen donors giving rise to the three-line ^{14}N EPR spectrum also have a binding energy of ~ 54 meV, and they constitute the most direct evidence yet obtained that the nitrogen donor detected in EPR spectra of cubic SiC and the pervasive 54 meV donor which characterizes the optical (PL) spectra are the same donor.

Some valuable insight concerning the probable location of the 54 meV donor and the A1 and B acceptors in the SiC lattice is provided by the DAP PL spectra [5]. (We simplify the discussion by referring to the donor as nitrogen.) The N-A1 close DAP spectrum is a type II spectrum [25] which means that the participating donors are located on one sublattice and the A1 acceptors on the other sublattice. For example, on the basis of atomic radii, it is suggested that the nitrogen donors substitute for carbon atoms and the aluminum acceptors for silicon atoms. On the other hand, the N-B DAP close pair spectrum is type I [25], meaning that donors and acceptors are located on the same sublattice. An internally consistent description, that is, one which is consistent with the requirements of the type I and II PL spectra and the sizes of the atoms involved, places both the nitrogen donors and the boron acceptors on the carbon sites.

Implicit in the above discussion is the fact that spectroscopic techniques such as PL and EPR automatically single out the high quality regions of the crystalline sample, and the spectral widths, lattice site configurations and symmetries, binding energies, etc. inferred from these spectra are characteristic of these high quality regions only. Conversely, transport measurements such as the Hall effect perform an average over the entire crystal (film) volume. The conductivities of high quality and highly defective regions of the sample are measured in parallel. Obviously, this can lead to some unavoidable ambiguities in any attempt to extract parameters such as donor binding energies and concentrations, compensation ratios, and thermally activated carrier concentrations.

We now discuss the possible relationship or contradiction between the 54 meV donor (apparently nitrogen) and the 15-20 meV donors which dominate the electrical properties [13,16-19] of the n-type CVD films of cubic SiC. It has been observed [25] that optical transitions which depend only upon the ground state energies can remain sharp and unshifted at relatively high impurity concentrations for which thermal activation energies or binding energies for carriers bound to the impurities can be depressed as much as 10-40% because of apparent overlap in the impurity excited states. In addition, SEGALL et al.[17,18] have invoked a concentration dependent reduction in the thermal activation energy to explain the apparent variation in donor binding energies inferred from temperature dependent Hall effect measurements on n-type CVD films of cubic SiC. However, thermal quenching studies of both the DAP PL spectra [8] and the EPR spectra [31] have measured 54 meV binding energies equivalent to those determined from the optical spectral energies. Furthermore, MOORE [32] has shown that if the published temperature dependent Hall effect data for CVD SiC films (from which donor ionization energies ranging from 15-40 meV have been inferred) are analyzed correctly, one consistently obtains activation energies in the range 15-20 meV, whose variation is easily accounted for by uncertainties in the fitting or analysis procedure. This means that there is not a continuous range of donor binding energies varying from the 54 meV measured optically to the lowest (~ 15 meV) value measured by Hall effect. Instead, the optical measurements detect one donor with a relatively precise value of 53-54 meV for its binding energy, and the Hall effect measurements yield a second shallower donor, with considerable uncertainty in its 15-20 meV binding energy.

Thus it appears that isolated nitrogen donors, which are located on undistorted lattice sites and have a 54 meV binding energy, cannot be responsible for the 15-20 meV donor binding energy inferred from temperature dependent Hall effect measurements. However, this does not mean that nitrogen impurities cannot be associated in some other configuration with this shallow donor. For example, the nitrogen impurities could substitute on either the carbon sublattice or the silicon sublattice in SiC, with different binding energies in the two cases, and

the 54 meV binding energy can represent only one of these two cases. In addition, nitrogen impurities as well as other electrically active lattice defects could be located or concentrated in inhomogeneous regions of the crystal. Under these circumstances the nitrogens could occupy highly distorted lattice sites or interstices, or be complexed with other defects and therefore have binding energies quite different from the 54 meV of the isolated, substitutional nitrogen donor.

Acknowledgments

The authors wish to thank P.E.R. Nordquist, Jr. and M.L. Gipe for providing some of the SiC samples, and P.B. Klein and W.J. Moore for many helpful discussions. This work has been partially supported by the Office of Naval Research.

References.

1. S. Nishino, J.A. Powell, and H. A. Will, *Appl. Phys. Lett.* **42** 460 (1983).
2. A. Addamiano and P.H. Klein, *J. Cryst. Growth* **70**, 291 (1984).
3. K. Sasaki, E. Sukuma, S. Misawa, S. Yoshida, and S. Gonda, *Appl. Phys. Lett.* **45**, 72 (1984).
4. H.P. Liaw and R.F. Davis, *J. Electrochem. Soc.* **131**, 3014 (1984).
5. S.G. Bishop, J.A. Freitas, Jr., T.A. Kennedy, W.E. Carlos, W.J. Moore, P.E.R. Nordquist, Jr., and M.L. Gipe, in: *Amorphous and Crystalline Silicon Carbide*, Springer Proc. in Physics, Vol. 34, ed. G.L. Harris and C.Y.-W. Yang (Springer-Verlag, Berlin, Heidelberg, 1987), p. 90.
6. J.A. Freitas, Jr., S.G. Bishop, A. Addamiano, P.H. Klein, H.J. Kim, and R.F. Davis, *Mats. Res. Soc. Symp. Proc.*, **46**, 581, (1985).
7. J.A. Freitas, Jr., S.G. Bishop, J.A. Edmond, J. Ryu, and R.F. Davis, *J. Appl. Phys.* **61**, 2011 (1987).
8. J.A. Freitas, Jr., S.G. Bishop, P.E. R. Nordquist, Jr., and M.L. Gipe: *Appl. Phys. Lett.* **52**, 1696 (1988).
9. W.J. Choyke, Z.C. Feng, and J.A. Powell, *J. Appl. Phys.* **64**, 3163 (1988).
10. J.A. Freitas, Jr. and S.G. Bishop, *Appl. Phys. Lett.* **55**, 2757 (1989).
11. J.A. Powell, D.J. Larkin, L.G. Matus, W.J. Choyke, J.L. Bradshaw, L. Henderson, M. Yoganathan, J. Yang, and P. Pirouz, *Appl. Phys. Lett.* **56**, 1442 (1990).
12. H. Okumura, M. Shinohara, E. Muneyama, H. Daimon, M. Yamanaka, E. Sakuma, S. Misawa, K. Endo, and S. Yoshida, *Japan. J. Appl. Phys.* **27**, L116 (1988).
13. W.E. Carlos, W.J. Moore, P.G. Siebenmann, J.A. Freitas, Jr., R. Kaplan, S.G. Bishop, P.E.R. Nordquist, Jr., M. Kong, and R.F. Davis, in *Proc. Mats. Res. Soc. Symp.* **27**, 253 (1987).
14. I. Nashiyama, H. Okumura, E. Sakuma, S. Misawa, K. Endo, S. Yoshida, H. Itoh, and N. Hayakawa, in: *Amorphous and Crystalline SiC II*, Springer Proc. in Physics, Vol. 43, eds. M.M. Rahman, C.Y.-W. Yang, and G.L. Harris (Springer-Verlag, Berlin, Heidelberg, 1988), p. 100.
15. I. Nashiyama, H. Okumura, E. Sakuma, K. Endo, and S. Yoshida, proceedings of this conference.
16. A. Suzuki, A. Uemoto, M. Shigeta, K. Furukawa, and S. Nakajima, *Appl. Phys. Lett.* **49**, 450 (1986).
17. B. Segall, S.A. Alterovitz, E.J. Haugland, and L.G. Matus, *Appl. Phys. Lett.* **49**, 584 (1986).
18. B. Segall, S.A. Alterovitz, E.J. Haugland, and L.G. Matus, *Appl. Phys. Lett.* **50**, 1533 (1987).
19. M. Shinohara, M. Yamanaka, H. Daimon, E. Sakuma, H. Okumura, S. Misawa, K. Endo, and S. Yoshida, *Japan J. of Appl. Phys.* **127**, L434 (1988).
20. W.J. Choyke, D.R. Hamilton, and L. Patrick, *Phys. Rev.* **133**A1163 (1964).
21. R.L. Hartman and P.J. Dean: *Phys. Rev.* **B2**, 951 (1970).
22. P.J. Dean, W.J. Choyke, and L. Patrick, *J. Lum.* **15**, 299 (1977).

23. J.A. Freitas, Jr., S.G. Bishop, P.B. Klein, P.E. R. Nordquist, Jr., and M.L. Gipe, in: *Amorphous and Crystalline SiC II*, Springer Proc. in Physics, Vol. 43, eds. M.M. Rahman, C.Y.-W. Yang, and G.L.Harris (Springer-Verlag, Berlin, Heidelberg, 1988), p. 106.
24. S.G. Bishop and J.A. Freitas, Jr., to be published in *J. Crystal Growth* (1990).
25. P.J. Dean, in: *Progress in Solid State Chemistry*, 8, eds. J.O. McCaldin and Y.G. Somarjai (Pergamon, Oxford) 1973, p. 1.
26. W.J. Choyke and L. Patrick, *Phys. Rev.* **B2**, 4959 (1970).
27. G. Zanmarchi, *J. Phys. Chem. Solids*, **29** (1968) 1727.
28. H. Kuwabara, S. Yamada, and S. Tsunckawa, *J. Lumin.* **12/13**, 531 (1976).
29. Yu.M. Altaiskii, I.M. Zaritskii, V.Ya. Zevin, and A.A. Konchits, *Sov. Phys.-Solid State* **12**, 2453 (1971).
30. J.A. Freitas, Jr. and W.E. Carlos, to be published.
31. I. Nashiyama and coworkers, private communication.
32. W.J. Moore, proceedings of this conference.

Optically detected magnetic resonance of cubic SiC grown by chemical vapor deposition on Si

T. A. Kennedy

Naval Research Laboratory, Washington, DC 20375

J. A. Freitas, Jr.

Sach/Freeman Associates, Landover, Maryland 20785

S. G. Bishop^{a)}

Naval Research Laboratory, Washington, DC 20375

(Received 7 May 1990; accepted for publication 27 August 1990)

Two distinct spectra are reported from an optically detected magnetic resonance study of epitaxial films of cubic SiC. The first is a Lorentzian, single line with $g = 2.0065 \pm 0.0015$, which is strong in Al-doped SiC. This line is attributed to residual donors. The second spectrum, observed in both Al-doped and undoped samples, is dominated by a pair of exchange-split lines with $g = 2.0024$ and $a = 0.095 \text{ cm}^{-1}$. Although a definite assignment of this spectrum cannot be made, spectral dependence studies show it is associated with a defect-related luminescence band in the energy range from 1.6 to 1.9 eV.

I. INTRODUCTION

Following the original growth of the cubic polytype of SiC by the Lely method about 20 years ago, thin films of this structure were grown by chemical vapor deposition on Si substrates starting around 1983.¹ A variety of methods have revealed the basic characteristics of these layers.² For example, transport measurements show that undoped films are invariably n type and heavily compensated. There are also photoluminescence bands present in as-grown SiC/Si samples or thermally annealed, free-standing SiC layers that are attributed to defects.³ Since optically detected magnetic resonance (ODMR) is a powerful tool for identifying defects and relating them to their luminescence, we were motivated to apply ODMR to SiC thin films.

Optically detected magnetic resonance is a combination of electron paramagnetic resonance (EPR) and photoluminescence (PL). Previous work using each of these techniques has been performed on cubic SiC. Photoluminescence of undoped layers contains lines attributed to N-bound excitons and two defect bands labeled D_1 and D_2 .³ Evidence from the conditions for observing D_1 and its phonon couplings suggest that an intrinsic point defect or defect pair is responsible for this band.^{4,5} A third defect band called G can be discerned in some samples.⁶ The G band is associated with dislocations or other extended defects.⁷ In Al-doped samples, there is a strong band attributed to N-Al donor-acceptor pairs.³ The electron paramagnetic resonance of undoped CVD films has a line due to donors.⁸ In samples with a low concentration of uncompensated donors, a hyperfine structure is observed which arises from the ^{14}N nucleus and thus identifies the donors as nitrogen. ODMR of donors has been reported in thermally quenched crystals of 3C-SiC.⁹

The ODMR of a wide variety of doped and undoped CVD layers has been studied and two distinct spectra were observed. The first is attributed to donor magnetic resonance

observed on the N-Al donor-acceptor pair (DAP) band. The second is a more complex spectrum which can be attributed either to a specific donor-acceptor pair with a fixed separation or to an exciton. The second spectrum is detected from 1.6 to 1.9 eV. This range includes both the D_1 and the G defect-related photoluminescence bands.

II. BACKGROUND

A wide variety of samples has been studied. All were grown on (100) Si by a CVD process¹⁰ and had thicknesses from 9 to 15 μm . Aluminum doping was obtained by introducing trimethylaluminum with the source gases. Some of the undoped samples were part of a study of the effect of varying the source-gas ratio C/Si.¹¹ All of the undoped samples were strongly n type and 90% compensated. Most of the PL and ODMR measurements were done on samples that were removed from their Si substrates and glued at the corners onto Si wafer chips for ease of handling. With this mounting, the strain due to mismatch is eliminated since the layer is no longer epitaxial to a Si substrate.

Photoluminescence spectra taken at 6 K for the two samples which gave the best ODMR data are shown in Fig. 1. The Al-doped sample is dominated by the DAP spectrum of the N-Al pairs with a zero-phonon line (ZPL) for distant pairs at 2.118 eV. There is some intensity at the positions of the D_1 band with ZPL at 1.97 eV and the G band with ZPL at 1.92 eV. The undoped sample has strong emission from N-bound excitons at 2.28 eV as well as the D_1 and G bands. Detailed photoluminescence studies of these bands have been presented.¹¹

The ODMR spectrometer is centered around an optical cryostat in a 9-in. electromagnet. The sample temperature is 1.6 K and fields up to 1.1 T are available. 50 mW of microwave power at 24 GHz are switched on and off by a p - i - n modulator and sent to a TE_{011} cavity with optical access. The luminescence was excited by the 476-nm line of a Kr laser at power density around 1 W/cm². The luminescence was collected, filtered, and detected with a Si photodiode. A

^{a)} Present address: Center for Compound Semiconductor Microelectronics, University of Illinois at Urbana-Champaign, Urbana IL 61801.

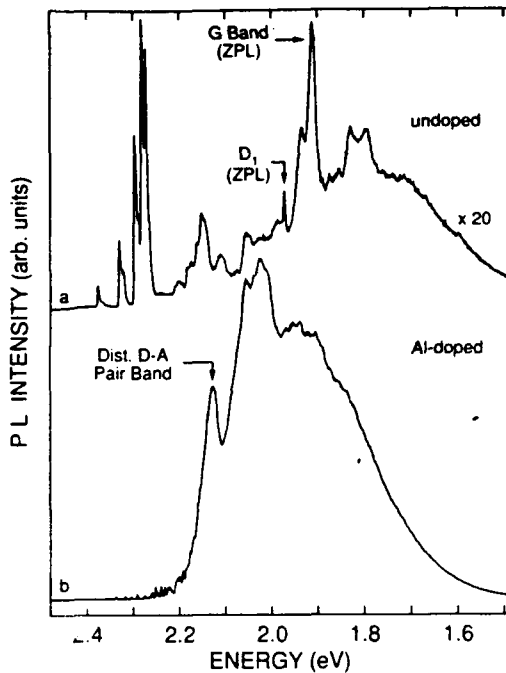


FIG. 1. Photoluminescence spectra at 6 K for an undoped sample and an Al-doped sample. The spectral range is the same for the D_1 and G bands and the excitonic ODMR which was observed in both samples. The donor-acceptor pair band for the Al-doped sample has the same range as the donor ODMR.

lock-in amplifier produces the ODMR signal which is the change in photoluminescent intensity which is coherent with the microwave switching. Signal averaging was used to enhance the signal-to-noise ratio.

Optically detected magnetic resonance arises from the spin dependence of the donor-acceptor pair recombination process. Detailed theoretical descriptions of ODMR have been presented.^{12,13} A simplified version adequate to the SiC results is presented here.

A donor-acceptor pair with a fixed separation undergoes recombination from the excited state with an electron on the donor and a hole on the acceptor to a ground state with the donor and acceptor unoccupied. If the donor and acceptor can be described using the hydrogenic, effective-mass theory, the magnetic properties of the initial state can be described by the following Hamiltonian:

$$\mathcal{H} = \mathcal{H}^D + \mathcal{H}^A + aS \cdot J, \quad (1)$$

where \mathcal{H}^D is the Zeeman interaction of the $S = 1/2$ donor, \mathcal{H}^A is the Zeeman interaction of the $J = 3/2$ acceptor, and the third term describes a weak exchange coupling between the donor and acceptor. The weak exchange interaction signifies that the pair chosen has a large donor-acceptor separation. Since most of the results obtained in this work concern the donors, the $J = 3/2$ acceptor is simplified to an effective spin-1/2 acceptor, such as might be found for a deep acceptor. With this assumption, the energy levels in a magnetic field B are

$$E(M_s, M_s') = E(\pm 1/2, \pm 1/2) = \pm g_D \beta B / 2 \pm g_A \beta B / 2 \pm a/4, \quad (2)$$

where g_D is the splitting factor for the donor and g_A is the factor for the acceptor. Magnetic resonance for the donor occurs at two transition energies

$$h\nu = g_D \beta B \pm a/2. \quad (3)$$

These states and microwave transitions are shown in Fig. 2. Selection rules for radiative recombination favor the $(-1/2, +1/2)$ and $(+1/2, -1/2)$ states since the ground state has $S = 0$. Thus magnetic resonance can alter the spin-state populations and affect the radiative recombination, producing ODMR.

Two distinct cases can be distinguished based on the rate of spin relaxation compared to the rate of recombination. If the recombination rate is faster, the two radiative states will empty. Magnetic resonance will cause a net transfer from the slowly recombining states to the faster states and an increase in photoluminescence. This is called the nonthermalized case. If the spin-lattice relaxation is faster, the spin levels will acquire a thermal distribution—the lowest state is most populated and the highest state is least populated. Spin resonance of the lower states will cause a net transfer to a more radiative state and thus an increase in photoluminescence. However, spin resonance of the upper states will cause a net transfer out of the radiative state and thus a decrease in photoluminescence. This is termed the thermalized case.

This theory describes the ODMR of a single pair. The most important modification for some of the SiC results concerns the changes when there is a distribution of pairs with different donor-acceptor separations. This will be discussed with the results.

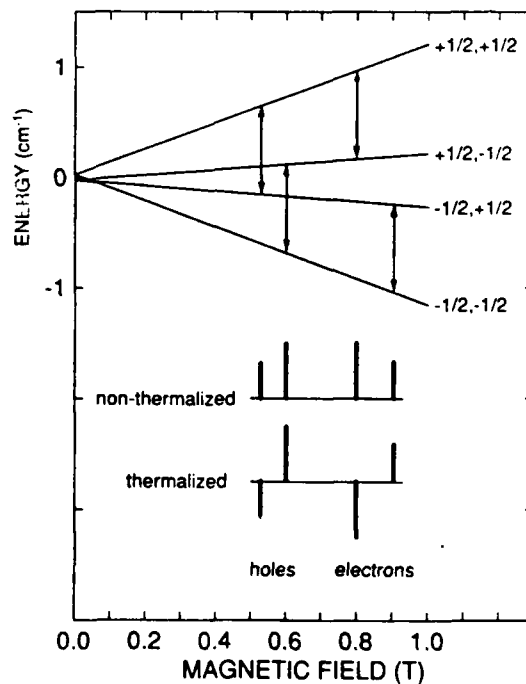


FIG. 2. Zeeman energy levels and ODMR intensity changes for a weakly exchange-coupled electron and hole. The electron is taken to be at a neutral donor and the hole at a neutral acceptor which is a fixed distance from the donor. The arrows denote microwave transitions and the thick lines resonant changes in photoluminescence intensity.

III. DONOR RESONANCE IN Al-DOPED SiC

All Al-doped samples exhibit a strong, positive ODMR signal near the free-electron g value. See Fig. 3. For these data, the luminescence was excited by the 476-nm line from a Kr^+ laser at a power density of about 1 W/cm^2 . The g value is 2.0065 ± 0.0015 .

The shape and width of this ODMR are influenced by the conditions of the experiment. In Fig. 3, the exciting power density is fixed but the microwave chopping rate is varied. The changes in shape denote the existence of a distribution of donor-acceptor pair separations. Closer pairs have both a faster recombination rate and a stronger exchange splitting, as given by Eq. (3). In the present case, the spectra of particular pairs are not resolved. However, the higher modulation frequency data is dominated by closer pairs, while the slow-frequency data includes the distant pairs with very small exchange splittings. Hence, the slow data appears sharp and has greater amplitude than the fast data.

For even the distant pairs, the linewidth is about 1 mT. This is much larger than the 0.12-mT hyperfine splitting observed for N donors using EPR.^{8,14} Thus the hyperfine splitting cannot be detected in this sample because of the exchange broadening of the distant pairs. This condition depends on the concentration of donors and the concentration of acceptors in the sample—it is possible that the hyperfine could be observed in a sample with a very low donor concentration. Recall that most of the CVD-grown films have a high donor concentration and high compensation.

The spectral dependence of this ODMR line has been studied by placing different long-pass filters in front of the detector and measuring the strength of the ODMR. The strength is defined as the ODMR signal amplitude divided

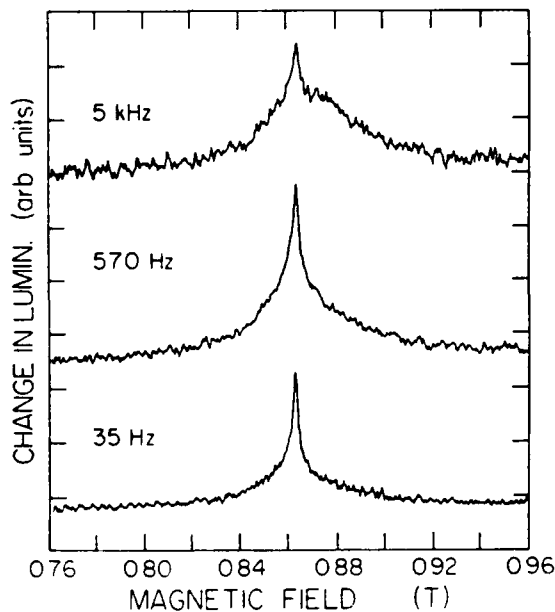


FIG. 3. ODMR of the Al-doped sample for three microwave modulation frequencies. The changing line shape indicates a distribution of recombination times and, hence, donor-acceptor separations.

by the photoluminescence intensity. The single line is observed in the energy range from 1.9 to 2.2 eV, which corresponds to the range of the N-Al DAP luminescence (see Fig. 1).

Comparison on the g value of 2.0065 ± 0.0015 with published results confirms the assignment of this line to donors. Previous EPR studies have found 2.0068 ± 0.005 (Ref. 14) and 2.0055 (Ref. 8) for donors in cubic SiC. Acceptors are not generally observed in cubic materials because the splitting of the degenerate valence band by random strains broadens the acceptor resonance beyond detection. Acceptor ODMR has been observed in (hexagonal) 6H-SiC where the crystal field removes the degeneracy of the valence band.^{15,16}

Can the chemical identify of the donor be deduced from the donor g value? No references were found for the magnetic resonance of donors other than N in any polytype of SiC. In Si, different shallow donors exhibit g values which vary by 1×10^{-4} .¹⁷ Therefore, it seems unlikely that the donor can be assigned to a particular element from its g value.

In summary, this ODMR provides a link between the strong DAP luminescence in Al-doped samples and a donor magnetic resonance at 2.0065. The identification of the donor through hyperfine interaction remains an exciting prospect. This could be realized with samples with lower concentrations of donors and acceptors or possibly by reducing the electron concentration of existing samples using electron irradiation.

IV. EXCITONIC RESONANCE

A distinct, new ODMR spectrum has been observed in an Al-doped sample but also in undoped samples. See Fig. 4. This spectrum is only observed for very slow microwave modulation rates and with moderate excitation intensities.

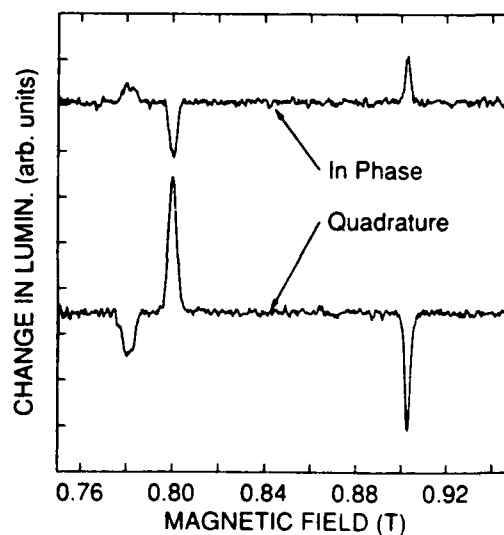


FIG. 4. ODMR of the undoped sample at a very low modulation frequency (10 Hz). Since the spectrum is strongly in quadrature at this frequency, the actual response is below 10 Hz. The negative-positive pair of lines is attributed to an exchange-split electron resonance. The lines near 0.780 T have not been firmly identified.

At 10 Hz, the spectrum in-phase with the modulation is still weaker than the spectrum in quadrature. There is a pair of lines centered near the donor g value with the lower field line negative and the higher positive for the in-phase spectrum. From the discussion in Sec. II, this is the signature of an electron resonance which is exchange-split by a hole at a particular separation (see Fig. 2). The g value for the pair is 2.0024 and the exchange splitting a is 102 mT. The negative-positive character indicates that the spin levels are thermalized and hence the spin-lattice relaxation is fast compared to 10 Hz, the microwave modulation frequency, for this defect.

A weaker, broader positive line is observed at 0.781 T. This line may actually be a slightly split pair of lines and it is always observed when the exchange-split electron lines are observed. From the model for an exchange-split electron and hole, it is natural to assign this line to the upper line of the exchange-split hole resonances. Wider scans than those of Fig. 4 do not reveal the line at lower field. Furthermore, the entire spectrum is isotropic, while hole lines frequently exhibit considerable anisotropy.^{15,16} Hence, there are a number of problems in assigning this line.

The spectral dependence of this new ODMR spectrum was also studied using long-pass filters. The ODMR arises from luminescence in the range from 1.6 to 1.9 eV, corresponding to the D_1 band, the G band, and possibly other emission (see Fig. 1).

The spectrum is not detected for very low excitation powers. The optimal excitation power density is about 1 W/cm² with the resonance lines broadening for higher powers.

The interesting feature of this spectrum is the unique separation between the electron and hole. It is difficult to think of how a donor-acceptor pair would occur with only a single separation and hence we consider excitons. A similar ODMR has been observed for the "type-II" excitons in AlAs/GaAs superlattices in which the electron is confined in the AlAs layer and the hole in the GaAs layer.¹⁸ The electron resonances are exchange-split with a strength which depends on the width of the layers. In the present case, there are two possibilities for such structure. First, the excitons could be associated with dislocations which have a unique structure separating electron and hole. The G band has been associated with extended defects or dislocations⁷ while the D_1 luminescence band has been associated with a defect or defect complex.^{5,19} Second, the epilayers are known to contain antiphase boundaries which might separate the electron and hole. Additional information or experiment is required before a definite assignment of this spectrum can be made.

Recently it has proved difficult to detect this spectrum in samples which previously exhibited strong signals. It is possible that the defect complexes or antiphase boundaries become decorated with defects after long period of time and the ODMR is lost. Alternatively, there may be something subtle in the ODMR conditions which has not been reproduced in the recent attempts. The detection of ODMR from thermalized spins is only possible over a very narrow range of parameters.

V. CONCLUSION

ODMR studies of CVD-grown cubic SiC films reveal two distinct spectra. The first is a single line observed in Al-doped samples. From its g value, line shape, and spectral dependence, it can be assigned to neutral donors. It is clearly associated with a luminescence band attributed to N-AI pairs. The second spectrum is more complex. It is dominated by two lines due to electron resonance split by a unique exchange interaction. This suggests that the defect responsible has a specific structure, such as a defect complex or antiphase boundary. From the spectral dependence of this line, the ODMR may arise from the D_1 or the G luminescence band.

ACKNOWLEDGMENTS

We thank P. E. R. Nordquist, Jr. and M. L. Gipe of the Naval Research Laboratory who grew the samples used in this work. We also acknowledge partial support by the Office of Naval Research.

- ¹S. Nishino, J. A. Powell, and H. A. Will, *Appl. Phys. Lett.* **42**, 460 (1983).
- ²S. G. Bishop, J. A. Freitas, Jr., T. A. Kennedy, W. E. Carlos, W. J. Moore, P. E. R. Nordquist, Jr., and M. L. Gipe, in *Amorphous and Crystalline Silicon Carbide*, edited by G. L. Harris and C. Y.-W. Yang (Springer, Berlin, 1989), p. 90.
- ³See, for example, J. A. Freitas, Jr., S. G. Bishop, A. Addamiano, P. H. Klein, H. J. Kim, and R. Davis, in *Microscopic Identification of Electronic Defects in Semiconductors*, edited by N. M. Johnson, S. G. Bishop, and G. D. Watkins (Materials Research Society, Pittsburgh, 1985), p. 581.
- ⁴W. J. Choyke and L. Patrick, *Phys. Rev. B* **4**, 1843 (1971).
- ⁵W. J. Choyke, in *Radiation Effects in Semiconductors, 1976*, edited by N. B. Uriil and J. W. Corbett, *Inst. Phys. Conf. Ser. No. 31* (Institute of Physics, London, 1977), p. 58.
- ⁶J. A. Freitas, Jr. and S. G. Bishop, *Appl. Phys. Lett.* **55**, 2757 (1989).
- ⁷W. J. Choyke, Z. C. Feng, and J. A. Powell, *J. Appl. Phys.* **64**, 3163 (1988).
- ⁸W. E. Carlos, W. J. Moore, P. G. Siebenmann, J. A. Freitas, Jr., R. Kaplan, S. G. Bishop, P. E. R. Nordquist, Jr., M. Kong, and R. F. Davis, in *Novel Refractory Semiconductors*, edited by D. Emin, T. L. Aselage, and C. Wood (Materials Research Society, Pittsburgh, 1987), p. 253.
- ⁹N. G. Romanov, V. A. Vetrov, and P. G. Baranov, *Sov. Phys. Semicond.* **20**, 96 (1986).
- ¹⁰A. Addamiano and P. H. Klein, *J. Cryst. Growth* **70**, 291 (1984).
- ¹¹J. A. Freitas, Jr., S. G. Bishop, P. E. R. Nordquist, Jr., and M. L. Gipe, *Appl. Phys. Lett.* **52**, 1695 (1988).
- ¹²J. J. Davies, J. E. Nicholls, and B. C. Cavenett, *Semicond. Insula* **4**, 101 (1978).
- ¹³R. T. Cox and J. J. Davies, *Phys. Rev. B* **34**, 8591 (1986).
- ¹⁴Yu. M. Altaiskii, I. M. Zaritskii, V. Ya. Zevin, and A. A. Konchits, *Sov. Phys.—Solid State* **12**, 2453 (1971).
- ¹⁵Le Si Dang, K. M. Lee, G. D. Watkins, and W. J. Choyke, *Phys. Rev. Lett.* **45**, 390 (1980).
- ¹⁶P. G. Baranov, V. A. Vetrov, N. G. Romanov, and V. I. Sokolov, *Sov. Phys.—Solid State* **27**, 2085 (1985).
- ¹⁷D. K. Wilson and G. Feher, *Phys. Rev.* **124**, 1068 (1961).
- ¹⁸H. W. van Kesteren, E. C. Cosman, F. J. A. M. Greidanus, P. Dawson, K. J. Moore, and C. T. Foxon, *Phys. Rev. Lett.* **61**, 129 (1988).
- ¹⁹J. A. Freitas, Jr., S. G. Bishop, J. A. Edmond, J. Ryu, and R. F. Davis, *J. Appl. Phys.* **61**, 2011 (1987).

MICRO-PHOTOLUMINESCENCE STUDIES OF DIAMOND FILMS

J.A. FREITAS, JR.* , U. STROM, J.E. BUTLER, and K.A. SNAIL

Naval Research Laboratory, Washington, D.C. 20375-5000

*Sachs-Freeman Assoc. Inc., Landover, MD 20785-5396

ABSTRACT

A micro-photoluminescence spectrometer has been used to measure the 77K photoluminescence spectra of combustion deposited diamond films with a spatial resolution of $3\mu\text{m}$. The spatial variations in the micro-luminescence spectra have been correlated qualitatively with the flame chemistry and the substrate temperature.

INTRODUCTION

Photoluminescence (PL) is well established as one of the most powerful spectroscopic techniques to characterize defects in semiconductors. The use of PL spectroscopy involves the measurement and interpretation of the spectral distribution of the radiation emitted by the sample during the recombination processes. In a typical process carriers are photo-excited into the conduction and/or valence band. These photo-excited carriers usually become trapped at a defect (impurity or structural defect) before they recombine, and the nature of the trap center can often be determined from the PL spectrum. Luminescence may also be observed as a result of the relaxation of electrons and/or holes which have been promoted from the ground state to an excited state of a localized center. This process is typically strong phonon coupled and its associated PL spectra are characterized by a broad vibronic emission band. Because crystalline quality can be inferred from intensity and line width of emission bands and impurities can sometimes be identified from the spectral position (energies), PL has proven to be extremely useful during all phases of the development of new materials systems or growth techniques [1].

We have previously used room and low temperature PL spectroscopy to characterize polycrystalline diamond films prepared by filament assisted and by combustion assisted chemical vapor deposition [2,3]. In those experiments a strong spectral emission variation was observed when the exciting laser beam was aimed at different positions on the sample surface. This observation motivated us to set up an experiment which allowed us to carry out low temperature PL measurements with spatial resolution consistent with our sample morphology. Details of the micro-photoluminescence (μ -PL) system will be presented in the next section.

EXPERIMENTAL

In the present work we are discussing only experiments carried out on polycrystalline films deposited on Si substrates by combustion assisted chemical vapor deposition (CACVD). Films deposited by other techniques and on other substrates will be discussed elsewhere.

Sample Characteristics

The two diamond films (S#1 and S#2) studied in the present work were deposited in ambient air using a commercial oxygen-acetylene brazing torch with a 0.89 mm i.d. orifice. Mass flow controllers were used to control the acetylene and hydrogen total flow rate of 3 slm and to keep constant an oxygen/acetylene mass flow ratio (R) of ca. 1.02. The flame was directed down onto a Si substrate placed on a molybdenum screw in contact with a water cooled copper block. The substrate temperature was adjusted by varying the thermal contact to the copper block [4].

The substrates for samples S#1 and S#2 are square shaped pieces of n-type Si (100) wafer approximately 8 mm on a side. Both substrates were intentionally scratched with 5-6 μm diamond polishing paste followed by ultrasonic cleaning in acetone and methanol. The deposition time was 4 hours in case of S#1, and 3 hours 25 minutes in case of S#2. The temperatures of the central parts of the substrates were 850 ± 50 °C and 900 ± 50 °C, respectively.

A micrograph of the area between the central part and the boundary of the film S#1 is shown in Fig. 1. One observes crystallites as large as 150 μm as well some which are only a few microns large. Sample S#2, not shown here, exhibits the same morphology as S#1, however the crystallites are smaller than in sample S#1. Both films show an annular pattern of isolated diamond crystals with low density in the center (directly under the inner flame cone), increasing to a maximum density 2 mm radially outward, from the center, and decreasing to a low and eventually zero density at 3 to 4 mm, near the edge of the substrate.



Fig. 1. Micrograph of the film S#1. The scale is 50 μm for the small division.

Instrumental

A schematic of the $\mu\text{-PL}$ spectrometer is shown in Fig. 2. We have used the 457.9 nm line of an argon ion laser to excite the PL. The samples were placed on a

liquid nitrogen cold finger cryostat, modified to have the samples facing down, to allow mounting on the microscope stage. The microscope was an inverted Carl Zeiss Axiovert model 405 with near UV-IR optics and long working distance objectives. The microscope has been modified to allow simultaneous laser and lamp illumination, only laser, or only lamp illumination. The laser spot size used in this work was $\approx 3 \mu\text{m}$ (which can be reduced to $\leq 1 \mu\text{m}$) and the laser power density varied between 350 and 530 W/cm^2 .

The microscope optics was coupled to a scanning single spectrometer by two lenses as shown in Fig. 2. A color glass filter was used to reduce the scattered laser intensity background. A GaAs photomultiplier tube, operated in a photon counting mode and controlled by a personal computer was used for data acquisition and manipulation.

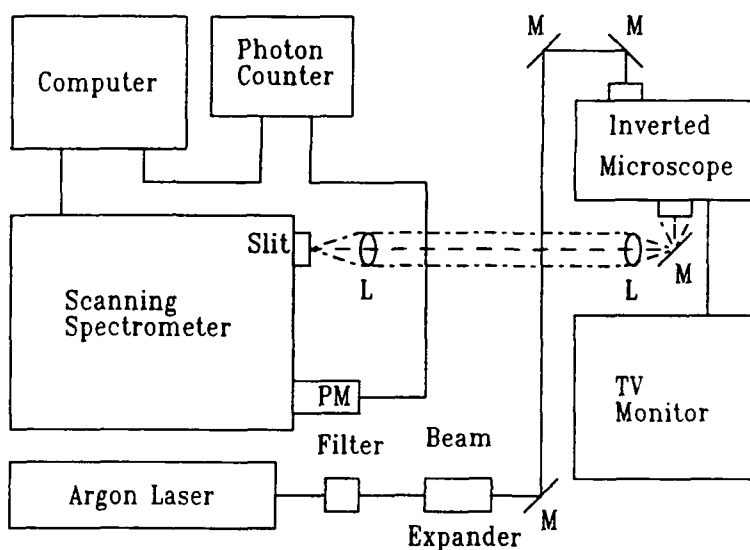


Fig. 2. Schematic view of the micro-photoluminescence spectrometer. M and L stand for mirror and lens, respectively.

RESULTS AND DISCUSSION

Uniformity is one of the basic requirements for optical-electronic applications of any semiconductor film. We have chosen PL to characterize our films because this technique has proven to be a useful non-destructive technique to map spatial variation of the opto-electronic properties of semiconductor films. In our previous PL experiments [2,3], even by reducing the laser spot size to 30-50 μm and using a specially designed device to move the sample by steps of a few microns under laser illumination, we were unable to associate the observed spectral change with any specific morphological features of the film. By using the μm -PL spectrometer described in the previous section this limitation was removed.

Fig. 3 displays the μ -PL spectrum associated with four crystallites in different parts of the film S#1. All four crystallites represented here show (100) faces because we want to separate the spatial dependence from a possible crystallographic growth zone dependence. The spatial position of each crystallite was measured from the film boundary, as shown in Fig. 3. In the following discussion we will identify each crystallite by its position, from the film edge, as indicated in Fig. 3.

The PL spectra of the crystallite at 250 μm is dominated by zero phonon lines (ZPL) at 1.95 eV and 2.16 eV and their associated phonon replicas, and by a broad featureless band centered around 2.35 eV. The 1.95 eV and 2.16 eV systems are assigned to vacancy-nitrogen (V-N) pairs and to a vacancy-nitrogen complex (V-V-N), respectively. Details of this assignment are discussed in Ref. [5,6]. The crystallite at 500 μm shows qualitatively the same spectrum associated with the crystallite at 250 μm , but the 2.16 eV center is the dominant spectral feature. In the spectra associated with the crystallite at 1050 μm and 1300 μm we do not observe any contribution from the 1.95 eV center, however the 1300 μm crystallite spectrum shows a small but noticeable peak at 1.68 eV. This new feature, although not well identified, seems to be associated with diffusion of Si atoms in the crystallite, and may be complexed with either Si, N or the carbon vacancy [7,8].

Oakes and coworkers [9] reported recently micro-Raman and SEM studies of CACVD diamond films, where they observed large substrate surface temperature gradients. They concluded that the inhomogeneities detected in their films were caused principally by flame species inhomogeneities rather than the temperature variation across the sample.

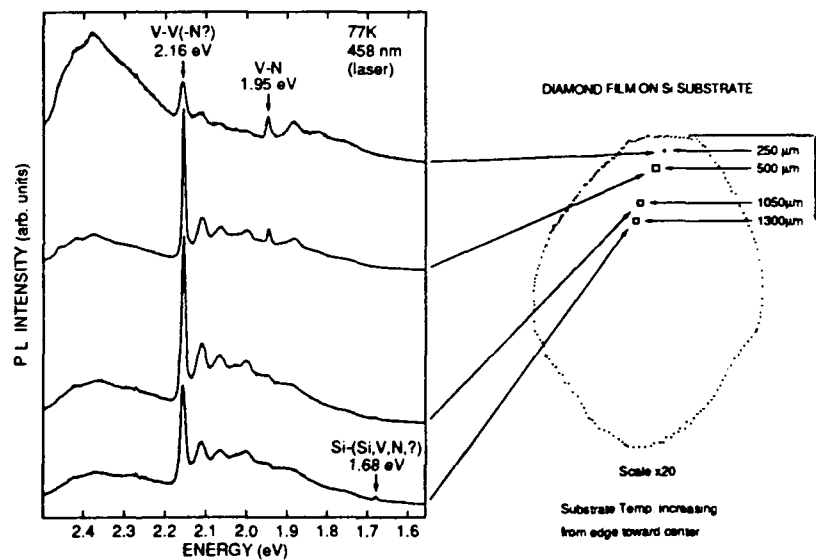


Fig. 3. Photoluminescence spectra of four (100) surface crystallites of sample S#1. Film locations are represented schematically in the right side of the figure.

The presence of different atomic species in the flame is an important factor in the incorporation of defects in the crystallites. This is evident from the intensity reduction of the 1.95 eV system in the crystallites which grow more toward the center of the film, where one can expect lower nitrogen content [2,3]. However, it is important to point out that the increase in substrate temperature toward the center of the film may be favorable for the incorporation of defects with higher formation and/or annealing temperature [5], e.g. the 2.16 eV center and the 1.68 eV center (Si diffusion).

We have also probed different crystallographic structures in film S#1 in the translation range of 30 to 50 μm . As an example, small microcrystals (few microns or less) grown on top of a large (100) single crystal (50 μm or larger) show basically the same PL spectra, with a small PL intensity reduction probably attributable to scattering. In case of a (100) single crystal grown on top of another (100) single crystal (both around 50 μm size), we observe very similar PL scattering, and the small PL variation could be due to crystal misorientation. We emphasize here that large spectral variations are observed in translations of 250 μm or larger distances over which the gas flame composition and temperature are also expected to vary.

The PL measurements of S#2 were carried out following the same procedure as in S#1, nevertheless special attention was given to different crystallographic shapes. Some of the PL spectra from S#2 are presented in Fig. 4. The spectrum (a) is from a crystallite with a hexagonal shape (with $\sim 50 \mu\text{m}$ diagonal) located at the boundary where the nucleation starts. This spectrum is dominated by an unidentified strong broad band centered around 2.35 eV and a strong 1.95 eV system band. Note that not much intensity is observed at 2.16 eV. However, in spectrum (b), associated with a (100) crystallite located about 350 μm toward the center of the film from crystallite (a), we observe a significant change in the spectral intensity associated with the 2.16 eV center. In this spectrum the 1.95 eV and 2.16 eV centers have equivalent relative

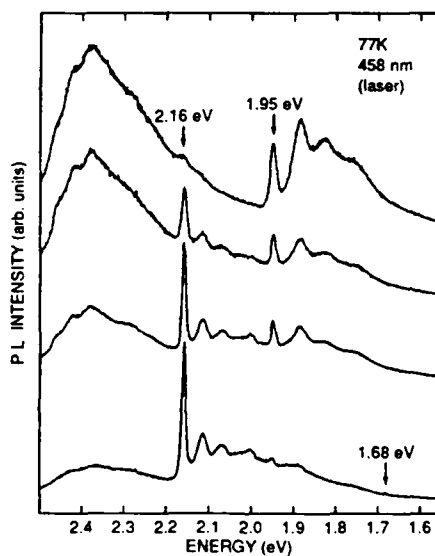


Fig. 4. Photoluminescence spectra of four crystallites of sample S#2. The locations of the microcrystals in the film are described in the text.

intensities and these are similar to the intensity distribution observed in the spectrum identified as 250 μm shown in Fig. 3. The intensity variation observed between spectrum (a) and (b) in Fig. 4 suggests that the nitrogen atoms in the flame environment are easily absorbed in crystallites nucleated close to the film boundary [2,3,10]. The spectrum (c), from the crystallite with a (100) surface, located 200 μm from (b) toward the center of the film, shows a relative increase of the 2.16 eV center in comparison with others spectral features. The spectrum (d), obtained from an area situated at about 700 to 800 μm from the crystallite (c), contains mostly submicron and few microns large crystallites. In this spectrum, the 2.16 eV center is the dominant spectral feature. Also observed, like in the last spectrum of Fig. 3, is the small peak at 1.68 eV associated with the Si diffusion. The overall spectral variations observed in the film S#2 are very similar to those observed in the film S#1. This established that for the quality of films considered here, the defect incorporation in the diamond microcrystals does not depend significantly on the crystallographic orientation.

CONCLUSION

A novel micro-PL spectrometer has been described which features micron sized spatial resolution at cryogenic temperatures. The spectrometer has been applied to investigate the spatial PL variations for polycrystalline diamond films deposited with an acetylene torch technique. Variations in the PL spectra were observed which can be qualitatively related to the variation with substrate temperature and possibly the flame species inhomogeneities. Future work will establish the relative importance of these experimental parameters and the effect of varying the substrate type.

REFERENCES

- [1] S.G. Bishop and J.A. Freitas, Jr., *J. of Crystal Growth*, **106**, 38 (1990).
- [2] J.A. Freitas, Jr., J.E. Butler, S.G. Bishop, W.A. Carrington, and U. Strom, *Proc. of MRS: Symp. in Diamond, Boron Nitride, Silicon Carbide and Related Wide Bandgap Semiconductors*, eds. J.F. Glass, R.F. Messier, N. Fujimori, Boston, MA, **162**, pg 237 (1989).
- [3] J.A. Freitas, Jr., J.E. Butler and U. Strom, *J. Mat. Res.*, **5**, 2502 (1990).
- [4] J.E. Butler, F.G. Celli, D.B. Oakes, L.M. Hansen, W.A. Carrington, and K.A. Snail, *Proc. of the Conf. on High Temperature Material Chemistry*, April 3-7, 1989, to be published in *High Temp. Sc. and/or Pure and App. Sc.*
- [5] J. Walker, *Rep. Prog. Phys.*, **42**, 1605 (1979).
- [6] G. Davies, *Rep. Prog. Phys.*, **44**, 787 (1981).
- [7] A.T. Collins, *this Conference Proc.*
- [8] J. Ruan, W.J. Choyke, W.D. Partlow, *this Conference Proc.*
- [9] D.B. Oakes, J.E. Butler, K.A. Snail, W.A. Carrington and L.M. Hansen, *J. App. Phys.*, in press.
- [10] Y. Yokota, H. Kawarada, and A. Hiraki, *Proc. of MRS: Symp. in Diamond, Boron Nitride, Silicon Carbide and Related Wide Bandgap Semiconductors*, eds. J.F. Glass, R.F. Messier, N. Fujimori, Boston, MA, **162**, pg 237 (1989).

High-temperature epitaxy of diamond in a turbulent flame

¹K. A. Snail, ²C. L. Vold and ¹C. M. Marks

¹Optical Sciences Division, Code 6522, ²Material Sciences & Technology Division, Code 6322, Naval Research Laboratory, Washington, DC, 20375-5000 (USA)

J. A. Freitas Jr

Sachs Freeman Associates, 1401 McCormick Drive, Landover, MD, 20785-5396 (USA)

Abstract

Diamond has been grown epitaxially on 1.5 mm diameter, natural diamond seed crystals at temperatures of 1200–1300 °C in a premixed, turbulent oxyacetylene flame. During a typical 1 h deposition, a polyhedral-shaped single crystal was observed to grow on top of a <100> oriented cylindrical seed crystal. The growth surface is composed of both {100} terraces and {110} ridges, arranged into well-formed pyramidal shaped structures with very long range order. Raman analyses show a lack of non-diamond carbon and a 1332 cm⁻¹ peak which is indistinguishable from natural type IIa diamond. Low-temperature photoluminescence measurements indicate a greatly reduced level of localized radiative defects. Laue X-ray diffraction measurements have confirmed the epitaxial nature of the deposit, and preliminary X-ray rocking curve analyses are presented. This is the first report of the high-temperature epitaxial growth of diamond in a turbulent flame.

1. Introduction

Recently, Janssen *et al.* [1] reported that diamond could be grown epitaxially on {110} natural diamond seed crystals at temperatures of 900 ± 100 °C and growth rates of 50 μm/h in an atmospheric pressure, oxyacetylene flame. In spite of the high growth rates, the deposited material had good crystalline and optical quality [1, 2]. In related work, we have reported that macroscopic (~1.7 mm × 150 μm) faceted diamond crystals can be grown epitaxially at high temperatures ($T > 1200$ °C) in an atmospheric pressure, laminar oxyacetylene flame [3, 4]. The growth rates observed on {100} seeds (150–200 μm/h) and the maximum deposition temperature observed on {110} seeds (~1500 °C) are some of the highest ever reported for the epitaxial synthesis of diamond. In collaboration with the University of Minnesota, we also investigated whether a high-temperature epitaxy (HTE) type process is possible with a plasma jet reactor. The results of these studies indicate that diamond can be grown epitaxially at high temperatures (1200–1400 °C) and high rates (> 200 μm/h) on {100} and {110} natural diamond seed crystals which are positioned in the plume of a DC triple plasma torch [5, 6]. In this paper we present the first evidence for the HTE growth of single crystal diamond in a turbulent flame. This study was motivated by the observation that undoped polycrystalline diamond films grown at low temperatures (<1000 °C) in a turbulent flame are clear [7] and exhibit a reduced level of radiative defects [8, 9]. Recently,

boron doped single crystal diamond films have also been grown in a turbulent oxyacetylene flame at high temperatures [10].

2. Experimental set-up

The apparatus used in this study is similar to that described in previous work [3, 8] and is shown in Fig. 1. High purity oxygen (99.99%) and acetylene (99.6%) were used as source gases, with the acetylene passed through an activated charcoal trap to remove residual acetone. The feed gases were metered to a commercial brazing torch with a mass flow control system. The oxygen and

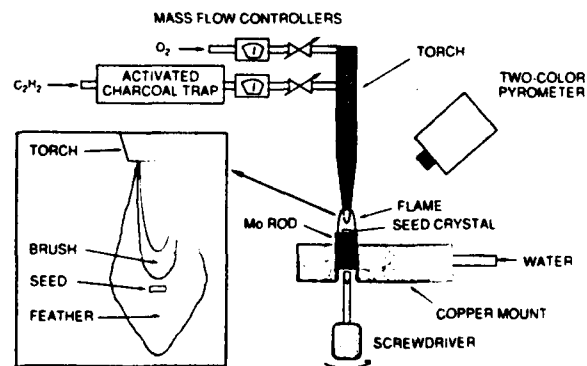


Fig. 1. Experimental set-up showing brazing torch, substrate mount assembly, two color pyrometer, and mass flow controllers. The flame shape and sample position in the flame are shown in the inset.

acetylene flow rates were 10.42 slm and 10.08 slm, respectively, and the orifice diameter of the torch was 1.85 mm. The substrates consisted of 0.25 mm thick, natural type IIa diamond heat sinks which were laser cut into circular cross-sections (1.5 mm diameter), polished on the top {100} face, and bonded to the ends of 1.5 cm long pieces of threaded molybdenum rod with a gold-tantalum brazing process. The seed crystal was positioned in the acetylene feather of a turbulent flame, just beyond the flame brush, as shown in Fig. 1, and the deposition lasted for 60 min.

The braze material insured good thermal contact between the diamond seed crystals and the molybdenum rod during depositions. Since the thermal conductivity of the seed crystals and braze material is relatively high, the seed crystal is expected to be isothermal with a temperature equal to or slightly greater than the molybdenum rod temperature. The temperature of the seed crystals was controlled by varying the penetration of the molybdenum rod into a threaded hole in a water-cooled copper cylinder. The temperature of the substrates was measured with a two-color (2.1 and 2.4 μm) pyrometer which was insensitive to the flame emissions.

Fluid flow in a tube is frequently characterized by its Reynolds number, defined as $Re = vd\rho/\mu$, where v is the average gas velocity, d is the tube diameter, ρ is the gas density, and μ is the gas viscosity. Assuming a temperature of 300°K and a 1:1 mixture of oxygen:acetylene, we estimated [11] that the gas viscosity in the tube before the flame front was 1.5×10^{-4} g/cm s. For the flow conditions corresponding to the flame used in this study, we estimate the Reynolds number in the tube supporting the flame to be $>12\,000$. For Reynolds numbers less than 2300 the flow in a tube supporting a flame is normally laminar and above that value the flow becomes progressively more turbulent. Reynolds numbers over 3200 are generally associated with fully developed turbulent flow [12, 13]. Premixed turbulent flames exhibit a rounding and broadening of the primary flame front, and a characteristic hissing sound [12]. The reaction zone becomes blurred or "wrinkled" instead of smooth, so that the reaction occurs over a much larger effective area which is not necessarily continuous [14]. The broadening occurs when the scale of the turbulence (*i.e.* the eddy diameter) is significantly greater than the flame front thickness [13]. The flame used in this study exhibited a rounded, thick flame front [8] and a loud hissing sound.

The laminar and turbulent operational regimes [15] of a Bunsen burner are shown as a function of the average gas velocity and the burner diameter in Fig. 2. We expect that oxyacetylene torches will exhibit similar, but not identical, characteristics. The laminar and turbulent regimes are separated by a hyperbolic wedge defined by the Reynolds number values corresponding to the

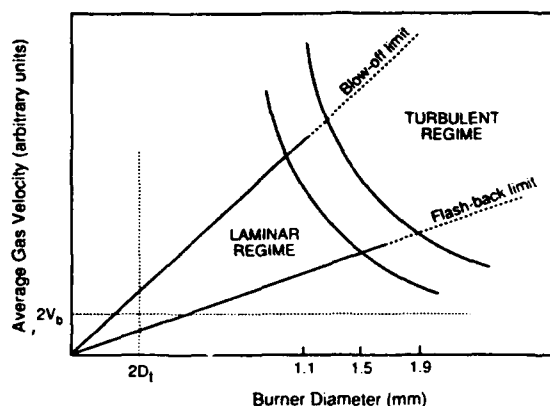


Fig. 2. Operational regimes of premixed, single orifice torches. Note the flashback limit, the blow-off limit, and the hyperbolic wedge separating the laminar and turbulent regimes.

laminar-turbulent transition at the flame front. Note that both the laminar and turbulent regimes are bounded from below by the flash-back limit, and from above by the blow-off limit. These limits correspond to the flame either propagating back down the burner tube or becoming unstable and detaching from the burner tip, respectively. The blow-off and flash-back limits are defined semi-empirically in terms of two critical velocity gradients which are expressed in terms of the quenching distance, D_1 (0.1 mm for a stoichiometric mixture), and the average gas velocity. Since the velocity profile in the burner tube changes significantly when the flow changes from laminar to turbulent, the critical velocity gradients and slope of the blow-off and flash-back limits shown in Fig. 2 may also change in passing through the laminar-to-turbulent transition.

3. Results

Optical and electron micrographs of a cylindrical {100} seed crystal after 1 h growth at 1250 °C in a turbulent flame are shown in Figs 3(a) and 3(b), respectively. The deposited material has an octagonal shape when viewed from above with the shapes of the side faces alternating between trapezoids and truncated parallelograms. These are the shapes expected around the 'waist' of a cubo-octahedral crystal which is truncated along a $\langle 100 \rangle$ axis perpendicular to the plane of the waist (the plane of the waist contains four $\langle 100 \rangle$ axes). The trapezoidal and truncated parallelogram shaped faces would thus correspond to the $\langle 111 \rangle$ and $\langle 100 \rangle$ crystallographic directions, respectively [4].

The top {100} growth surface of the sample is covered with multiple pyramidal shaped structures which appear to be composed of both {100} and {111} surfaces (see Fig. 3(a)). Note the long range (200–800 μm) order of the growth and the rigid locking of most features to low

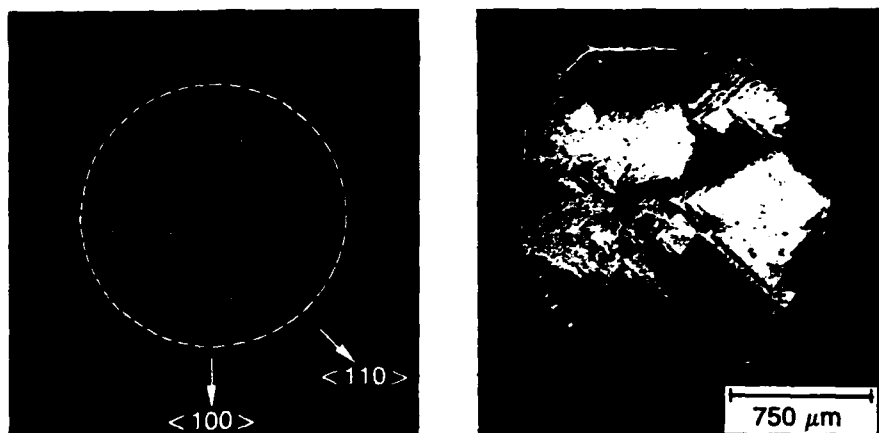


Fig. 3. (a) Optical and (b) electron micrographs of diamond crystal grown on 1.5 mm diameter $\{100\}$ seed in a turbulent oxyacetylene flame at 1250 °C for 1 h.

index crystallographic directions. The optical micrograph shown in Fig. 3(a) was taken with a short depth of field microscope, however both the bases and tops of the pyramid type structures appear to be in focus. Considering the size of these pyramids, this suggests that the slopes of the pyramids' side faces are too small for the faces to be of a $\langle 111 \rangle$ orientation. Measurements of the height and lateral extent of one section of a pyramid side face were performed with an optical microscope equipped with a micrometer. The slope was less than 0.05, suggesting that these side faces would not have the proper orientation to be a $\{111\}$ face. The fine structure of the pyramidal structures did not show up well in the scanning electron micrograph of the same (uncoated) sample, as shown in Fig. 3(b). The pyramids did appear to have an enhanced secondary electron yield, which may have been related to charging. Smaller pyramidal growth structures have been observed in $\{100\}$ growths before [16], however, the side faces were incorrectly identified as $\{111\}$ faces. Preliminary atomic force microscope (AFM) studies of a sample grown under similar conditions suggest that the side faces of some pyramids are composed of very well-ordered $\{100\}$ terraces and $\{110\}$ ridges with a typical height: length ratio of 100 nm: 4 μm . These relative dimensions agree with the microscope slope measurements mentioned earlier. An AFM micrograph of the tip of a growth pyramid is shown in Fig. 4.

The thickness of the deposited layer was measured by examining a side $\{100\}$ face with an optical microscope equipped with a micrometer; the growth rate determined from this measurement was 35 $\mu\text{m}/\text{h}$. The distances from two orthogonal $\{100\}$ side faces to their respective opposite $\{100\}$ side faces were measured to be 1.552 and 1.561 mm, giving a lateral $\langle 100 \rangle$ growth rate of 26–31 $\mu\text{m}/\text{h}$. This is slightly lower than the growth rate calculated from the film thickness; the discrepancy may

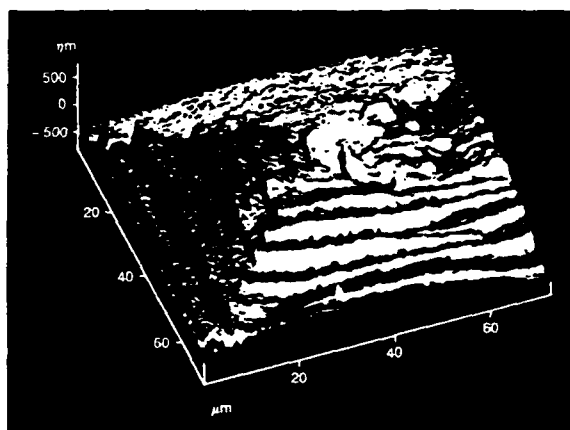


Fig. 4. Atomic force micrograph of top of pyramidal structure similar to that observed on sample shown in Fig. 3a. Note the staircase structure with $\{100\}$ terraces and $\{110\}$ ridges.

be due to growth non-uniformities, residual braze compound on the seed and/or a smaller seed diameter than the specified value. Normally, the seed crystal dimensions are within 1–2 μm of the dimensions quoted by the supplier.

Although true $\{111\}$ faces did not exist on the top growth surface of the seed, $\{111\}$ faces did grow out of the side wall of cylindrical, $\langle 100 \rangle$ oriented seeds. The $\langle 111 \rangle$ growth rate was thus determined by examining the dimensions of one side $\{111\}$ face of the crystal shown in Fig. 3 and calculating the distance between two parallel planes, one of which was co-planar with the deposited face, the other of which contained the top edge of the seed crystal. A growth rate of 57 $\mu\text{m}/\text{h}$ was calculated in this way for the $\langle 111 \rangle$ direction. The side $\{111\}$ faces frequently appeared to have a large misorientation (1–4°) from the expected orientation, but this may be due to measurement errors associated with poorly formed faces, and with astigmatic effects in our scanning

electron microscope. This misorientation did not affect the growth rate calculation significantly. The ratio of the growth rates in the $\langle 111 \rangle$ to $\langle 100 \rangle$ directions is thus in the range of 1.63–2.19, depending on the value used for the $\langle 100 \rangle$ direction. For a $\langle 111 \rangle / \langle 100 \rangle$ growth rate ratio of ≥ 1.732 , a cubic morphology will be the final crystal shape [17]. The growth rate in the $\langle 110 \rangle$ direction is probably much higher than either the $\langle 100 \rangle$ or $\langle 111 \rangle$ directions, since no macroscopic $\{110\}$ faces appear. Several different techniques for estimating the $\langle 110 \rangle$ growth rate all suggest values well over $100 \mu\text{m/h}$.

The first order Raman spectrum of a single crystal diamond film grown at $T_s = 1250^\circ\text{C}$ in a premixed, turbulent oxyacetylene flame is shown in Fig. 5. For comparison, the first order Raman spectrum of a natural type IIa diamond sample is also presented in Fig. 5. The 514.5 nm argon laser line with a power density of $\sim 40 \text{ W cm}^{-2}$ was used as the light source, and all measurements were performed at room temperature. The scattered light was dispersed by a double spectrometer with a bandpass of $\sim 0.25 \text{ cm}^{-1}$. The film's TO/LO phonon (continuous line) peaks at $1333.20 \pm 0.25 \text{ cm}^{-1}$, while natural diamond's TO/LO phonon (dotted spectrum) has its maximum at $1333.50 \pm 0.25 \text{ cm}^{-1}$. For line-shape and line-width comparisons, the film's spectrum was red shifted (0.25 cm^{-1}) and the natural diamond spectrum was normalized to the film's phonon peak intensity. As one can see, there is excellent agreement between the two spectra, within experimental error. A low-resolution wide-range spectrum, not presented here, showed no evidence of amorphous and/or graphitic components.

The low-temperature (6 K) photoluminescence (PL) spectrum of the sample analyzed in Fig. 5 is shown in Fig. 6. The 488.0 nm argon laser line with an intensity of 20 mW was used as the exciting light source. The PL spectrum of the seed crystal was not measured before

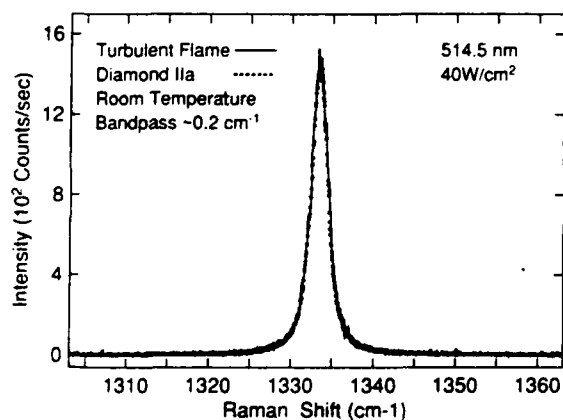


Fig. 5. High-resolution Raman spectrum of a homoepitaxial diamond film grown on a $\{100\}$ type IIa seed with a turbulent, oxyacetylene flame. (—) the deposited crystal, and (.....) a natural type IIa diamond.

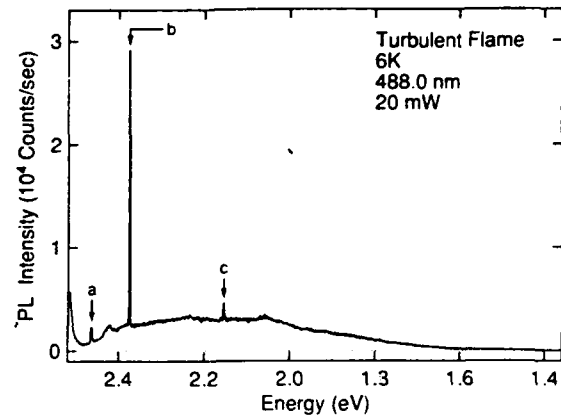


Fig. 6. Low-temperature photoluminescence spectrum excited with a 488 nm line of a homoepitaxial diamond film grown in a turbulent flame. The peaks labeled "a" and "c" correspond to the zero phonon line of the H3 defect band and the 2.156 eV defect band, respectively. The peak "b" at 2.375 eV is the first-order diamond phonon line.

the deposition. The spectrum is characterized by a broad, almost featureless, band extending from 2.31 to 1.6 eV and three sharp peaks labeled as "a", "b", and "c". The gradual decrease in the spectral intensity observed at the high-energy end of the spectrum is due to Rayleigh scattering of the laser light. The peak "a" at 2.465 eV has been assigned [18] to the zero phonon line (ZPL) of the H3 defect band (N–V–N), which is easily identified by the broader unlabeled phonon replica at 2.421 eV (43.4 meV from the ZPL). The strong sharp peak "b" at 2.375 eV is the first order TO/LO phonon (1333.2 cm^{-1}). The peak labeled "c" at 2.156 eV is assigned to the ZPL of the 575 nm system, the structure of which has not yet been identified (V–?) [18]. The 575 nm system has been previously observed in polycrystalline [19] and monocrystalline [4] diamond films deposited in laminar flames. The 575 nm and 637 nm (1.947 eV ; N–V pair) [19] systems are the dominant defect bands observed in homoepitaxial films deposited in a laminar oxyacetylene flame [4]. The absence of the 637 nm center and the strong reduction of the 575 nm and H3 centers suggest that nitrogen is significantly excluded and vacancies are not incorporated as efficiently into films deposited under turbulent conditions [8]. These Raman scattering and PL results imply that high-quality diamond films can be deposited using a turbulent oxyacetylene flame.

The combination of the polyhedral shape of the deposited crystal shown in Fig. 3 and the quality of the deposited crystal's Raman spectrum shown in Fig. 5 suggest that the growth is monocrystalline diamond. Laue X-ray diffraction analysis of the deposited crystal shown in Fig. 3 has confirmed that it is monocrystalline. These Laue photographs did, however exhibit a certain degree of asterism, implying the presence of defects in the diamond structure. The nature of these defects were considered by making measurements of X-ray rocking

curve breadths from the face of the seed diamond opposite that of the epitaxial deposit, and from the epitaxial deposit itself.

The crystal was affixed to a glass slide using a small amount of grease, and this assembly was positioned on the focusing circle of an X-ray powder diffractometer. The detector was positioned and fixed at the 2θ angle corresponding to the Cu $K\alpha_1$ reflection from the (400) plane, approximately 119.45° . Several omega scans were then performed, rotating the diamond crystallite approximately 10° about its face normal between scans. This procedure was performed upon the face of the seed diamond opposite that of the epitaxial deposit to establish a baseline for the rocking curve measurements to which the measurements from the epilayer may be compared. The measurements were then repeated on the epitaxially grown deposit. The line breadths were characterized by subtracting the background and then evaluating the integral breadth. Despite the relatively poor resolution, two points are noted: (i) the integral breadths are quite variable, even on a single face. This variability seems to be caused by the intrinsic characteristics of the diamond's defect structure, and is manifested as multi-peaked rocking curves, as shown in Figure 7; (ii) The average rocking curve breadth for the epitaxial deposit (0.426 degrees) is nearly twice that of the diamond seed (0.245 degrees).

The rocking curves presented here are a direct measurement of the angular dispersion of the diamond subgrains from which the single crystal diamond lattice is built. Propagation of lattice defects in the seed appear to be propagated into the epilayer and this accentuated as the diamond growth front moves forward in the turbulent flame. It is also noted that rocking curves measured from the epilayer side will also contain a contribution from the substrate and the defected side $\{111\}$ faces (see Fig. 3). No attempt has been made to separate these contributions to the intensity. Insufficient resolution precludes extracting more quantitative information concerning the angular dispersion of the sub-

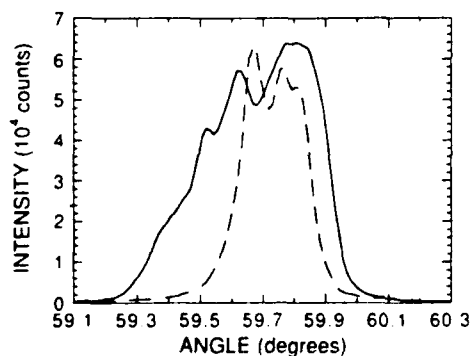


Fig. 7. X-ray rocking curve spectra obtained with a powder diffractometer for the (400) plane of (-----) the seed crystal, and (—) the deposited epilayer.

grains. Double crystal diffractometer measurements would be desirable, and, under favorable conditions, may yield additional insight into the structure of the individual grains.

4. Discussion

Diamond grown in a turbulent oxyacetylene flame exhibits a lower growth rate, a different growth morphology and a greatly reduced level of radiative defects, as compared to diamond grown in a laminar flame. These features of diamond growth in turbulent flames are unexpected and surprising. If diamond growth in laminar flames is transport limited, then the higher effective diffusion coefficient (the "eddy viscosity") in turbulent flow could lead to higher diamond growth rates. The decrease in growth rates observed (*e.g.* for $\langle 100 \rangle$ direction at 1250°C , laminar, $\sim 150 \mu\text{m/h}$; turbulent, $\sim 30 \mu\text{m/h}$) suggests that diamond growth in flames is not transport limited and/or the flux of growth and etchant species has been altered drastically in going from laminar to turbulent conditions (so as to favor increased etching). Recent studies [20] of the variation of diamond growth rates with substrate temperature in a filament assisted chemical vapor deposition environment show an Arrhenius dependence with an activation energy of 22–24 kcal/mol, suggesting that diamond growth may be limited by a surface reaction.

Capelli *et al.* [21] have suggested that spatial variations in the diamond growth rate observed in an atmospheric pressure, inductively coupled plasma may be due to atomic hydrogen flux changes which are related to variations in the boundary layer thickness. Higher growth rates were observed near regions of thinner boundary layers. A study of the radial variation of the Raman spectra of diamond deposited in a laminar flame using a stagnation flow geometry showed that for smaller flame front-to-sample distances, the growth rate was lowest at the stagnation point (where the boundary layer presumably is the thickest), but the diamond quality was highest [22]. For the turbulent flame described earlier, we have observed that the growth rate and diamond quality are fairly uniform over $>1 \text{ cm}$ diameter areas. The boundary layer remains laminar, but its thickness decreases significantly compared to a fully laminar flow condition. This decrease in boundary layer thickness is expected [23], however the decrease in growth rate suggests that the mechanisms behind the growth of diamond in turbulent flames may be more than a simple extension of the laminar flame case.

One factor affecting the flux of species to the substrate is the tendency for turbulent flame fronts to wander laterally and actually become discontinuous [24]. The wandering and breaking of the flame front can occur at

a high frequency (~1 kHz) and could conceivably lead to alternating periods of growth and etching, by varying the amount of room air entrained into the flame, and/or by allowing unburnt pockets of oxygen and acetylene to leak through the flame front. Since diamond and graphite burn rapidly [25] at 1250 °C, only short periods of exposure to oxygen would be required to decrease the growth rate. Experiments with atmospheric pressure, turbulent plasma torches [26] have demonstrated that ambient gases can be entrained into a plasma torch's plume with an engulfment process. If this phenomena is present in a turbulent oxyacetylene flame, then it could also lead to alternating periods of growth and etching at the substrate, which could decrease the diamond growth rate if the ratio of etching to growth periods is sufficiently long.

A decrease in the density of radiative defects has been observed in depositions performed with a turbulent flame using both single crystal diamond substrates at high temperatures (>1250 °C) and metal substrates at low temperatures (~900 °C) [8, 9]. In both cases, the substrates were positioned about 1 mm from the end of the turbulent flame front's brush. In the laminar case, the substrates were not always positioned as close to the flame front, which might result in an increased exposure to entrained room air and possible changes in the species fluxes striking the substrate. Additional experiments with very lean laminar flames would also be useful to determine whether a lower growth rate alone is sufficient to reduce the defect density in the deposited diamond. The alternating growth and etching cycles discussed earlier could also be responsible for the improved diamond quality. Tzeng *et al.* [27] have demonstrated that periodic increases in the oxygen:acetylene flow ratio into the etching regime for short intervals can improve the Raman spectra of flame grown diamond. For a given ratio of growth:etching time, higher frequency oscillations between growth and etching produced higher quality diamond.

To conclude, it has been demonstrated that single crystal diamond can be grown epitaxially at high temperatures (>1200 °C) in a turbulent oxygen-acetylene flame on <100> oriented natural diamond seed crystals. Studies with <110> oriented diamond substrates will be reported on in a future publication. Compared to diamond grown in a laminar flame, the diamond deposited on {100} seeds in a turbulent flame exhibits a reduced level of nitrogen and vacancy incorporation, a lower growth rate, and growth steps which are rigidly locked to low index crystallographic directions. The <110> oriented ridges observed are consistent with a (2 × 1) dimer reconstruction of the {100} face.^{28,29} Even without a complete understanding of diamond growth in turbulent flames, however, the reduced level of radiative defects suggests

that diamond synthesized in a turbulent flame may be a good candidate for use in electronic devices.

Acknowledgements

The authors would like to thank Bruce Haggard and his colleagues at Wyko Corporation for characterizing several diamond samples with a Wyko MicroProbe 3D atomic force microscope.

References

- 1 G. Janssen, W. J. P. Van Enckevort, J. J. D. Schaminee, W. Vollenberg, L. J. Giling and M. Seal, *J. Crystal Growth*, 104 (1990) 752.
- 2 G. Janssen, W. Vollenberg, L. J. Giling, W. J. P. Van Enckevort, J. J. D. Schaminee, and M. Seal, *Surface & Coatings Technology* 47 (1991) 113-126.
- 3 K. A. Snail and L. M. Hanssen, *J. Crystal Growth*, 112 (1991) 651.
- 4 K. A. Snail, J. A. Freitas Jr, C. L. Vold, and L. M. Hanssen, *Proc. 2nd Int. Symp. on Diamond Materials, Washington, DC, May, 1991*, Electrochemical Society, Pennington, NJ, 1991, Vol. 91-8, p. 81.
- 5 Z. Lu, K. A. Snail, C. M. Marks, J. Heberlein, and E. Pfender, *Proc. 2nd Int. Symp. on Diamond Materials, Washington, DC, May, 1991*, Electrochemical Society, Pennington, NJ, 1991, Vol. 91-8, p. 99.
- 6 K. A. Snail, C. M. Marks, Z. Lu, J. Heberlein, and E. Pfender, *Materials Letts* (in press).
- 7 K. A. Snail and C. J. Craigie, *Appl. Phys. Letts*, 58 (1991) 1877.
- 8 K. A. Snail, C. J. Craigie, R. G. Vardiman, C. M. Marks, and J. A. Freitas Jr, *Proc. 2nd Int. Symp. on Diamond Materials, Washington, DC, May, 1991*, Electrochemical Society, Pennington, NJ, 1991, Vol. 91-8, p. 91.
- 9 J. A. Freitas Jr, U. Strom, K. Doverspike, C. M. Marks and K. A. Snail, Optical evidence of reduction of radiative defects in diamond films grown by acetylene-oxygen flames. *Proc. MRS Symposium on Wide Band-Gap Semiconductors, Boston, MA, Dec. 1991*, Materials Research Society, Pittsburgh, PA, 1991 (in press).
- 10 J. W. Glesener, J. A. Freitas Jr, A. A. Morrish and K. A. Snail, Electrical characterization of boron doped single crystal diamond grown in a flame. *Proc. MRS Symposium on Wide Band-Gap Semiconductors, Boston, MA, Dec. 1991*, Materials Research Society, Pittsburgh, PA, 1991 (in press).
- 11 R. H. Perry and C. H. Chilton (eds), *Chemical Engineer's Handbook*, 5th edn, McGraw-Hill, New York, 1973, p. 3-210.
- 12 A. G. Gaydon and H. G. Wolfhard, *Flames: Their Structure, Radiation and Temperature*, Chapman & Hall, London, 1979, p. 14.
- 13 J. A. Barnard and J. N. Bradley, *Flame and Combustion*, Chapman and Hall, New York, 1985, p. 74.
- 14 A. Thomas, *Comb. & Flame*, 65 (1986) 291.
- 15 I. Glassman, *Combustion*, Academic Press, New York, 1987, p. 157.
- 16 V. A. Laptev, In Y. Tzeng, M. Yoshikawa, M. Murakawa, and A. Feldman (eds), *Applications of Diamond Films and Related Materials*, Elsevier, Amsterdam, 1991, p. 9.
- 17 J. S. Kim, M. H. Kim, S. S. Park and J. Y. Lee, *J. Appl. Phys.*, 67 (1990) 3354.
- 18 G. Davies, *Rep. Prog. Phys.*, 44 (1981) 787.
- 19 J. A. Freitas Jr, J. E. Butler, and U. Strom, *J. Mater. Res.*, 5 (1990) 2502.
- 20 E. Kondoh, T. Ohta, T. Mitomo and K. Ohtsuka, *Appl. Phys. Letts.*, 59 (1991) 488.

- 21 M. A. Capelli, T. G. Owano and C. H. Krueger, *J. Mater. Res.*, **5** (1990) 2326.
- 22 D. B. Oakes, J. E. Butler, K. A. Snail, W. A. Carrington and L. M. Hanssen, *J. Appl. Phys.*, **69** (1991) 2602.
- 23 H. Tennekes and J. L. Lumley, *A First Course in Turbulence*, MIT Press, Cambridge, MA, 1989, p. 13-14.
- 24 M. D. Fox and F. J. Weinberg, *Proc. Roy. Soc., A* **268** (1962) 222.
- 25 C. E. Johnson, W. A. Weimer, D. C. Harris, *Mat. Res. Bull.*, **24** (1989) 1127.
- 26 R. Spores and E. Pfender, *Surf. & Coat. Techn.*, **37** (1989) 251.
- 27 Y. Tzeng, R. Phillips, S. Govil and A. Joseph, *Proc. 2nd Intl. Symp on Diamond Materials, Washington, DC, May 1991*, Electrochemical Society, Pennington, NJ, 1991, Vol 91-8, p. 49.
- 28 W. J. P. van Enckevort, G. Janssen, W. Vollenberg, M. Chermín, L. J. Giling & M. Seal *Surface & Coatings Technology* **47** (1991) 39-50.
- 29 K. Okada, S. Komatsu, S. Matsumoto and Y. Moriyoshi, *Jrnl. Crystal Growth* **108** (1991) 416-420.

Optical studies of donors and acceptors in cubic SiC

J. A. Freitas Jr.

Sachs/Freeman Associates, Inc., Landover, MD 20785 (U.S.A.)

P. B. Klein

Naval Research Laboratory, Washington, DC 20375 (U.S.A.)

S. G. Bishop

University of Illinois, Urbana, IL 61801 (U.S.A.)

Abstract

Previous and recent results of continuous wave and pulsed photoluminescence (PL) studies of undoped and aluminum-doped 3C-SiC deposited on Si(100) substrates are reviewed. In undoped samples the band edge PL spectra are dominated by sharp lines assigned to excitons bound to neutral nitrogen donors, while deep PL emissions are associated predominantly with structural defects. In contrast, the PL spectra of aluminum-doped samples are dominated by recombination involving N-Al donor-acceptor pairs. The photoluminescence excitation spectra of undoped films are also discussed.

1. Introduction

SiC is well known as a potential material for the fabrication of devices operating under extreme conditions. However, difficulties encountered in the growth of large bulk crystals have limited its practical application. The recent success of homo- and heteroepitaxial growth of SiC films by chemical vapor deposition (CVD) has renewed interest in this promising wide band gap semiconductor [1-3].

Despite the fact that the SiC film deposition and device-processing techniques have improved in the last few years to the point where device fabrication [4] is now feasible on a commercial scale, some basic material properties are still not well understood. One of the most undesirable characteristics of films deposited on Si(100) substrates is the high concentration of misfit dislocations and stacking faults. One attempt to solve this problem was by off-axis deposition on silicon substrates [5, 6]. Although some improvement was observed in film morphology and anti-phase boundaries, no change was verified in the density of stacking faults [6]. A different approach was reported by Kong *et al.* [3], in which cubic SiC films were deposited on 6H-SiC(0001) substrates. These films showed a large decrease

in the density of line and planar defects, but unfortunately a high density of double-positioning boundaries (DPBs) was observed [7]. Recently, it has been reported that cubic SiC films deposited on 6H-SiC substrates may show a very low concentration of DPBs if one uses the Si(0001) face of Lely 6H-SiC crystals [8].

Although better quality cubic SiC films may be achieved by deposition of 6H-SiC substrates, the deposition of films on silicon substrates is still very attractive because of the low cost of good quality wafers and the possibility of growing multiple-layered structures. In the present work we discuss the properties of donors and acceptors in undoped and aluminum-doped 3C-SiC deposited on silicon substrates as determined by photoluminescence (PL) and photoluminescence excitation (PLE) spectroscopies.

2. Experimental details

Undoped 3C-SiC films were grown epitaxially on Si(100) substrates by CVD [1, 2]. These films are invariably n type. The dominant residual donor as determined by transport measurements has a binding energy in the range 15-20 meV, but the layers are highly compensated (approximately

95%) by background acceptors [9–12]. The incorporation of defects was investigated by growing several samples with different values of C:Si source gas ratio. Aluminum doping was achieved by introducing trimethylaluminum with the source gases [2]. The film thickness varies from 9 to 15 μm and each film was removed from its substrate to reduce the strain due to lattice mismatch.

The PL spectra described here were obtained with the samples contained in a Janis Super-vari-temp cryostat, which allowed temperature variation from 1.5 to 330 K. Most spectra were obtained in continuous wave (CW) mode with excitation provided by either an argon ion laser (476.5 nm) or light from a xenon lamp and a double monochromator. Time decay studies of the PL spectra employed 10 ns pulses of 355 nm excitation light from a tripled Nd-YAG laser with peak power approximately 4 kW. The excited luminescence in all experiments was analyzed by a grating spectrometer and detected by a GaAs photomultiplier operated in a photon-counting mode.

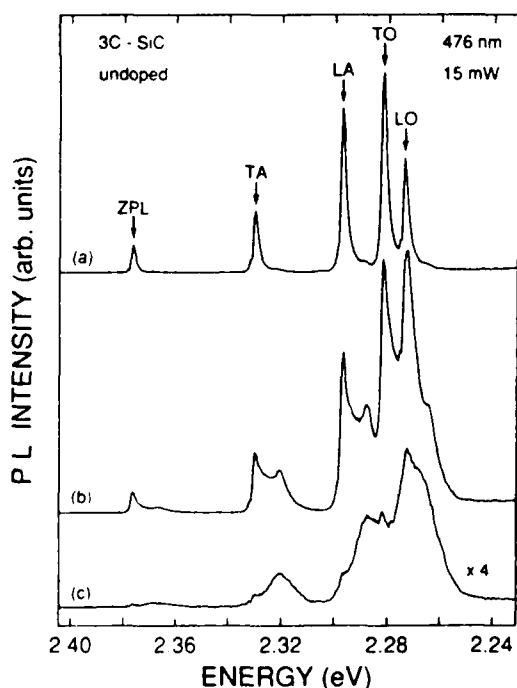


Fig. 1. PL spectra from two undoped cubic SiC CVD films grown with two different values of C:Si gas source ratio: (a) 2.4; (b), (c) 1.2. Spectra (a) and (b) were acquired with the samples at 5 K and spectrum (c) with the sample at 15 K. The weak shoulder in spectrum (b) has become dominant in spectrum (c).

3. Results and discussion

Low temperature (6 K or less), near-band-edge (about 2.38 eV) PL spectra of undoped CVD-grown cubic SiC films are characterized by five lines [13–17], which are basically equivalent to the five-line PL spectrum first observed by Choyke *et al.* in Lely-grown (bulk) crystals of cubic SiC [18]. This luminescence spectrum, shown as spectrum (a) in Fig. 1, is attributable to the recombination of excitons bound to isolated neutral nitrogen donors. Despite the similarity in the spectra of CVD films and Lely crystals, we observe that the spectral features are always red shifted and broadened in the CVD films. These differences in the PL spectra may be associated with internal strain and high concentrations of charged centers in CVD SiC layers. Recently it has been reported [8] that cubic CVD films deposited on hexagonal Lely-grown substrates exhibit a PL spectrum whose quality is very close to that of cubic Lely crystals.

In Fig. 1, spectrum (a) is obtained from a film deposited with a C:Si gas source ratio of 2.4. The zero-phonon line (ZPL) and each of the phonon replicas of the nitrogen bound exciton (NBE) exhibit a weak shoulder on the low energy side. It is found that the intensity of these shoulders is greatly enhanced for lower C:Si ratios as shown in spectrum (b) of Fig. 1, which corresponds to a C:Si ratio of 1.2 [15]. This observation suggests that the recombination centers responsible for these processes might be associated directly or indirectly with non-stoichiometric defects. Indeed, thermal quenching studies of the exciton PL spectra [15] yielded activation energies of 11 meV for the NBE and 17 meV for the shoulders, indicating that the shoulders originate from a different defect. This is shown in spectrum (c) of Fig. 1, which is the NBE spectrum of the sample (b) measured at 15 K instead of 5 K as in (a) and (b). The weaker shoulders of the 5 K spectrum (b) have now become dominant. Assuming that this emission line is due to an exciton bound to another donor, and that Haynes' rule [19] can be applied, one can estimate 90–120 meV for its binding energy. This energy value is much larger than the 15–20 meV donor observed by Hall measurements, which suggests that they are different donors.

In Fig. 2 we show the strong dependence of the PL spectrum (using the sample with a C:Si ratio of 1.2) upon excitation intensity. The spectra (a)

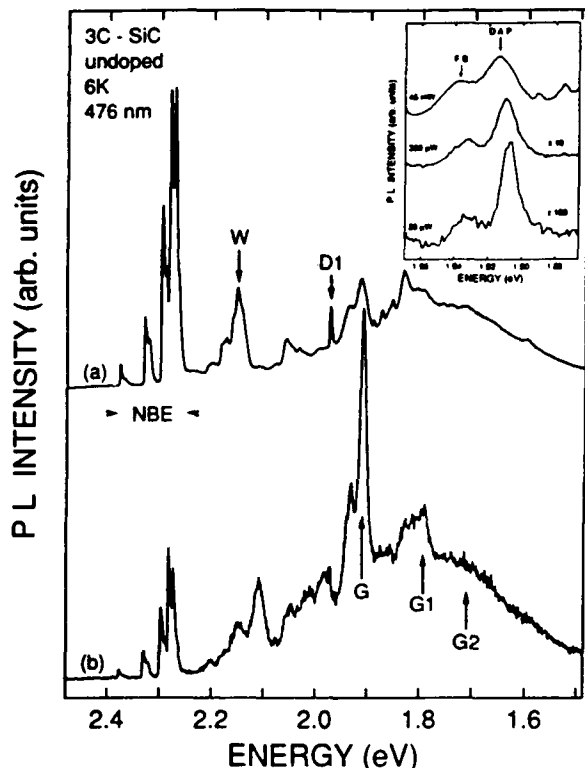


Fig. 2. Low temperature PL spectra obtained at (a) 2 W cm^{-2} and (b) 0.02 W cm^{-2} from film with C:Si ratio of 1.2. The inset shows variations in the FB and DAP G band PL spectra over a three-order-of-magnitude change in excitation intensity.

and (b) were obtained at high (2 W cm^{-2}) and low (0.02 W cm^{-2}) power respectively. Spectrum (a) is typical of a high power PL spectra reported for undoped n-type 3C-SiC CVD films. The band edge PL spectrum is dominated by NBE lines, but other features associated with structural defects are also observed at lower energy; the bands W (2.15 eV) D1 (ZPL at 1.972 eV) and G (ZPL at about 1.91 eV) [13, 14, 16, 17, 20] are indicated in the figure. We are particularly interested in the G band because it is the dominant feature of the low power PL spectra from all the undoped films that we have studied. This suggests that the G band has a long radiative lifetime compared with the NBE, W and D1 bands, which is characteristic of radiative recombination at an extended defect such as a donor-acceptor pair (DAP). The inset in Fig. 2 shows the G band as a function of incident laser power. The red shift of the G band peak position at lower powers and its association with a power-independent band at slightly higher energy are typical of DAP and

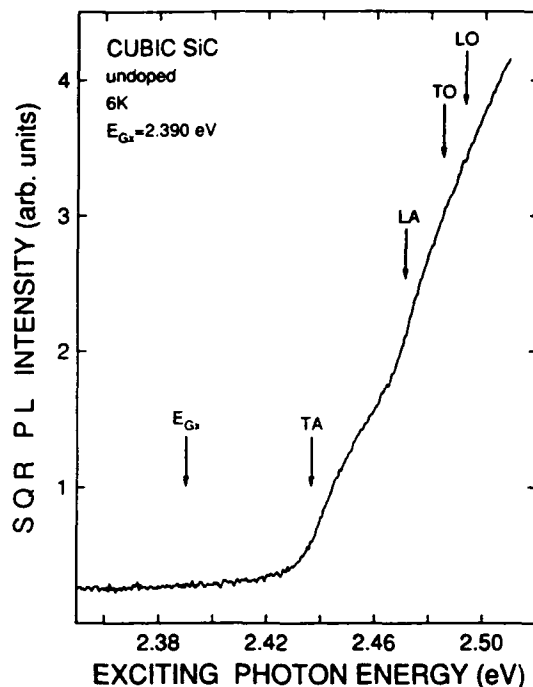


Fig. 3. Square root of integrated PL intensity as a function of photon energy for CVD cubic SiC film with C:Si gas source ratio of 1.2. The emitted phonons, measured from the PL spectra, are indicated in the spectrum.

free-to-bound (FB) emission at an acceptor site. Recently, Freitas and Bishop reported a thorough study of the G band and its phonon replicas as a function of excitation intensity and sample temperature [17, 21], which yielded an acceptor binding energy of 470 meV. On the basis of the observation of the G band in samples from different laboratories, they suggested the possibility that the G band may be at least partially responsible for the high compensation level observed by Hall effect measurements in undoped cubic SiC [9-12]. Despite the association of the G band with a deep acceptor level and its possible correlation with extended structural defects [16], the complete identification of the G band remains to be determined.

In Fig. 3 we show the PLE spectrum of the undoped film discussed in Fig. 2. These data were acquired with the sample at 6 K using a 0.22 mm double spectrometer and a xenon lamp as light source. The exciting light was excluded with appropriate color gas filters and the integrated PL intensity was plotted as a function of the double-spectrometer wavelength. The square root of the integrated PL intensity is plotted against the exciting photon energy (Fig. 3) in analogy with

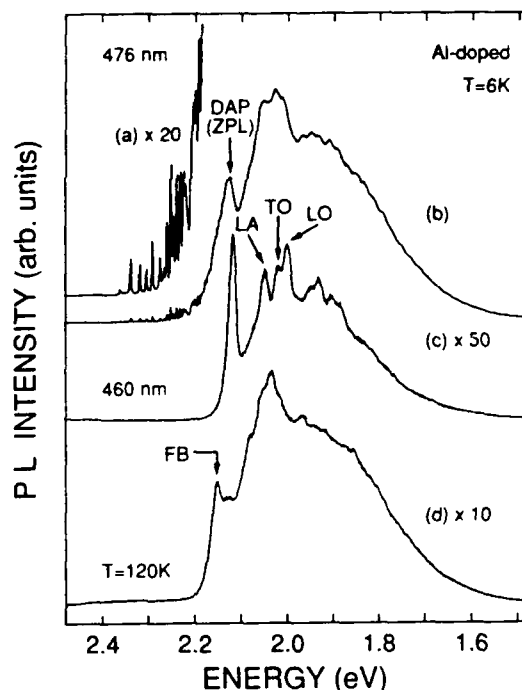


Fig. 4. CW PL spectra from aluminum-doped 3C-SiC film: (a) magnified sharp line, close pair spectra; (b) full spectrum showing close pair spectra, distant pair band at 2.12 eV and its phonon replicas at lower energy. Spectrum (c) was excited by 0.1 mW cm^{-2} of 460 nm light from a xenon lamp and a double monochromator. Spectrum (d), acquired with the sample at 120 K, shows the aluminum FB transition.

optical absorption measurements. The exciton energy gap ($E_{G,x}$) was obtained from ref. 18, but the positions of the phonon replicas were measured from the NBE PL spectrum of the sample. The observed shape is characteristic of phonon-assisted indirect transition [22]. Our result is in good agreement with absorption measurements reported by Choyke *et al.* in bulk 3C-SiC [18]. The "lack of sharpness" around the transverse acoustic (TA) phonon may be associated with the high background carrier concentration observed in these films. We have also carried out PLE experiments in aluminum-doped films, but these results will be discussed elsewhere.

A typical DAP spectrum observed in aluminum-doped 3C-SiC CVD film at 6 K [12, 15, 23] is shown in Fig. 4. The sharp line spectrum seen between 2.20 and 2.35 eV shown in curve (b) and magnified in curve (a) is similar to the DAP spectra reported by Choyke and Patrick [24] in aluminum-doped Lely-grown crystals and is attributed to radiative recombination at close nitrogen donor-aluminum acceptor pairs. At lower excitation intensity the distant pairs are

preferentially observed because of their longer radiative lifetime. As a result, the close DAP lines are not observed and the distant DAP band exhibits an expected narrowing and shift to lower energy [25] as shown in spectrum (c). At higher temperature, above 60 K (dependent on doping level and laser excitation power), the nitrogen donors are thermally ionized and the recombination process is dominated by transitions involving an electron in the conduction band and a hole bound to the neutral acceptor, or FB transitions. This behavior is presented in spectrum (d). A detailed study of the temperature dependence of DAP bands in cubic SiC films was reported by Freitas *et al.* in ref. 15, where the nitrogen donor and aluminum acceptor binding energies were determined to be 54 and 257 meV respectively.

Pulsed PL experiments in aluminum-doped samples show decay curves which cannot be assigned to a center with a unique relaxation time. Decay curves obtained in the spectral range associated with close pairs show shorter decay times than those measured from the distant pair band [26]. These observations are all consistent with the CW PL data.

4. Conclusions

On the basis of the above discussion it is evident that PL spectra of undoped cubic SiC films deposited on silicon substrates are characterized by nitrogen donors and a deep acceptor with binding energies of about 54 and 470 meV respectively. The deep acceptor, which seems to be associated with extended defects, may be partially responsible for the observed high compensation level in these films. The PLE spectrum shows the characteristic shape of indirect gap materials. The successful use of PLE suggests that this technique can be conveniently applied to study thin semiconductor films.

Acknowledgments

We would like to thank P. E. R. Nordquist Jr. and M. L. Gipe of the Naval Research Laboratory for providing the samples used in this experiment. This work was partially supported by the Office of Naval Research.

References

- 1 S. Nishino, J. A. Powell and H. A. Will, *Appl. Phys. Lett.*, 42 (1983) 460.

- 2 A. Addamiano and P. H. Klein, *J. Cryst. Growth*, 70 (1984) 291.
- 3 H. S. Kong, J. T. Glass and R. F. Davis, *Appl. Phys. Lett.*, 49(1986) 1074.
- 4 R. F. Davis, G. Kelner, M. Shur, J. W. Palmour and J. A. Edmond, submitted for publication.
- 5 K. Shibahara, T. Saito, S. Nishino and H. Matsunami, *Proc. 18th Int. Conf. on Solid State Devices and Materials, Tokyo, 1986*, pp. 717-718.
- 6 J. A. Powell, L. G. Matus, M. A. Kuczmaerski, C. M. Chorey, T. T. Cheng and P. Pirouz, *Appl. Phys. Lett.*, 51 (1987) 823.
- 7 H. S. Kong, B. L. Jiang, J. T. Glass, G. A. Rozgonyi and K. L. More, *J. Appl. Phys.*, 63(1988) 2645.
- 8 J. A. Powell, D. J. Larkin, L. G. Matus, W. J. Choyke, J. L. Bradshaw, L. Henderson, M. Yoganathan, J. Yang and P. Pirouz, *Appl. Phys. Lett.*, 56(1990) 1353.
- 9 A. Suzuki, A. Uemoto, M. Shigeta, K. Furukawa and S. Nakajima, *Appl. Phys. Lett.*, 49(1986) 450.
- 10 B. Segall, S. A. Alterovitz, E. J. Haugland and L. G. Matus, *Appl. Phys. Lett.*, 49(1986) 584.
- 11 B. Segall, S. A. Alterovitz, E. J. Haugland and L. C. Matus, *Appl. Phys. Lett.*, 50(1987) 1533.
- 12 W. E. Carlos, W. J. Moore, P. G. Siebenmann, J. A. Freitas Jr., R. Kaplan, S. G. Bishop, P. E. R. Nordquist Jr., M. Kong and R. F. Davis, *MRS Symp. Proc.*, 97 (1987) 253.
- 13 J. A. Freitas Jr., S. G. Bishop, A. Adamiano, P. H. Klein, H. J. Kim and R. F. Davies, *MRS Symp. Proc.*, 46 (1985) 581.
- 14 J. A. Freitas Jr., S. G. Bishop, J. A. Edmond, J. Ryu and R. F. Davis, *J. Appl. Phys.*, 61 (1987) 2011.
- 15 J. A. Freitas Jr., S. G. Bishop, P. E. R. Nordquist Jr. and M. L. Gipe, *Appl. Phys. Lett.*, 52(1988) 1696.
- 16 W. J. Choyke, Z. C. Feng and J. A. Powell, *J. Appl. Phys.*, 64(1988) 3163.
- 17 J. A. Freitas Jr. and S. G. Bishop, *Appl. Phys. Lett.*, 55 (1989) 2757.
- 18 W. J. Choyke, D. R. Hamilton and L. Patrick, *Phys. Rev.*, 133(1964) A1163.
- 19 J. R. Haynes, *Phys. Rev. Lett.*, 4(1960) 361.
- 20 W. J. Choyke and L. Patrick, *Phys. Rev. B*, 2(1971) 6.
- 21 J. A. Freitas Jr. and S. G. Bishop, *MRS Symp. Proc.*, 162 (1990) 495.
- 22 T. P. McLean, *Progress in Semiconductors*, Vol. 5, Heywood, London, 1960, p. 55.
- 23 S. G. Bishop, J. A. Freitas Jr., T. A. Kennedy, W. E. Carlos, W. J. Moore, P. E. R. Nordquist Jr. and M. L. Gipe, in G. L. Harris and C. Y.-W. Yang (eds.), *Springer Proceedings in Physics*, Vol. 34, *Amorphous and Crystalline SiC*, Springer, Berlin, 1989, p. 90.
- 24 W. J. Choyke and L. Patrick, *Phys. Rev. B*, 2(1970) 4959.
- 25 P. J. Dean, in J. O. McCaldin and Y. G. Somarjai (eds.), *Progress in Solid State Chemistry*, Vol. 8, Pergamon, Oxford, 1973, p. 1.
- 26 J. A. Freitas Jr., S. G. Bishop, P. B. Klein, P. E. R. Nordquist Jr. and M. L. Gipe, in M. M. Rahman, C. Y.-W. Yang and G. L. Harris (eds.), *Springer Proceedings in Physics*, Vol. 43, *Amorphous and Crystalline SiC*, Springer, Berlin, 1989, p. 106.

139083

3307

200 0.

82084

OPTICAL EVIDENCE OF REDUCTION OF RADIATIVE DEFECTS IN DIAMOND FILMS GROWN BY ACETYLENE-OXYGEN FLAMES

J.A. Freitas, Jr.^{*}, U. Strom, K. Doverspike, C.M. Marks^{**} and K.A. Snail
Naval Research Laboratory, Washington, DC 20375-5000
^{*}Sachs/Freeman Associates Inc., Landover, MD 20785-5396
^{**}NRC Postdoctoral Fellow

ABSTRACT

Raman scattering and photoluminescence spectroscopies have been used to characterize polycrystalline diamond films deposited on molybdenum substrates by laminar and turbulent premixed oxygen-acetylene flames in air. Samples deposited under laminar flame conditions are characterized by a high degree of incorporation of nitrogen-vacancy complexes. However, samples deposited with a turbulent flame show a significant decrease in the concentration of these defects and a reduction of the amorphous carbon film component.

INTRODUCTION

One of the most challenging problems in diamond film research has been the growth of high quality, monocrystalline films on a heterogeneous substrate. Solution of the problem requires an improved understanding of the nucleation and growth mechanism, which in turn may depend on the details of the deposition technique.

Combustion assisted chemical vapor deposition (CACVD) in open atmosphere has attracted the attention of many research groups because of the instrumental simplicity and high growth rate (1,2). One of the basic problems with this technique, other than the polycrystallinity of the films, is the undesirable incorporation of nitrogen impurities during the film deposition (3,4). Recently, Snail et al. (5) have reported the synthesis of polycrystalline films in a turbulent flame with very low levels of incorporation of nitrogen impurities. These results are very important since they allow the possibility of the study of in situ doping.

In this work we report a comparative study of polycrystalline films deposited in molybdenum substrates using laminar and turbulent premixed oxygen-acetylene flames in air. Low and high resolution room temperature Raman scattering (RS) experiments were used to evaluate the film quality. Low temperature photoluminescence (PL) experiments were performed to monitor the incorporation of nitrogen and nitrogen-vacancy complexes.

EXPERIMENTAL TECHNIQUE

We have examined free-standing films deposited on molybdenum substrates by CACVD, in the laminar and turbulent flame regimes. The film deposition was performed in ambient air using a commercial oxygen-acetylene brazing torch with 1.17 mm and 1.85 mm diameter orifice tips for laminar (1) and turbulent (5) flame conditions, respectively. High purity oxygen (99.99%) and acetylene (99.6%) were used as source gases, with the acetylene passing through an activated charcoal trap to remove residual acetone (6). For the samples ex-

amined in this work the ratio (R_f) of the oxygen-acetylene flow varied from 1.017 to 1.080. The substrates were positioned in the feather about 1-2 mm from the primary flame front, and adjusted so as to maintain a surface temperature $\sim 900^\circ\text{C}$. The substrate temperature was adjusted by varying the fraction of the length by which a $3/8$ " threaded molybdenum rod was inserted into a threaded hole in the water cooled copper substrate mount (2). The substrate temperature, during the growth, was monitored with a two-color infrared pyrometer. The films deposited under laminar flame conditions are nearly transparent in the center, degrading to a gray-brown color at the edges, with crystallite size varying from sub-micron to a few microns. Similar morphology was observed in films deposited with flames in the turbulent regime, except for the absence of the colored rings. An observed decrease of the film growth rate under turbulent conditions by a factor of two or three, may be associated with simultaneous etching (5).

The RS measurements were carried out at room temperature. The 514.5 nm and 488.0 nm argon ion laser lines provided between 10 and 100 mW of laser power with the laser spot size of approximately 150-200 μm . The scattered light was dispersed by a scanning double grating spectrometer with 85 cm focal length and a built in spatial filter to increase the straight light rejection. The analyzed scattered light was detected by a GaAs photomultiplier tube, operated in a photon counting mode.

The PL measurements were performed with the sample at 5-6 K, by means of a liquid and/or continuous gas flow He cryostat. The sample temperature was monitored by a solid state sensor located in the copper sample holder, and its temperature was stabilized by a temperature controller with sensitivity of ± 0.1 K. We have used the UV and blue (351.1 nm, 457.9 nm, 476.5 nm and 488.0 nm) argon ion laser lines to excite the defects in our sample, however we will present only results with the 488.0 nm (2.54 eV) laser line. The light emitted by the samples was dispersed and analyzed by the same experimental set-up as was used for the RS experiment.

RESULTS AND DISCUSSION

The low temperature PL spectra of two films deposited in the laminar flame regime are presented in Fig. 1. The spectrum (a) is from a sample grown with $R_f = 1.017$ and substrate temperature (T_s) varying between 885 and 915 $^\circ\text{C}$. The spectrum (b) was obtained from a sample grown with $R_f = 1.031$ and $T_s = 890^\circ\text{C}$. Both spectra are similar in regard to the overall shape of PL spectrum and the number of observed defect PL bands. Differences in the spectra include the reduction of the zero phonon line (ZPL) linewidth (reduced by 4 to 5 times), in spectrum (b), and the relative intensity between the Raman peaks associated with the diamond and the amorphous carbon (a-C) content. The gradual increase in the spectral intensity observed on the high energy side of both spectra are due to laser Rayleigh scattering. The peak "1" at 2.465 eV is the ZPL of the H3 center, which may be associated with a single vacancy (V) complexing with a nitrogen (N) cluster (N-V-N?) (7). The peak "2" at 2.375 eV is the first order TO/LO phonon, and the first broad shoulder on its low energy side is the phonon associated with the a-C film content. Two other features, clearly observed in spectrum (b), are the small peaks at 2.282 eV ("3") and 2.156 eV ("4"). The first feature has not been correlated with any defect previously observed in natural diamond, and the second feature is the 575 nm center which has been tentatively assigned to a nitrogen-vacancy complex (V-N-V?) (7). The most intense peak ("5") in the spectra is the ZPL at 1.946 eV (637 nm center) which has been assigned to a single nitrogen-vacancy pair (N-V) (7,8).

Fig. 2 shows the first order low resolution Raman spectra of the same samples analyzed on Fig. 1. High resolution measurements (bandpass $\sim \pm 0.25$ cm^{-1}), carried out on these

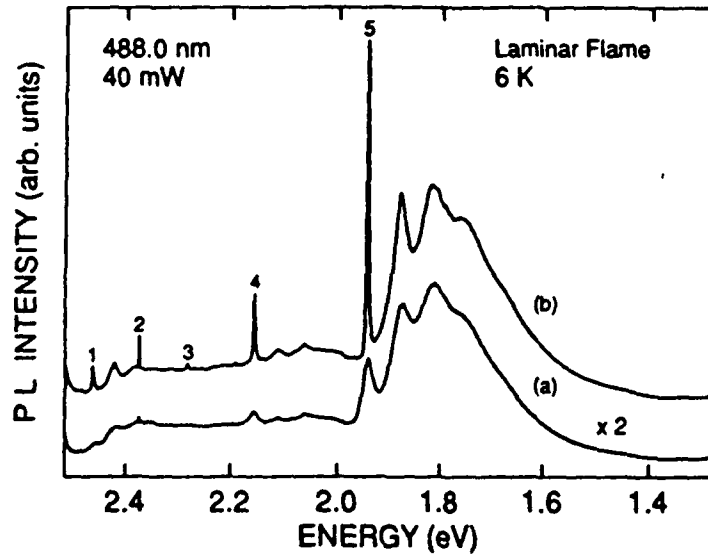


Fig. 1. Photoluminescence spectra obtained at 6K from two CACVD films deposited in the laminar flame regime. The peaks "1,3, and 4" are due to nitrogen-vacancy complexes. The peak "2" is the first order diamond phonon, and the peak "3" is an unidentified center. The spectra (a) and (b) have been offset in the vertical axis.

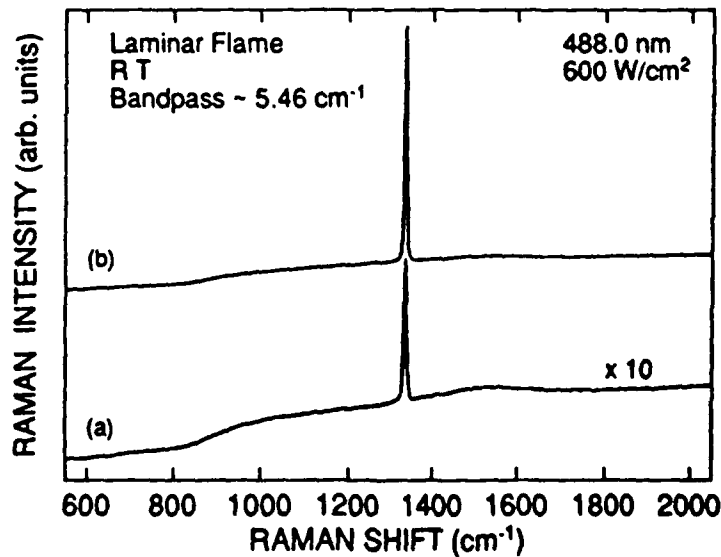


Fig. 2. Low resolution room temperature (RT) Raman spectra of the two films shown in Fig. 1. The phonons are represented as peak "2" in Fig. 1. The spectra (a) and (b) have been offset in the vertical axis.

samples, yield a phonon peak position at 1333.60 cm^{-1} and full width at half maximum (FWHM) of 4.53 cm^{-1} in spectrum (a), and 1333.30 cm^{-1} and FWHM = 2.94 cm^{-1} for the phonon in spectrum (b). In Fig. 2, taking the phonon intensity as reference, we observe a relative reduction of the PL background and the a-C component in this films.

The ~35% reduction of the linewidth of the ZPL and first order phonon lines is correlated with the decrease of the a-C component in the films. This observation is consistent with an increase in the average crystallite size (9) which yields higher quality diamond as well as reduced grain boundary regions, which are the likely location of the a-C deposits(10).

In Fig. 3 is shown the first order low resolution Raman spectrum of a polycrystalline diamond film deposited at $T_s = 900^\circ\text{C}$ in a premixed ($R_f = 1.08$) turbulent oxyacetylene flame. The extremely low PL background and a-C content in this film is noted. High resolution Raman measurements yield a phonon peak position at 1333.30 cm^{-1} and FWHM of 3.00 cm^{-1} . For calibration and comparison, we had performed high resolution RS measurement (bandpass $\pm 0.25 \text{ cm}^{-1}$) in a natural type IIa diamond heat sink. The result is a phonon peak position at 1333.50 cm^{-1} and FWHM of 2.40 cm^{-1} . The agreement (within experimental error) of the phonon peak position for films grown in the laminar and turbulent flame regimes with the type IIa diamond suggests that the films are rather strain free (10). The 25% phonon line broadening observed in the FWHM of our films in comparison with the type IIa diamond seems to be associated with the polycrystalline character of the films, in which grain sizes vary from the submicron level to a few microns. It needs to be emphasized that many crystallites and inter-grain regions are probed with the relatively large laser spot size used in the present experiment.

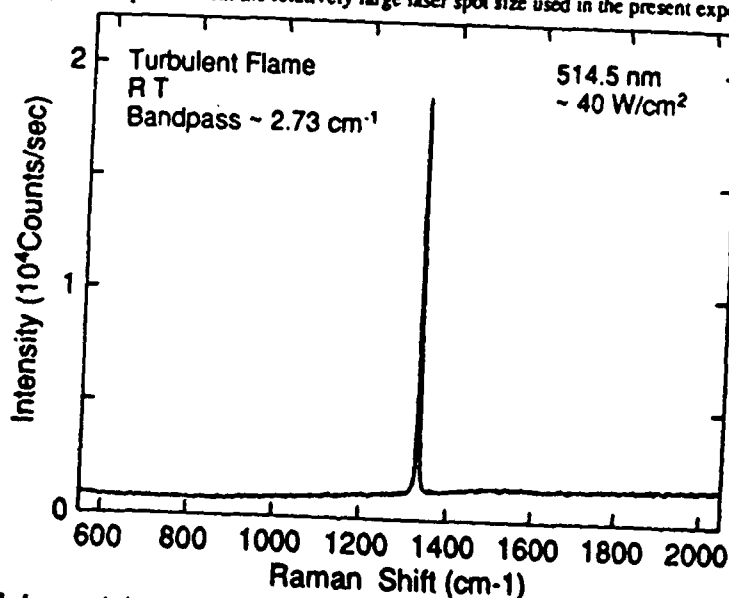


Fig. 3. Low resolution room temperature (RT) Raman spectrum of an CACVD film deposited under turbulent flame condition. The phonon peak position is represented as peak "2" in the PL spectra (Fig. 1. and Fig. 4.)

The low temperature PL spectrum of the film analyzed in Fig. 3 is presented in Fig. 4. This spectrum is quite different from those shown in Fig. 1, since the dominant feature is the

strong first order phonon peak at 2.375 eV. The defect ZPLs and side band phonons are extremely weak, and can be observed only with a high gain scale. The continuous decrease in PL intensity from the begin of the spectrum to 2.48 eV is due to the laser Raleigh scattering. The broad feature between 2.1 and 2.0 eV is probably due to the spectrometer response. The dominant emission of the 637 nm center (N-V) as observed in Fig. 1, has been reduced to a weak band from 1.95 to 1.70 eV, in Fig 4. The regularly spaced small peaks from 1.75 to 1.4 eV are due to interference effects in the film. It is emphasized that the strong PL background dominated by intense side band phonons generally observed in laminar flame deposited samples, has been replaced by a weaker, almost featureless background in the sample deposited under turbulent flame conditions. The weakness of the a-C component observed in the low energy side of the phonon in Fig. 4 is also noted.

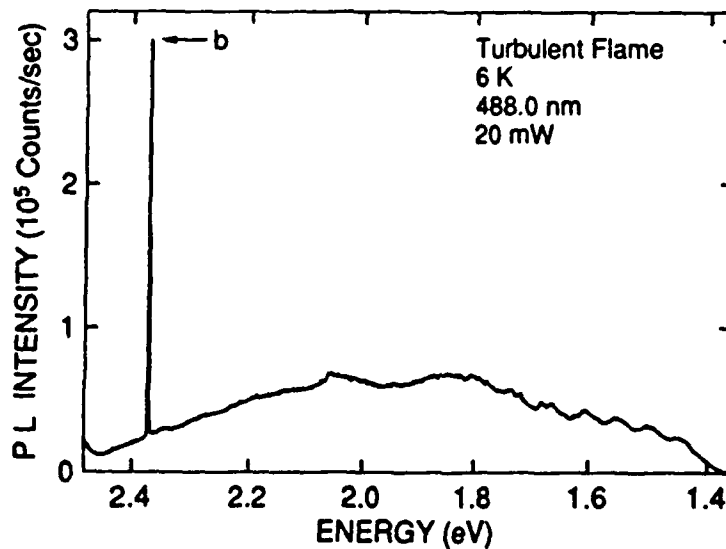


Fig. 4. Low temperature (6 K) photoluminescence spectrum of the CACVD film analyzed in Fig. 3. The peak "2", the first order diamond phonon, is the singly dominant feature observed.

CONCLUDING REMARKS

Low and high resolution RS experiments were successfully carried out on polycrystalline films deposited on molybdenum substrates by CACVD to evaluate the material quality. Although good quality films can be deposited with laminar flames, films deposited in the turbulent flame regime show very low amorphous carbon content and very small PL background. Low temperature PL measurements of films deposited under laminar flame conditions exhibit the presence of strong luminescence bands associated with nitrogen-vacancy complexes probably incorporated during the film deposition (3). PL experiments performed in samples deposited under turbulent flame conditions reveal an extremely low level of nitrogen-vacancy complexes. This result is extremely important because low level of intrinsic impurities and defects are basic requirements to achieve controlled doping.

ACKNOWLEDGMENTS

This work was supported in part by the Office of Naval Research.

REFERENCES

1. L.M. Hanssen, W.A. Carrington, J.E. Butler, and K.A. Snail, *Mat. Lett.*, **7**, 289 (1988).
2. L.M. Hanssen, K.A. Snail, W.A. Carrington, J.E. Butler, S. Kellog, and D.B. Oakes, *Thin Solid Films*, **196**, 271 (1991).
3. J.A. Freitas, Jr., J.E. Butler and U. Strom, *J. Mater. Res.*, **5**, 2502 (1990).
4. J.A. Freitas, Jr., U. Strom, J.E. Butler, and K.A. Snail *Proc. of The 2nd Intl. Conf. on New Diamond Science and Technology* (MRS, Washington, DC September 1990), p. 723.
5. K.A. Snail, C.J. Craigie, R.G. Vardinam, C.M. Marks, and J.A. Freitas, Jr., *Proc. of The 2nd Intl. Symp. on Diamond Materials (ECS - 2)*, Washinton, DC May 1991, vol. 91-8, p. 91.
6. D.C. Manning, *Atomic Absorption Newsletter*, **7**, 44 (1968).
7. J. Walker, *Rep. Prog. Phys.* **42**, 1605 (1979).
8. G. Davies, *Rep. Prog. Phys.*, **44**, 787 (1981).
9. A.T. Collins and S.H. Robertson, *J. Mat. Sci. Lett.* **4**, 2223 (1971).
10. Y. Sato, C. Hata, T. Ando and M. Kamo, *Proc. of The 2nd Intl. Conf. on New Diamond Science and Technology* (MRS, Washington, DC September 1990), p. 537.

PROG. OF THE 2nd INT. SYMP. ON
DIAMOND MATERIALS
PART. VOL. 91-8
THE ELECTROCH. SOC.
(1991)

**GROWTH OF HIGH QUALITY DIAMOND FILMS IN A
TURBULENT FLAME**

K. A. Snail, C. J. Craigie[^], R. G. Vardiman^{*}, C. M. Marks, and J. A. Freitas, Jr.⁺
Optical Sciences Division, Code 6522

^{*}Materials Science and Technology Division, Code 6325
Naval Research Laboratory
Washington, DC 20375-5000

[^]Optical Sciences Center
University of Arizona
Tucson, AZ 85721

⁺Sachs Freeman and Associates
1401 McCormick Drive
Landover, MD 20785-5396

ABSTRACT

High quality polycrystalline diamond films have been synthesized in a turbulent premixed, oxygen-acetylene flame, using a commercial brazing torch. The quality of the films was measured by high resolution Raman spectroscopy, scanning and transmission electron microscopy, hemispherical transmittance measurements in the UV, visible and infrared, and photoluminescence spectroscopy. Turbulence was achieved by operating the torch with a sufficiently high Reynolds number. The presence of turbulence was confirmed by observations of changes in the flame shape, the characteristic sound of the flame, and calculation of the Reynolds number.

Most combustion processes either involve or are dependent on turbulence. While several groups have investigated diamond growth in laminar flames (1,2), none have examined the turbulent case. One of the outstanding features of turbulent flames is that the rates of transfer and mixing can be several orders of magnitude higher than in laminar flames (3). This is due to the presence of eddies, which can have an effective diffusion coefficient which is larger than the molecular diffusion coefficient by one to two orders of magnitude, depending on the Reynolds number (4). Consequently, the transport of molecules, heat and momentum can be greatly enhanced in turbulent, as compared to laminar flow. If the

diamond growth rate in laminar premixed flames is transport limited, then that rate could be significantly increased by the introduction of turbulence. Recently we have reported on the growth of high quality diamond films in a turbulent, premixed, oxygen-acetylene flame (5). In this paper we provide more details about the growth conditions and additional analyses of the quality of the deposited diamond films.

The apparatus used in this study consisted of a commercial oxygen-acetylene brazing torch, a gas mass flow control system, a water cooled copper (Cu) substrate mount, and a two-color infrared (IR) pyrometer that was used to monitor the substrate temperature during growth (see Figure 1). The substrates consisted of ~1.5 cm long sections of 3/8"-16 molybdenum (Mo) threaded rod, slotted on one end and polished with silicon carbide and diamond grit on the other. The temperature of the Mo substrates was controlled by adjusting the penetration of the substrates into a threaded hole in the water cooled Cu substrate mount. A more detailed description of this experimental setup can be found elsewhere (6). High purity oxygen (99.99%) and acetylene (99.6%) were used as source gases, with the acetylene passed through an activated charcoal trap to remove residual acetone (7). For this study the ratio (R_f) of the flow rate of oxygen to acetylene was chosen so that a small excess acetylene feather existed just beyond the primary flame front. The substrates were positioned in the feather about 1-2 mm from the primary flame front (see Fig. 1), and adjusted so as to maintain a surface temperature of ~900°C for one hour. Photographs of flame shapes were performed with a Bausch and Lomb StereoZoom7 microscope and a standard polaroid attachment.

Figures 2a and 2b show photographs of premixed oxygen-acetylene flames generated with 0.89 mm and 1.85 mm diameter orifice tips, respectively. The oxygen/acetylene flow ratio and the average gas velocity at the orifice are the same for both flames. Turbulent flow can cause a rounding and broadening of the primary flame front, as shown in Figure 1b, and introduce a characteristic hissing sound (8). The rounding of the flame front may be due to the rounding of the velocity profile observed when the flow in a tube changes from laminar to turbulent. The broadening occurs when the scale of the turbulence (i.e. the eddy diameter) is significantly greater than the flame front thickness (9). Instantaneous micro-Schlieren photographs have revealed that the thickened flame front seen by the eye is really the time averaged envelope of a fluctuating, corrugated flame front (10). The Reynolds number ($Re = vdp/\mu$) of the flow in the tube supporting the flames shown in Fig. 2a and 2b was calculated to be 5,900, and 12,200 respectively, assuming a temperature of 300°K and a 1:1 mixture of oxygen: acetylene. Higher gas temperatures

could lower these Re values (due to the viscosity's \sqrt{T} dependence), but the temperature rise of the gases in the burner tip was estimated to be negligible. The high Reynolds numbers quoted here for flow in the tube supporting a laminar flame may be related to the observation (11) that Bunsen burner flames can appear laminar when the gas flow in the burner tube is turbulent.

The laminar and turbulent operational regimes (12) of a Bunsen burner are shown as a function of the average gas velocity and the burner diameter in Figure 3. We expect that oxygen-acetylene torches will exhibit similar, but not identical, characteristics. Note that both the laminar and turbulent regimes are bounded from below by the flashback limit, and from above by the blow-off limit. These limits correspond to the flame either propagating back down the burner tube or becoming unstable and detaching from the burner tip, respectively. The blow-off and flash back limits are defined semi-empirically in terms of two critical velocity gradients which are expressed in terms of the quenching distance and the average gas velocity. The quenching distance corresponds to the tube diameter below which a flame cannot propagate, due to heat losses to the walls; this sets a lower limit on the burner diameter. For stoichiometric mixtures of oxygen and acetylene, the quenching distance is about 0.1 mm. The laminar and turbulent regimes are separated by a hyperbolic wedge defined by the Reynolds number values corresponding to the laminar-turbulent transition at the flame front. Since these Reynolds numbers are not defined at the flame front, the values may be higher than the normal 2,300-3,200 values that are quoted for turbulent flow in tubes. The velocity profile in the burner tube changes significantly when the flow changes from laminar to turbulent, and hence the critical velocity gradients and slope of the the blow-off and flash-back limits shown in Fig. 3 may also change in passing through the laminar-to-turbulent transition.

The first order Raman spectrum of a polycrystalline diamond film grown at $T_S = 900$ °C in a premixed ($R_f = 1.08$), turbulent oxygen-acetylene flame was measured at low power with a bandpass of 2.7 cm^{-1} and is shown in Figure 4. Note the absence of any significant graphite or a-C components in the spectrum and the small luminescence background increases with larger shifts from the excitation wavelength. A measurement of the high resolution Raman spectrum of the same sample was also performed. The film's diamond peak position is located at $1333.3 \pm 0.2 \text{ cm}^{-1}$ and it's linewidth (FWHM) is 3.0 cm^{-1} . For comparison, a natural type IIA diamond sample was also analyzed; the peak position and FWHM were found to be 1333.5 cm^{-1} and 2.4 cm^{-1} , respectively.

The low temperature photoluminescence spectra of the polycrystalline sample analyzed in Figure 4 is shown in Figure 5. We have used a 488 nm laser line and a power of 20 mW for this measurement. Note that the spectra exhibits no detectable vacancy and/or nitrogen related complexes that have been observed (12) in diamond grown in laminar oxygen-acetylene flames. The regularly spaced small peaks from 1.4-1.7 eV are due to interference effects in the film. Note that the spectrum is dominated by a strong first order Raman peak at 2.375 eV, and a broad almost featureless luminescence band. The broad band may be due to the recombination of extended defects, as observed in natural diamond. The features at 1.8-1.9 eV and 2.0-2.1 eV are probably due to the spectral response of the spectrometer. A transmission electron micrograph of a film grown under similar conditions is shown in Figure 6a. The grain size is 1-2 μm . Twinning, although frequent, is not as heavy as in FACVD films which were grown and analyzed at NRL. Stacking faults may also be observed, as shown in Fig. 6b.

Diamond crystals grown on Si coated Mo substrates under the proper conditions (i. e. substrate temperature, flow ratio, position in flame) in a turbulent oxy-acetylene flame are transparent enough to allow one to image the substrate through individual crystals with an optical microscope; thin films (~10-30 μm thick) grown on Mo substrates are white and sufficiently transparent to read newsprint through. We have been able to grow well faceted crystals at substrate temperatures of 500-1200°C, depositions outside of this range have not been attempted. The UV, visible and NIR hemispherical transmittance of 10 μm thick diamond films synthesized in a turbulent flame is high throughout the UV, visible and NIR (5). A sharp absorption edge is observed at ~222nm, indicating the absence of the defect center associated with substitutional nitrogen (13). A slightly higher transmittance is observed when the rough side of the film is oriented towards the spectrophotometer's beam. This is due to total internal reflection at the rough surface of the film (14).

The diamond growth rates observed under the conditions reported in this paper are lower than those observed with a laminar oxygen-acetylene flame (2.6). In a turbulent flame, the flux of active species to the growing diamond surface is expected to increase significantly compared to a laminar flame. Recently we have determined that the boundary layer next to a substrate positioned in a flame similar to that shown in Figure 2b is laminar. Hence, the increased species flux associated with turbulent flow may not be fully realized. The increase in quality and lower growth rates for diamond synthesized in a turbulent flame suggests that the flux of growth to etchant species (15) at the substrate surface has shifted in

the direction of etching. If the entrainment of room air increases with flow rate and/or turbulence, then additional etchant species, e.g. OH, may be transported to the substrate. A thinner boundary layer may also change the ratio of growth to etchant species at the substrate if the lifetimes of critical species are close to the transport time across the boundary layer. Finally, if the level of turbulence is sufficiently high, the flame front can be discontinuous, leading to burning in isolated pockets and further changes in the growth chemistry. Previous reports of high quality diamond growth in flames (16,17,18) did not indicate that turbulent flames were employed, and flame shape drawings and/or experimental parameters from these papers suggest that the flames were laminar.

REFERENCES

- ¹Y. Hirose and M. Mitsuizumi, *New Diamond* 4(3), 34 (1988).
- ²L. M. Hanssen, W. A. Carrington, J. E. Butler, and K. A. Snail, *Mats. Ltrs* 7, 289 (1988).
- ³H. Tennekes and J. L. Lumley, *A first course in turbulence*, MIT Press, (Boston, 1972).
- ⁴U. Frisch and S. A. Orszag, *Physics Today*, p. 24, (January 1990).
- ⁵K. A. Snail and C. Craigie, *Appl. Phys. Ltrs.* 58, 1875 (1991).
- ⁶L. M. Hanssen, K. A. Snail, W. A. Carrington, J. E. Butler, S. Kellogg, and D. B. Oakes, *Thin Solid Films* 196, 271 (1991).
- ⁷D. C. Manning, *Atomic Absorption Newsletter* 7, 44 (1968).
- ⁸A. G. Gaydon and H. G. Wolfhard, *Flames: Their structure, radiation and temperature*, Chapman & Hall, p. 14, (London, 1979).
- ⁹J. A. Barnard and J. N. Bradley, *Flame and Combustion*, Chapman and Hall, p. 74 (New York, 1985).
- ¹⁰M. D. Fox and F. J. Weinberg, *Proc. Roy. Soc. A* 268, 222 (1962).
- ¹¹I. Glassman, *Combustion*, Academic Press, p. 167, (New York, 1987).
- ¹²J. A. Freitas, J. E. Butler, and U. Strom, *J. Matl. Res.* 5, 2502 (1990).
- ¹³M. Seal, *Interdisc. Sci. Rev.* 14, 64 (1989).
- ¹⁴T. P. Thorpe, A. A. Morrish, L. M. Hanssen, J. E. Butler, and K. A. Snail, *Proc. of the Conf. on Diamond Optics III*, SPIE Vol. 1325, p. 230, Intl. Soc. for Optical Engineering, (Bellingham, WA, 1990).
- ¹⁵S. J. Harris and A. M. Weiner, *Appl. Phys. Ltrs.* 55, 2179 (1989).
- ¹⁶Y. Hirose, S. Amanuma, N. Okada, and K. Komaki, *Proc. of the 1st Intl. Symp. on Diamond and Diamond-Like Films*, ECS Proc. Vol. 89-12, p. 80, May 7-12, 1989 (Los Angeles).
- ¹⁷K. A. Snail, W. A. Carrington, L. M. Hanssen, and A. A. Morrish, *Proc. Conf. on Diamond Optics II*, SPIE Vol. 1146, p. 144, Intl. Soc. for Optical Engineering, (Bellingham, WA, 1989).
- ¹⁸Y. Tzeng, C. C. Tin, R. Phillips, T. Srivinyunon and Y. Chen, *Appl. Phys. Ltrs.* 57, 789 (1990).

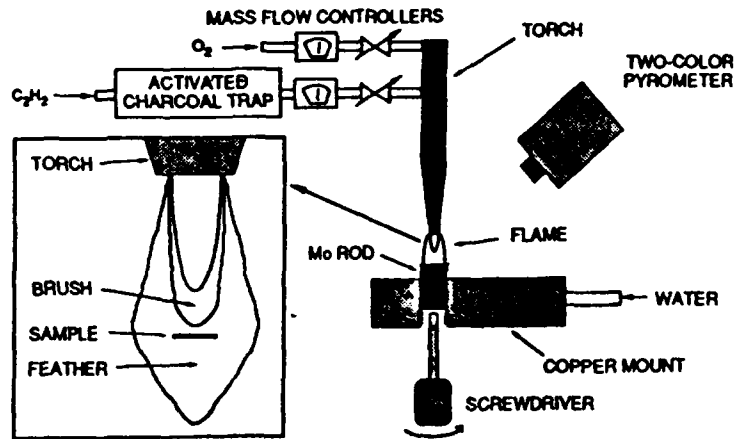


Figure 1. Experimental setup showing mass flow controllers, two color pyrometer, brazing torch and substrate mount assembly. The flame shape and sample position are indicated in the inset.

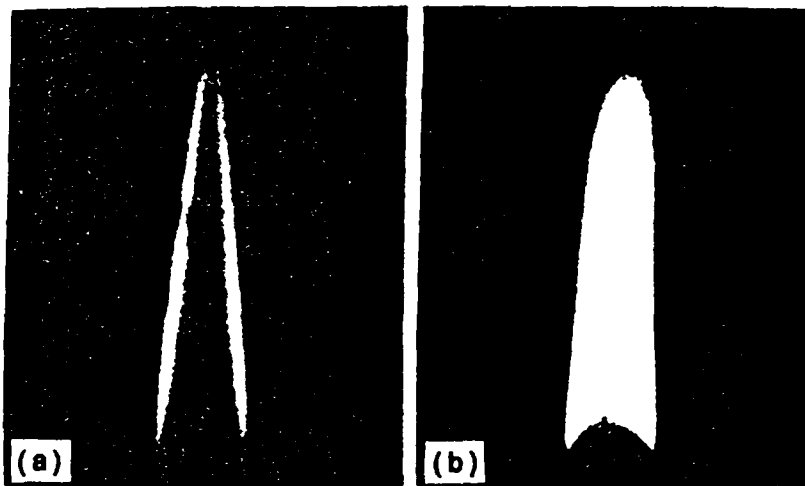


Figure 2. Photographs of premixed oxygen-acetylene flames which are (a) laminar and (b) turbulent. Note the rounding and broadening of the flame front in the turbulent case, compared to the thinner conical flame front in the laminar case.

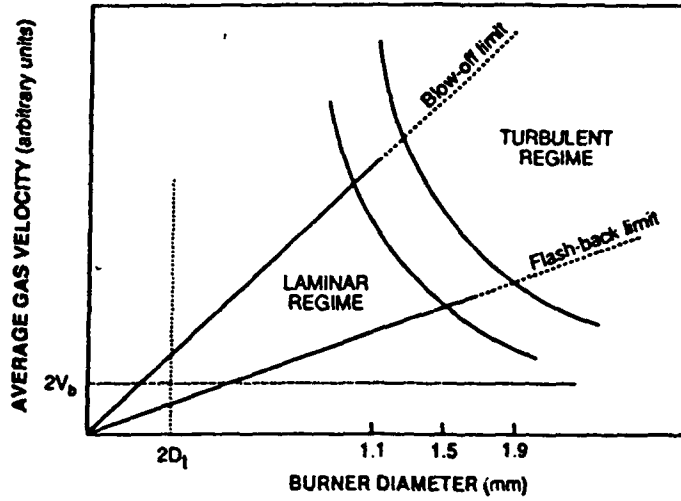


Figure 3. Operational regimes of premixed, single orifice torches. Note the flashback limit, the blow-off limit, and the hyperbolic wedge separating the laminar and turbulent regimes.

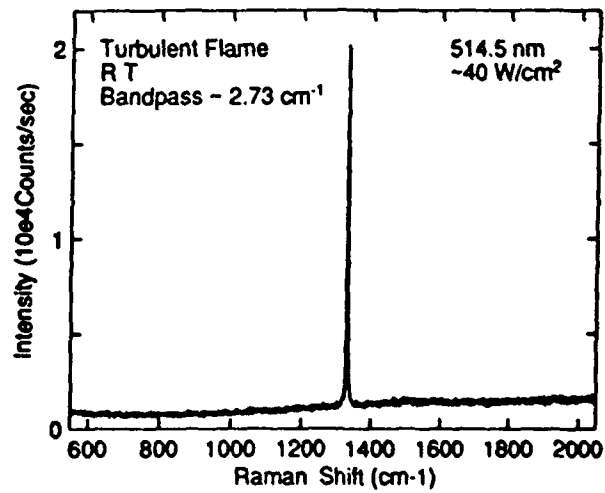


Figure 4. Raman spectrum of a polycrystalline diamond film grown in a turbulent, premixed oxygen-acetylene flame at $T_s = 900^\circ\text{C}$.

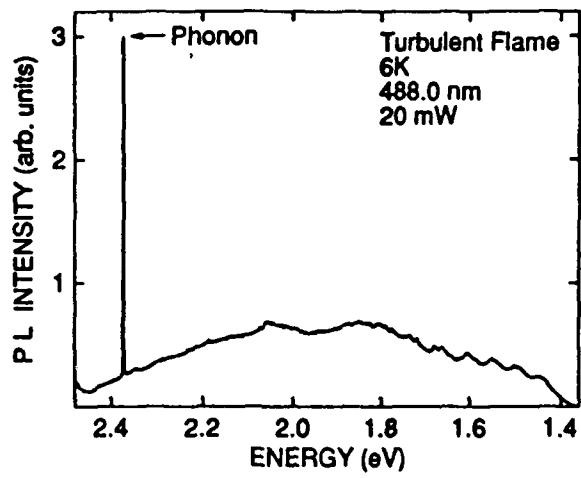


Figure 5. Low temperature photoluminescence spectrum of a diamond film grown in a turbulent oxygen-acetylene flame. Note the absence of defect bands associated with vacancies and nitrogen related complexes.

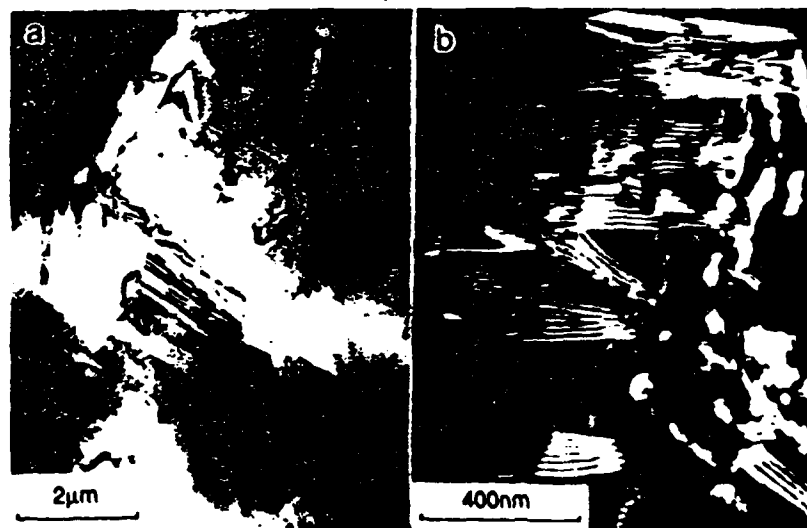


Figure 6. TEMs of a diamond film grown in a turbulent flame: (a) bright field, showing twins (b) dark field, showing stacking faults.

PROC. OF THE 2ND INT. SYMP.
DIAMOND MATERIALS
PART. VOL. 91-8
THE ELECTROCH. SOC.
(1991)

HIGH RATE HOMOEPITAXIAL SYNTHESIS OF DIAMOND IN A FLAME

K. A. Snail, J. A. Freitas^{*}, C. L. Vold^{*}, and L. M. Hanssen[†]
Optical Sciences Division, Code 6522

^{*}Material Sciences & Technology Division, Code 6322
Naval Research Laboratory
Washington, DC 20375-5000

[†]Sachs Freeman Associates
1401 McCormick Drive
Landover, MD 20785-5396

[†]Current Address: Bldg. 220, Rm. B-306,
National Institute of Standards and Technology,
Gaithersburg, MD 20899, U.S.A.

Abstract

Homoepitaxial growth of high quality, faceted diamond crystals at rates exceeding 150 microns/hour has been observed on millimeter sized {100} and {110} natural diamond seed crystals, using a laminar, premixed oxygen-acetylene flame in air. The key element in achieving such high growth rates has been a substrate temperature in the 1150-1500°C range. Microscope and naked eye observations show the original cylindrical shaped seed crystals growing into polyhedral shaped crystals with identifiable {100} and {111} faces. Examination under optical and scanning electron microscopes reveals terraces on the {100} faces. The deposited diamond is clear and exhibits Raman spectra almost identical to that of natural diamond. Laue Xray diffraction analyses have confirmed the epitaxial nature of the growth. The deposition temperatures and growth rates reported are the highest ever observed for the homoepitaxial synthesis of diamond crystals at low pressures.

Introduction

In the fall of 1988 we observed an unusual phenomena during multi-hour diamond depositions with an oxygen-acetylene flame. Frequently,

large (~100-350 microns) single crystals of diamond would begin to grow on Si substrates after about 1-3 hours [1, 2]. These large crystals typically had smooth, oriented {100} faces, and electron channeling measurements [3] indicated that the crystals were monocrystalline and that the strain in the crystal lattice was indistinguishable from natural diamond. The Raman spectra of a typical crystal exhibited a sharp 1332 cm^{-1} peak, no evidence of a-C or graphite, and a very low fluorescence background. The crystals often were found on pedestals which thermally isolated them from the substrate. Capelli [4] has used an energy balance argument to show that diamond crystals in an oxygen-acetylene flame would equilibrate above 1200°C if thermally isolated from their substrate. Unreported in the presentation of previous studies [1, 2, 3] was the observation that during long multi-hour depositions a two color pyrometer always registered temperatures >1250°C (the limit of the instrument) whenever large (>100 μm) single crystals appeared on the substrate, and that the crystals themselves had a visible brightness that was considerably brighter than the 900-1000°C substrate.

Based on these observations, we performed a series of homoepitaxial growths in a laminar, premixed oxygen-acetylene flame at substrate temperatures of 1150-1500°C. The results of these depositions are described in the following sections and in an upcoming publication [5].

Experimental Setup

The apparatus used in this study is similar to that described in previous work [6,7]. Oxygen and acetylene were metered to a commercial brazing torch with a mass flow control system. The temperature of the substrates was measured with a two-color pyrometer which was insensitive to the flame's emission. The substrates consisted of 0.5 mm thick, natural type I and type IIa diamond heat sinks with circular or square cross sections, polished on the top {100} or {110} faces, and brazed to the ends of 1.5 cm long pieces of threaded molybdenum rod with a Au-Ta compound. Although the braze material melted during the high temperature depositions, no degradation in thermal contact between the seed crystals and the Mo rod was observed during depositions up to 1500°C. Since the thermal conductivity of the seed crystals and braze material is relatively high, the seed crystal is expected to be isothermal and its temperature equal to or slightly greater than the Mo rod temperature. The temperature of the seed crystals was controlled by adjusting the penetration of the Mo rod into a water cooled Cu cylinder. A more detailed description of these procedures can be found elsewhere [5].

Results

A series of growths on three $\langle 100 \rangle$ and one $\langle 110 \rangle$ oriented diamond crystal substrates were performed at substrate temperatures of 1150, 1250, 1360, and 1500°C ($\pm 30^\circ\text{C}$), respectively. Depositions at temperatures below 1000°C consisted of small, rectangular shaped, oriented single crystal domains on $\{100\}$ seed crystals, and rough surface morphologies on $\{110\}$ seed crystals which were similar to the results reported by Janssen et al. [8]. Growths below 1000°C on both $\{100\}$ and $\{110\}$ seed crystals exhibited oriented polycrystalline growth around the perimeter the seed crystals (see Figure 1). A substrate temperature of at least 1150-1200°C appeared necessary to grow a macroscopic faceted crystal which covered the entire top surface of the seed crystal. These results are strongly dependent on the position of the seed crystal in the flame. Growth of macroscopic (e.g. 1.7 mm x 150 μm) polyhedral crystals from 1.5 mm diameter cylindrical seed crystals was observed in ~20-30 minutes at 1250°C on a $\langle 100 \rangle$ oriented crystal, and in ~10-15 minutes at 1500°C on a $\langle 110 \rangle$ oriented crystal. Large (~100 microns) randomly oriented diamond crystals were also observed to grow at each temperature on the Au-Ta braze covering the top surface of the Mo rod.

Electron micrographs of a cylindrical $\{100\}$ seed crystal before and after a one hour growth at 1250°C are shown in Figures 2a and 2b, respectively. The thickness of the deposited layer was estimated with an optical microscope equipped with a micrometer; it varied from 100-165 microns depending on position on the $\{100\}$ face. The deposited material has an octagonal shape when viewed from above (Fig 2b), with the shapes of the side faces alternating between trapezoidal and truncated parallelograms. These are the shapes expected around the 'waist' of a cubo-octahedral crystal which is truncated along a $\langle 100 \rangle$ axis which is perpendicular to the plane of the waist (the plane of the waist contains four $\langle 100 \rangle$ axes). The trapezoidal and truncated parallelogram shaped faces would thus correspond to the $\langle 111 \rangle$ and $\langle 100 \rangle$ crystallographic directions, respectively, as shown in Figure 3.

The first order Raman spectrum of the deposited crystal side of the 1250°C sample (see Fig. 2) was measured with a low laser power (40 W/cm^2), a 514.5 nm laser line, and a bandpass comparable to the phonon peak's line width, and is shown in Figure 4. Note the absence of graphite and a-C components in the spectra and the low luminescence background. High resolution Raman spectra were also acquired from this crystal. The deposited crystal's diamond peak position was located at $1333.1 \pm 0.2 \text{ cm}^{-1}$ and it's linewidth (FWHM) was 2.6 cm^{-1} . For comparison, we also

measured a natural type IIA diamond; the values obtained were 1333.5 cm^{-1} and 2.4 cm^{-1} , respectively.

The increase in the luminescence background observed in the Raman spectrum at higher frequency shifts is due to a defect band which has a zero phonon line (ZPL) at 2.155 eV, as shown in Fig. 5. The low temperature (6K) photoluminescence spectra shown in Figure 5 was excited with a 488 nm laser line and with a power of ~5mW. The two strongest bands (d,e) are located at 2.155 eV and 1.946 eV; these have been assigned (9) to a nitrogen vacancy complex and a nitrogen-vacancy (N-V) pair, respectively. Two weaker bands (a,f) at 2.464 eV and 1.682 eV correspond to the H3 center and a possible Si-related defect (9). A weak band (c) that has not been assigned to any previously observed defect was seen at 2.282 eV. The peak (b) at 2.375 eV is the 1st order Raman peak.

The observation of the polyhedral shape of the deposited crystal shown in Figure 2b and the quality of the deposited crystal's Raman spectra shown in Figure 4 suggested that the growth is monocrystalline. Laue X-ray diffraction patterns of both the seed crystal and deposited crystal sides of the 1250°C sample are shown in Figures 6a and 6b, respectively. Analysis of these patterns confirmed that the deposited diamond is monocrystalline with a <100> orientation which is epitaxially oriented with respect to the {100} seed crystal. The optical transparency of the deposited crystal is excellent [5].

At high substrate temperatures in a laminar flame, growth on the {100} surface proceeds mainly via steps which can be many hundreds of microns long. The period of the steps increased with the deposition temperature [5], and ranged from 1-2 microns at 1150°C to 40-60 microns at 1360°C. The seed crystals subjected to higher deposition temperatures had larger misorientations, which would tend to produce a smaller initial step period. This suggests that the step period does increase rapidly with temperature. Under certain conditions, continuous growth across the top surface of the seed crystal is lost, but local well formed domains of epitaxial growth which are 100's of microns on a side are observed to grow at rates exceeding 200 $\mu\text{m/hr}$ in the <100> direction.

A deposition on a cylindrical {110} seed crystal was performed at a temperature of 1500°C. After only 15-20 minutes at this temperature, crystal faces corresponding to the {111}, {110} and {100} directions appeared around the perimeter of the top {110} face of the seed crystal, giving an octagonal shape when viewed from above [5]. A very low growth

rate in the center of the seed crystal's {110} face was observed; the Raman spectra of this area of the face exhibited a strong graphitic character. The Raman spectra of the epitaxially grown faces exhibit a diamond peak height to fluorescence background ratio of >35:1. Poorly formed cubo-octahedral crystals were also observed to grow on the Au-Ta braze material [5]. This is the highest temperature ever reported for both epitaxial and non-epitaxial diamond growth at low pressures.

Discussion

In 1976 Chauhan et al. [10] reported on a study of carbon deposition on 0-1 micron diamond powders which used methane-hydrogen gas mixtures without activation of the gas phase. Their results showed diamond growth at temperatures of 1140-1475°C (determined from density measurements), and a maximum initial diamond growth rate of <0.02 microns/hour which exponentially decayed with time. The exponential decay of the initial rate was explained by the covering of the diamond surface by graphitic carbon. In 1981 Spitsyn et al. reported [11] on homoepitaxial growth studies in a controlled transport reaction (CTR) environment. They stated, "high perfection single crystalline [diamond] layers were obtained on the {110} face of natural diamond at 750°C... As the temperature is increased further, the growth rate of [the] homoepitaxial film increases ... and reaches a maximum at ~1000°C. Further increase in temperature results in a reduction of the growth rate and in deterioration of the structure of the diamond layers, so that HEED analysis reveals graphite inclusions." As far as we know, no refereed publications reported on the homoepitaxial growth of diamond above 1200°C between 1976 and 1990.

Several authors [12,13] have argued that the chemisorption states of hydrogen on diamond surfaces [14], with their desorption peaks at approximately 900 and 1050°C, will prevent a growing diamond surface from maintaining its sp^3 hybridization at higher temperatures. The upper temperature limit for CVD diamond growth would then be due to the desorption of atomic hydrogen and the subsequent reconstruction and graphitization of the growing diamond surface. The actual hydrogen coverage of a diamond surface in a CVD environment will depend on a dynamic balance of the flux of hydrogen and other species from the gas phase, as well as the abstraction and desorption kinetics on the surface. Estimates of the hydrogen disassociation fraction in atmospheric pressure oxygen-acetylene flames suggest that the hydrogen flux in a flame environment could be as much as an order of magnitude higher than

in CVD reactors [5]. Thus, the high atomic hydrogen flux in an atmospheric pressure oxygen-acetylene flame could permit a growing diamond surface to remain hydrogen terminated well above the hydrogen desorption temperatures determined under UHV conditions.

A recent U.S. patent application [15] and two publications [16, 17] reported diamond growth at temperatures above 1400°C. Scanning electron micrographs in both publications show a columnar type morphology with square, <100> oriented diamond crystals situated on top of the columns. The columns act to thermally isolate the large diamond crystals from the substrate, thus generating the very high crystal temperatures that we first observed in 1988 [1, 2, 3, 5].

The existence of a new high temperature, high rate growth regime for the homoepitaxial synthesis of macroscopic, high quality diamond crystals has been demonstrated by this work. Knowing that DC and RF plasma jets can also induce a high disassociation fraction of hydrogen, we recently initiated a collaboration with the High Temperature Laboratory at the University of Minnesota. The results of this work indicate that monocrystalline diamond can also be grown with a high temperature epitaxy (HTE) type process in a DC triple torch reactor [18, 19]. The work reported in these papers may eventually enable the growth of relatively inexpensive, large (1-10 ct.) single crystals and boules of diamond. Such diamond is not readily available from natural or synthetic sources and is needed to develop diamond-on-diamond electronic devices, heat sinks and bulk optical components.

Acknowledgements

The authors would like to thank Richard G. Priest and Phillip Klein for many useful discussions on the mechanisms of crystal growth, and Michael Seal for brazing and supplying the diamond seed crystals. James E. Butler is to be thanked for some of the initial Raman characterization of the deposited crystals, and for arranging to have the seed crystals mounted.

References

- ¹L. M. Hanssen, W. A. Carrington, D. B. Oakes, J. E. Butler, and K. A. Snail, Preprints Book, American Chemical Society Yearly Mtg., Vol. 34, #2, p. 444, April 1989 (Dallas).
- ²L. M. Hanssen, W. A. Carrington, D. B. Oakes, J. E. Butler, and K. A. Snail, Final Prog. & Pres. Summaries, p. T7, SDIO/IST-ONR Diamond Tech. Init. Symp., 11-13 July 1989, (Crystal City, VA).
- ³R. G. Vardiman, C. L. Vold, K. A. Snail, J. E. Butler and C. S. Pande, *Mats. Ltrs.* 8, 468 (1989).
- ⁴M. A. Capelli and P. H. Paul, *J. Appl. Phys.* 67, 2596 (1990).
- ⁵K. A. Snail and L. M. Hanssen, "High temperature, high rate homoepitaxial growth of diamond in an atmospheric pressure flame", *J. Crystal Growth*, in press.
- ⁶D. B. Oakes, J. E. Butler, K. A. Snail, W. A. Carrington, and L. M. Hanssen, *J. Appl. Phys.* 69, 2602 (1991).
- ⁷L. M. Hanssen, K. A. Snail, W. A. Carrington, J. E. Butler, S. Kellog, and D. B. Oakes, *Thin Solid Films* 196, 271 (1991).
- ⁸G. Janssen, W. J. P. van Enckevort, J. J. D. Schaminee, W. Vollenberg, L. J. Giling, and M. Seal, *J. Crystal Growth* 104, 752 (1990).
- ⁹J. A. Freitas, J. E. Butler, and U. Strom, *J. Matl. Res.* 5, 2502 (1990).
- ¹⁰S. P. Chauhan, J. C. Angus, and N. C. Gardner, *J. Appl. Phys.* 47, 4746 (1976).
- ¹¹B. V. Spitsyn, L. L. Bouilov and B. V. Derjaguin, *J. Crystal Growth* 52, 219 (1981).
- ¹²P. G. Kosky and D. S. McAtee, *Mats. Ltrs.* 8, 369 (1989).
- ¹³B. B. Pate, *Surf. Sci.* 165, 83 (1986). See section 9.
- ¹⁴S. Matsumoto and N. Setaka, *Carbon* 17, 485 (1979).
- ¹⁵K. A. Snail, L. M. Hanssen and J. E. Butler, "Epitaxial synthesis of diamond crystals at high growth rates", U.S. Patent Application #548,719, filed July 6, 1990.
- ¹⁶Y. Matsui, H. Yabe, and Y. Hirose, *Jap. Jml. Appl. Phys.* 29, 1552 (August, 1990).
- ¹⁷R. Komanduri, K. A. Snail and L. Fehrenbacher, *Phil. Mag. Ltrs.* 62, 283 (October, 1990).
- ¹⁸Z. Lu, K. Snail, C. Marks, J. Heberlein, and E. Pfender, "High rate homoepitaxial growth of diamond in thermal plasma", late paper, Electrochemical Society Annual Meeting, May 5-10, 1991 (Washington, DC).
- ¹⁹K. Snail, C. Marks, Z. Lu, J. Heberlein, and E. Pfender, "High temperature, high rate homoepitaxial synthesis of diamond in a triple torch plasma reactor", *subm. to Appl. Phys. Ltrs.*, Apr. 1991.

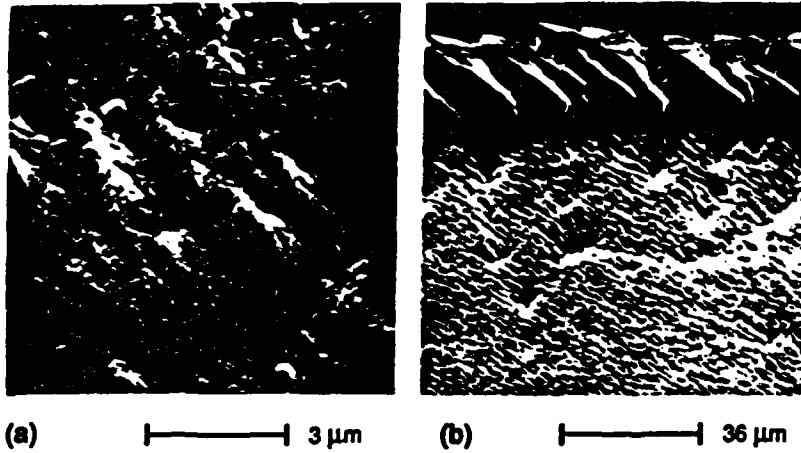


Figure 1. Scanning electron micrographs of a) top surface of {110} type IIA seed crystal after 1 hr deposition at 950°C showing rough growth surface similar to that observed by other groups, and b) edge of same seed after deposition showing oriented polycrystalline growth on side of seed.

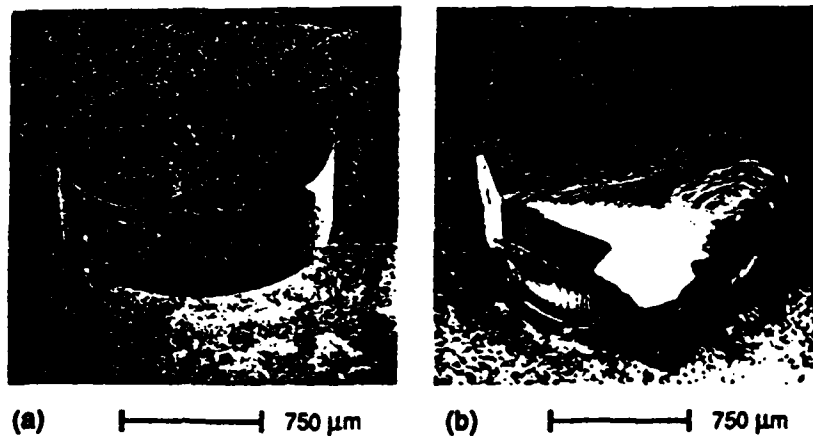


Figure 2. Scanning electron micrographs of circular <100> oriented seed crystal grown at 1250±30°C in a oxy-acetylene flame: a) before deposition, and b) after deposition showing faceted growth with octagonal shape.

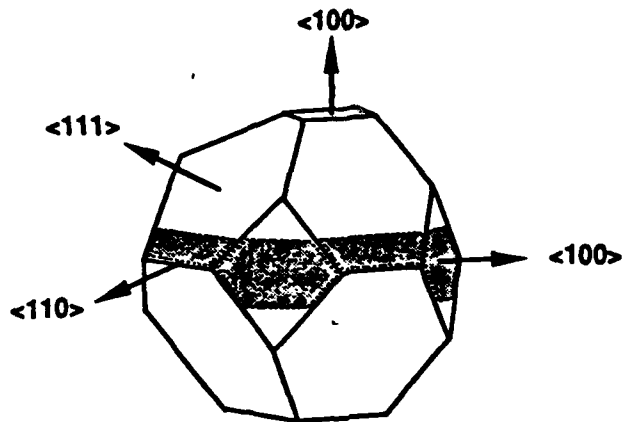


Figure 3. Cubo-octahedral crystal showing growth sectors observed (gray) in deposit on {100} seed crystal shown in Fig. 2b.

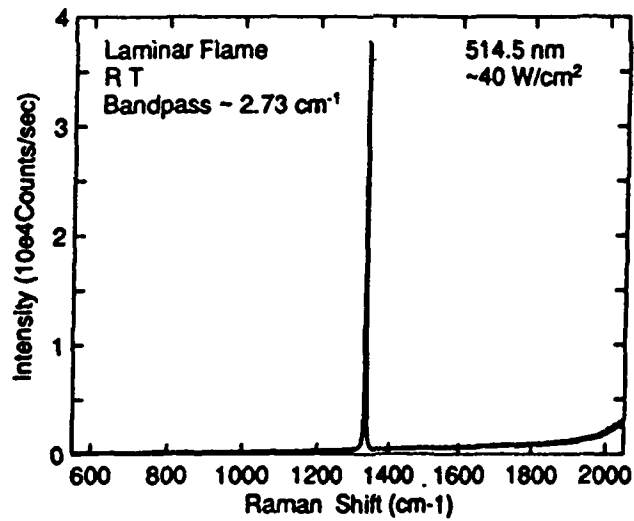


Figure 4. Raman spectrum of the diamond crystal shown in Fig. 2b. The diamond peak position and its FWHM are 1333.1 cm^{-1} and 2.6 cm^{-1} .

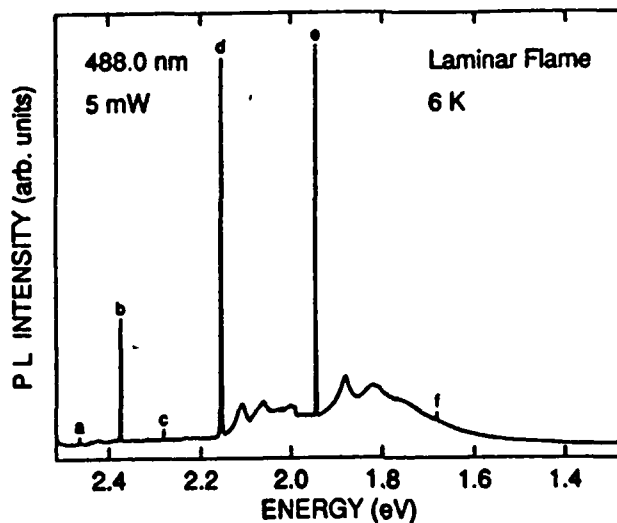


Figure 5. Low temperature photoluminescence spectrum of diamond crystal shown in Fig. 2b. Note the peaks at 2.464 (a), 2.282 (c), 2.155 (d), 1.946 (e) and 1.682 (f) eV. The first order Raman peak (b) is at 2.375 eV.

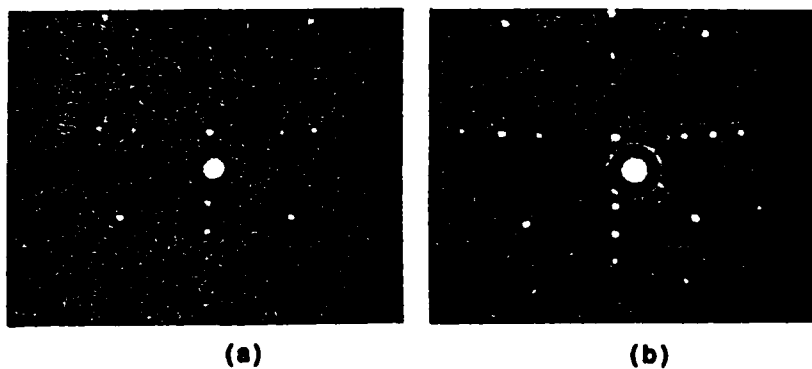


Figure 6. Laue X-ray diffraction pattern of a) seed crystal side of 1250°C sample after growth, and b) deposited crystal side of same sample. Note that the deposited layer is monocrystalline, of $\langle 100 \rangle$ orientation, and epitaxially oriented with respect to the seed crystal.

DEPOSITION OF FLAME GROWN DIAMOND FILMS IN A CONTROLLED ATMOSPHERE

Kathleen Doverspike*, James E. Butler**, and Jaime A. Freitas, Jr.***

* Naval Research Laboratory, Code 6861, Washington, D.C. 20375-5000

** Naval Research Laboratory, Code 6174, Washington, D.C. 20375-5000

*** Sachs/Freeman Assoc. Inc. Landover, MD 20785-3396

ABSTRACT

Polycrystalline diamond films were synthesized both by using an open atmosphere combustion flame, and also using a combustion flame in an enclosed chamber. By operating the pre-mixed oxy-acetylene torch in a chamber, we were able to vary the atmosphere around the flame in a controlled manner and study the effects on the diamond films. Varying the atmosphere around the flame is of interest to control the incorporation of unwanted gases, such as room air, and to obtain finer control over the flame properties. We report on the properties of films grown in the open atmosphere and in the chamber with oxygen and argon.

Introduction

The combustion flame technique has been demonstrated at several laboratories to be a viable technique to obtain high quality diamond films with a high growth rate ($>100\mu\text{m/hr}$)[1-10]. In this paper, we report on the growth of free standing polycrystalline diamond films grown by the combustion process using an oxy-acetylene torch in the open atmosphere, and in an enclosed chamber where the environment can be controlled. Diamond growth using an oxy-acetylene torch occurs in the fuel rich acetylene feather just outside the primary flame front. The torch is a premixed design, where oxygen and acetylene are combined in the mixing chamber and then burn near the primary flame front (*inner cone*) where temperatures can reach up to about 3300K[11]. The overall combustion reaction at the inner cone is [12]:



with many reactive intermediates (eg. H, OH, C₂, and C₂H) involved in the overall reaction. If the torch is run in a fuel rich mode, the unburnt hydrocarbons, reactive intermediates, CO, and H₂ form a region (*feather*) bounded by another flame front caused by oxygen diffusion from the surrounding atmosphere. Although the oxygen and acetylene gases are premixed in the torch, the outer regions of the feather can be described as a diffusion flame because of the oxygen diffusion from the atmosphere. When the torch is operated in the open atmosphere, there is an ample supply of room air available for diffusion into the flame fully oxidizing the combustion products to CO₂ and H₂O in the outer region. Fourier transform infrared spectroscopy has shown that the feather region contains a large concentration of CO and the outer part of the feather and the outer region of the flame contain an appreciable amount of OH, H₂O and CO₂[13]. Laser-induced fluorescence and mass spectrometry have shown the feather region also contains an appreciable amount of nitrogen[12]. This indicates that the atmospheric air not only oxidizes the combustion products in the outer region, but does indeed diffuse into the feather region.

Since environmental gases around the flame diffuse into the area of the flame where diamond growth occurs, these environmental gases are an important variable that warrants further attention. Varying the atmosphere around the flame is also a method of controlling the incorporation of unwanted dopants, such as nitrogen, and of obtaining a finer control over the flame properties. In the present paper, we will discuss films that were made (A) in the open atmosphere, (B) in the enclosed chamber using argon as the auxiliary gas, and (C) in the enclosed chamber using oxygen as the auxiliary gas.

Experimental

All of the diamond films were synthesized using a premixed oxy-acetylene welding torch with a nozzle diameter of 1.17 mm. The flow rates of the oxygen and acetylene (99.6%) were controlled by mass flow controllers with the total flow rate being held constant at 7 SLM. The films were grown on molybdenum screws that were placed in a threaded hole in a water-cooled copper block. The temperature of the screw was controlled by the depth of penetration into the copper block and was monitored by using a two-color pyrometer. The temperature of the films that will be discussed was 900°C ($\pm 20^\circ$). In order to enhance the nucleation, the surface of the molybdenum screw was polished with 600 mesh silicon carbide followed by 1 μm diamond paste, and then ultrasonically cleaned in acetone and methanol. Because of the large difference in the thermal expansion of diamond and molybdenum, the film delaminates as the substrate cools. All the samples discussed in this paper were thus free standing diamond films.

A similar apparatus to that described above was placed in an enclosed chamber in order to control the atmosphere around the flame. Prior to lighting the torch, the chamber was evacuated to approximately 1 torr and then backfilled with the auxiliary gas, either argon or oxygen. An exhaust valve was opened during the growth process, so the experiments were done at slightly above atmospheric pressure.

Micro-Raman analysis was performed using the 514.5 nm line of an argon ion laser and a spatial resolution of less than 1 μm [14]. The Raman line width measurements were performed in the photoluminescence apparatus using a 488.0 nm line with a laser spot size of about 100 μm [15]. The photoluminescence experiments were carried out at 6K in a Janis supervaritemp cryostat. Scanning electron microscopy (SEM) was performed on these samples using a Cambridge S200 instrument.

RESULTS

Results are reported on three types of samples grown in (A) the open atmosphere, (B) the enclosed chamber using argon as the auxiliary gas, and (C) the enclosed chamber using oxygen as the auxiliary gas. Sample A was grown using an oxy-acetylene torch operating in the open atmosphere with an $\text{O}_2/\text{C}_2\text{H}_2$ ratio of 1.04. Sample B was grown using an oxy-acetylene torch operating in an enclosed chamber with an $\text{O}_2/\text{C}_2\text{H}_2$ ratio of 1.10 and an argon flow of 5 SLM. Sample C was grown with an $\text{O}_2/\text{C}_2\text{H}_2$ ratio of 1.03 and an oxygen flow of 7 SLM. Just prior to ending the growth of sample C, the auxiliary flow was changed to argon while the sample cooled down to room temperature. A fourth sample was grown using the same sample conditions as sample C, but when this experiment was terminated, the auxiliary oxygen continued to flow. Therefore, the substrate cooled from 900°C to room temperature (about 2 minutes) in an atmosphere containing a large concentration of oxygen. The total flow rate through the torch for all of these samples was held constant at 7 SLM. The growth time for each of the samples was 60 minutes, while the temperature of the substrate, measured with a two-color pyrometer, was approximately 900°C ($\pm 20^\circ$).

The crystallite morphology of the films can be seen in the SEM micrographs of Figure 1a-d. Micro-Raman spectra of samples A, B, and C are shown in Figure 2a-c, while Figure 3a,b show the photoluminescence spectra of sample A and sample C.

The shape of the feather in an argon environment was very long and slender drastically different from the rounded appearance in the open atmosphere. For a given position in the flame, the temperature of the substrate also appears to be affected by the environmental gases. We have also observed that no water vapor condenses in the chamber in an argon atmosphere, but in an oxygen atmosphere water is seen condensing on the walls of the chamber.

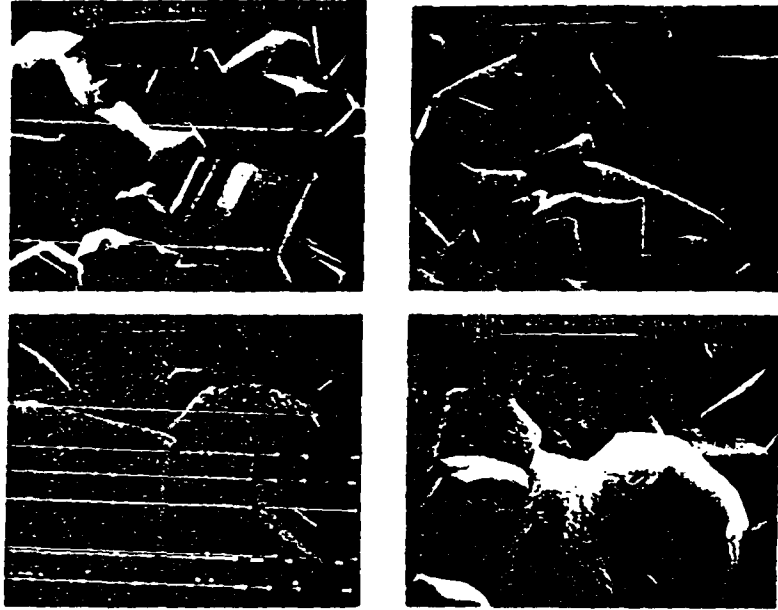
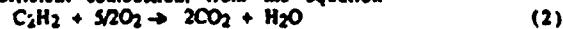


Figure 1. Morphology of films grown in various atmospheres (a, upper left) open atmosphere, (b, lower left) argon atmosphere, (c, upper right) oxygen atmosphere (cooled in argon), and (d, lower right) oxygen atmosphere (cooled in oxygen).

DISCUSSION

The temperature in various parts of the acetylene feather has been shown to be between 2200 and 3000K with a substrate in place[13]. We have found that the temperature of the substrate in the feather is lower in an argon atmosphere, and can easily be varied over a 100K range by changing the environmental gases, without varying the depth of penetration of the substrate into the water-cooled copper block. The lower temperature in an argon atmosphere is not unexpected, since there is no additional oxygen to promote the further combustion of the unburnt fuel, and thus, less heat is provided by the flame. In an argon atmosphere where the only source of oxygen is through the torch, a slightly higher oxygen/acetylene ratio was used to attain similar growth as compared to an oxygen atmosphere. The feather is essentially starved of oxygen in an argon atmosphere that would normally diffuse into the flame and burn with the excess fuel creating a secondary flame front. Therefore, the feather is not bound by this secondary flame front in an argon atmosphere and only a small increase in the acetylene flow rate is needed to extend the slender feather several inches. In the open atmosphere, small increases in the acetylene increased the length of the feather very gradually. Since diamond growth occurs in this feather region, the composition of the environmental gases is important.

Assuming complete efficient combustion, from the equation



and an $\text{O}_2/\text{C}_2\text{H}_2$ ratio of approximately 1, then the flow rate of additional oxygen in the chamber should be about 3/2 the flow rate of C_2H_2 through the torch in order to

obtain the fully oxidized combustion products. We see evidence of this visually, by water condensing on the walls of the chamber when sufficient oxygen is present.

The well crystallized faces, typical of growth in the open atmosphere, is shown in Figure 1a. An interesting feature of the film grown in argon is the smooth (100) faces shown in Figure 1b. This is not unexpected, since growth can occur on the (100) face one atom at a time resulting in a smooth face, whereas growth on faces such as the (111) face often proceeds by a step mechanism[16]. Although the smooth (100) faces is not surprising in general, it is interesting that this is so clearly seen in the flame grown polycrystalline samples when there is a decreased oxygen content in the environment.

The morphology of the sample grown in 100% oxygen and cooled primarily in argon is shown in Figure 1c. The grains are much smaller (1 μm) in the outside region and show a micro-Raman spectra similar to 2c. This may be related to an increased concentration of atomic O and OH expected in the outer region of the flame. OH, and to a lesser extent atomic O have been thought to be very effective etchants of various forms of carbon[17]. This is in contrast to the outer edge in the atmospheric grown films where the quality of the diamond is lower possibly due to the increased incorporation of nitrogen[14]. In the past, this has been attributed to a high entrainment of room air (mostly nitrogen) in the outer part of the flame causing the decreased quality of diamond in the outer region of the film[18].

Figure 1d shows the morphology of a film grown in 100% oxygen and allowed to cool in an oxygen environment. Many pits are evident on the grains, and we believe they are most likely a result of etching by oxygen species after the flame was extinguished. This indicates that not only is graphite and amorphous carbon being etched, but the diamond faces show signs of considerable etching. It is interesting that some grains indicate preferential etching with fewer pits being seen on the (100) face which is known to be the slowest etched face in both natural and synthetic diamond[19].

As can be seen in the micro-Raman spectra in Figure 2a the films grown in the open atmosphere show no signs of graphitic or amorphous carbon. The films grown in the chamber with 100% oxygen (Figure 2c) also indicate high quality diamond, although there may be a small amount of amorphous carbon present in these films. Although we have been successful in growing diamond in an argon atmosphere, the quality of the diamond film decreases (Figure 2b). The broad band centered around 1500cm^{-1} is indicative of amorphous carbon, and the background fluorescence is also much larger, which indicates a larger number of defects in the sample. It appears that the oxygen entrainment into the feather region plays an important role in suppressing the formation of amorphous carbon in the films. The Raman line width was measured with a laser spot size of $100\ \mu\text{m}$ in order to get an indication of the overall quality of the film including intergranular regions. The Raman full width half maximum (FWHM), a measure of the crystalline quality, was found to be $4.7\ \text{cm}^{-1}$ for the film grown in oxygen and slightly wider, $7.0\ \text{cm}^{-1}$, for the film grown in argon.

Photoluminescence spectroscopy can also be used to monitor the quality of the film by examining the diamond 1^{st} order phonon line shape, and the zero phonon line and phonon replicas of defect bands[15]. Shown in Figure 3a,b are the photoluminescence spectra of a film grown in the open atmosphere and with 100% oxygen in the chamber. In Figure 3a the line at 2.16 eV (d) is believed to be due to a double vacancy-nitrogen complex[20], while the line at 1.95 eV (e) is from a vacancy-nitrogen pair[21] and the line labeled(a) is a nitrogen complex band[20]. The band labeled b is the diamond 1^{st} order phonon line, while b^o is indicative of a small amount of graphite present in this sample. The broad band labeled f is due to the spectrometer response when this sample was measured. For the film grown in the chamber (Figure 3b) we see no evidence of the nitrogen defect bands, which indicates that we have reduced the defects associated with nitrogen when we operate in the enclosed chamber and control the environmental gases. There was some evidence of nitrogen defect bands (although still smaller in intensity than the open atmosphere films) in other samples that were grown in the chamber, and may be related to impurities in the gases used (oxygen, acetylene or argon).

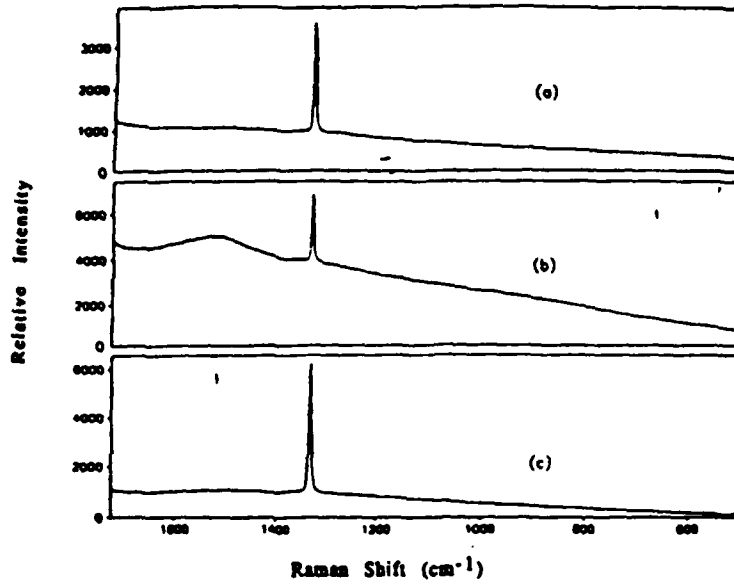


Figure 2. Micro-Raman of films grown in (a) open atmosphere, (b) an argon atmosphere, (c) an oxygen atmosphere.

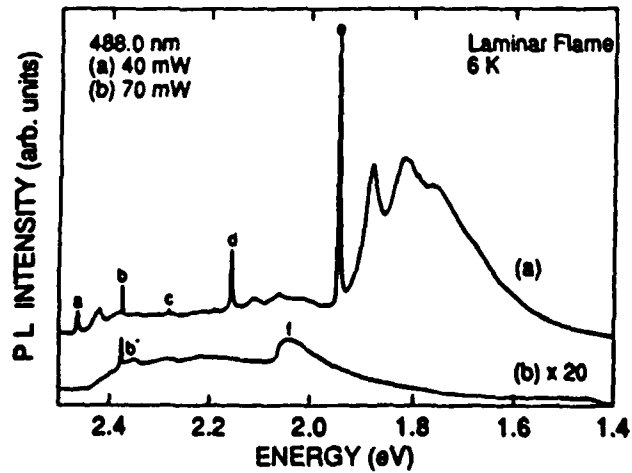


Figure 3. Photoluminescence spectra of films grown in (a) open atmosphere, (b) an oxygen atmosphere

CONCLUSION

In this paper, we have demonstrated the growth of polycrystalline free standing diamond films using a pre-mixed oxy-acetylene torch in an enclosed chamber. We have demonstrated some of the effects that the atmosphere has not only on the flame, but also on the quality and the morphology of the diamond films. When the torch is the only source of oxygen, the films show an increased amount of amorphous carbon present. When the atmosphere is primarily oxygen, the quality of the film is much better even to the outer edge of the film. We have also shown the drastic etching effect that is observed when the films are allowed to cool to room temperature in an oxygenated atmosphere. The photoluminescence results also indicate that there may also be a reduction in the incorporation of nitrogen in the films by controlling the atmosphere around the flame.

ACKNOWLEDGEMENTS

We would like to acknowledge D.J.Vestyck, Jr. for the micro-Raman analysis and D.K.Gaskill for some helpful discussions. This work was partially supported by the Office of Naval Research.

REFERENCES

1. Y.Hirose and N.Kondo, Program and Book of Abstracts, Japan Applied Physics 1988 Spring Meeting, March 29, 1988, p.95.
2. L.M.Hanssen, W.A.Carrington, J.E.Butler and K.A.Snail, *Mat. Lett.* **2**, 289 (1988).
3. Y.Hirose, Proc. 1st Intl. Conf. on the New Diamond Science and Technology, Tokyo, Japan, Oct 24/26, 1988.
4. K.A.Snail, L.M.Hanssen, W.A.Carrington, D.B.Oakes, and J.E.Butler, Proc. 1st Intl. Conf. on the New Diamond Science and Technology, Tokyo, Japan, Oct 24/26, 1988.
5. W.Yarbrough, M.A.Stewart and J.A.Cooper, *Surf. and Coat. Tech.* **39/40**, 241 (1989).
6. P.Kosky and D.S.McAtee, *Mat. Lett.* **3**, 369 (1989).
7. L.M.Hanssen, W.A.Carrington, J.E.Butler and K.A.Snail, *Mat. Lett.*, **2** (7.8), 289 (1988).
8. Y.Tzeng, C.Cutshaw, R.Phillips, T.Srivinyunon, A.Ibrahim and B.H.Loo, *Appl. Phys. Lett.* **56**(2), 134 (1990).
9. M.A.Cappelli and P.H.Paul, *J.Appl.Phys.* **67**(5), 2596 (1990).
10. K.V.Ravi, C.A.Koch, H.S.Hu and A.Joshi, *J. Mater. Res.*, **5**(11), 2356 (1990).
11. A.G.Gaydon and H.G.Wolfard, Flames: Their Structure, Radiation, and Temperature, 4thed. (Chapman and Hall, New York, 1979).
12. Y.Matsui, A.Yuuki, M.Sahara and Y.Hirose, *Jap. J. Appl. Phys.* **28**(9), 1718 (1989).
13. P.W.Morrison, Jr., J.E.Cosgrove, J.R.Markham and P.R.Solomon, New Diamond Science and Technology, edited by R.Messier, J.T.Glass, J.E.Butler and R.Roy (Mater. Res. Soc. Proc., Pittsburgh, PA 1991) pp. 219-224.
14. D.B.Oakes, J.E.Butler, K.A.Snail, W.A.Carrington, L.M.Hanssen, *J. Appl. Phys.* **69**(4) 1991.
15. J.A.Freitas, J.E.Butler, U.Strom, *J. Mater. Res.* **5**(11), 2502 (1990).
16. R.E.Clausing, L.Heatherly, E.D.Specht and K.L.More, New Diamond Science and Technology, edited by R.Messier, J.T.Glass, J.E.Butler and R.Roy (Mater. Res. Soc. Proc., Pittsburgh, PA 1991) pp. 575- 580.
17. S.J.Harris and A.Weiner, *Appl. Phys. Lett.* **55** (21), 2179 (1989)
18. J.A.Freitas, Jr., U.Strom, J.E.Butler and K.A.Snail, New Diamond Science and Technology, edited by R.Messier, J.T.Glass, J.E.Butler and R.Roy (Mater. Res. Soc. Proc., Pittsburgh, PA 1991) pp. 723-728.
19. K.Tankala and T.Debroy, New Diamond Science and Technology, edited by R.Messier, J.T.Glass, J.E.Butler and R.Roy (Mater. Res. Soc. Proc., Pittsburgh, PA 1991) pp. 827-831.
20. J.Walker, *Rep. Prog. Phys.* **42**, 1605 (1979).
21. G.Davies and M.F.Hamer, *Proc. R. Soc. London A* **348**, 285(1976).

Microluminescence depth profiles and annealing effects in porous silicon

S. M. Prokes

Naval Research Laboratory, Washington, DC 20375

J. A. Freitas, Jr.

Sachs/Freeman Associates Inc., Landover, Maryland 20785

P. C. Searson

The Johns Hopkins University, Baltimore, Maryland 21218

(Received 10 March 1992; accepted for publication 11 May 1992)

Cross-sectional microluminescence measurements for $1 \Omega \text{ cm}$ $70 \mu\text{m}$ porous silicon samples show a continuous decrease of the photoluminescence band as a function of sample depth. No spectral shift is observed. For samples annealed at 390°C , in addition to spectral intensity reduction, we observe the same redshift in all luminescence spectra independent of depth. A study of this luminescence redshift as a function of annealing temperature reveals a striking similarity to results observed for optical band gap shrinking of $\alpha\text{-Si:H}$ as a function of hydrogen loss during annealing.

Visible luminescence in silicon was first reported by Anaham,¹ and subsequently other confirmations of this phenomenon have been published.^{2,3} It has been suggested¹ that as the porosity is increased, the silicon structures decrease to nanometer scale dimensions, leading to a quantum size effect in the silicon band structure.

However, previous results have shown⁴ that low temperature heat treatments of porous $0.1 \Omega \text{ cm}$ silicon (of 50% porosity) performed in an ultrahigh vacuum environment resulted in a significant hydride desorption correlated with redshifting of the photoluminescent (PL) peak and significant decrease of the PL intensity. The mechanism suggested to explain these results was attributed to luminescence from SiH_x and polysilane chains.

In this letter, we have examined the luminescence (PL) properties of porous Si in cross section using micro PL and we have examined the redshift of the PL as a function of annealing. Results show no apparent shifting of the PL energy with depth, but significant redshifting has been monitored as a function of annealing, suggesting a hydride-related luminescence process may be active in porous silicon.

The substrates were boron-doped $1 \Omega \text{ cm}$ p -type silicon (100) wafers. Porous $70\text{-}\mu\text{m}$ -thick silicon layers (40% porosity) were formed by etching in 25% HF at a current density of 10 mA/cm^2 . In the annealing experiments, the samples were loaded into a tube furnace and annealed under an argon ambient. The temperature was monitored using a type K thermocouple positioned next to the sample. The samples were also annealed in vacuum as described previously.⁴ In the conventional luminescence experiment, the 488 nm line of the Ar^+ laser and a cooled germanium detector were used. The spot size was roughly $0 \mu\text{m}$ at a power of 250 mW, and all the PL data were normalized to the detector/spectrometer response by using a tungsten lamp. The overall structure of the porous silicon before and after these anneals was examined using scanning electron microscopy (SEM), and no significant structural changes were observed in these temperature ranges.

The micro PL setup consisted of an Ar^+ laser, an

inverted Carl Zeiss Axiovert microscope (model 408), and a double spectrometer (SPEX model 1404), fitted with a GaAs photomultiplier and a photon counter system.⁵ The laser spot size used in this experiment was about $1.5 \mu\text{m}$, and spectra were obtained for laser powers between 0.2 and 2.1 mW using the 488 and the 514.5 nm lines. The micro PL spectra have also been corrected for a tungsten lamp.

Five spectra obtained as a function of sample depth using a $\approx 1.5 \mu\text{m}$ spot size at roughly $12 \mu\text{m}$ intervals are shown in Fig. 1. Note that the PL peak energies are the same as a function of depth into the sample, and only the intensity of the PL decreases with increasing distance from the top surface. This result differs from the results of Tischler *et al.*,⁶ who report blueshifted PL close to the sample surface in p^- samples. However, they examined the PL as a function of depth by etching back the porous silicon, which may have contributed to the reported shifting. In addition, it has been shown⁷ that for highly porous silicon in the range of $1\text{--}10 \Omega \text{ cm}$, a blueshift close to the sample surface occurs and is caused by significant strains in the highly porous samples, exhibited by a curved cell structure on the surface.

Figure 2 represents micro PL results for the same sample which was annealed at 390°C in an argon ambient for 1 min. The PL spectra show the same behavior as the unannealed sample (constant peak energy with depth), but each spectrum has redshifted (to 1.67 eV) and the intensity has decreased by a factor of 2 for all depths. These measurements were performed using both the 488 and the 514 nm line of the Ar laser and no differences were observed in the PL spectra.

The redshifting of the PL as a function of heating under an argon ambient and under vacuum was examined in the same samples using a conventional luminescence setup, shown in Fig. 3. At room temperature, a strong luminescence is seen roughly at 1.72 eV. As the annealing temperature increases, the PL redshifts significantly, by as much as 0.32 eV at 690°C , at which point it almost disappears. The results for anneals in an argon ambient and in an ultrahigh vacuum (10^{-10} Torr) were quite similar.

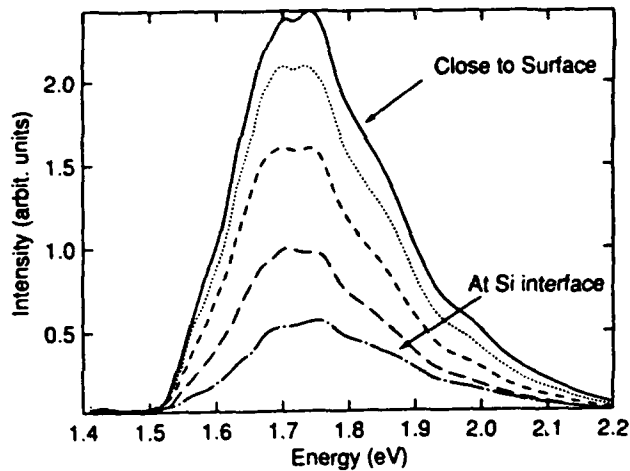


FIG. 1. Micro PL spectra taken in cross section for 1 Ω cm 70- μ m-thick porous silicon sample with peak positions at 1.72 eV. The PL peak measured closest to the Si interface refers to material roughly 60 μ m from the surface.

Figure 4 is a plot of the redshift in PL energy of the porous silicon sample versus the annealing temperature and the optical gap shrinking of *a*-Si:H as a function of annealing temperature measured by Yamasaki *et al.*⁸ It is quite apparent that for annealing in the range of 200–690 $^{\circ}$ C, the optical band gap shrinking of the *a*-Si:H due to loss of hydrogen⁸ and our PL peak redshifting in the same temperature range show identical behavior.

From the above results, several points should be noted. First, it is clear that no PL shifting occurred as a function of depth in these samples. The redshift observed upon a heat treatment to 390 $^{\circ}$ C is the same in all the spectra obtained as a function of depth. If vertical structural inhomogeneities are present in these samples, resulting in smaller particle sizes in the top layers as discussed by Tischler *et al.*,⁶ then one would expect a blueshifted luminescence in the top regions if the sole luminescence mechanism was that of quantum confinement. However, this is

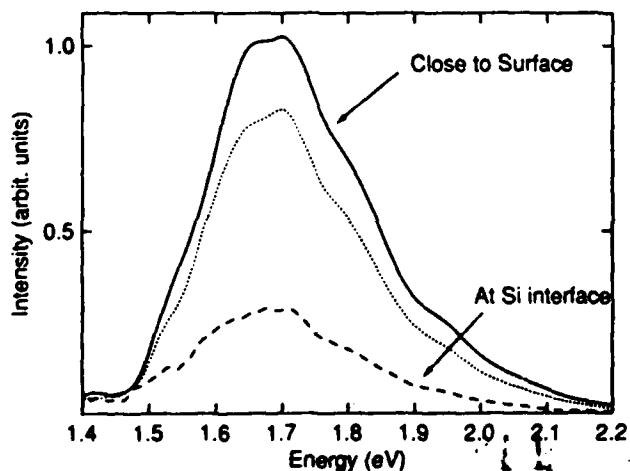


FIG. 2. Micro PL data in cross section after 1 min anneal at 390 $^{\circ}$ C of sample in Fig. 1, showing a redshift of all peaks to 1.67 eV and a drop in overall intensity.

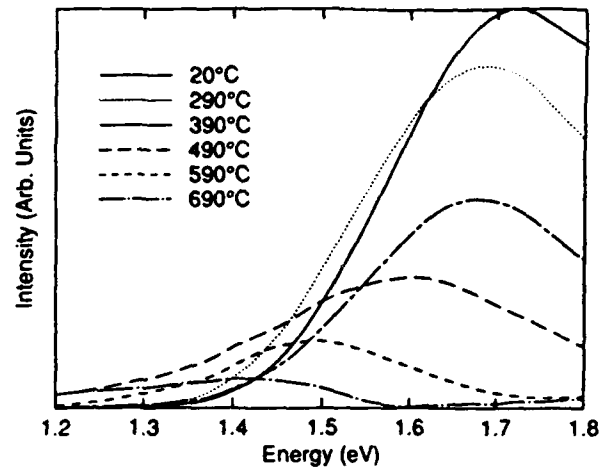


FIG. 3. PL peak as a function of 1 min anneals at various temperatures. The sample is the same as in Fig. 1.

not the case in these samples, even after annealing. This appears inconsistent with the quantum confinement luminescence mechanism, but it can be easily explained in terms of a hydride/polysilane type mechanism.⁴

Wolford *et al.*⁹ reported room temperature PL from hydrogenated amorphous silicon (*a*-Si:H). Their results indicate a 5 K luminescence in the range of 1.3–2.08 eV, blueshifting with increasing hydrogen content. The samples with the highest H content (PL at 1.7–2.0 eV) exhibited room temperature luminescence. The presence of hydrogen complexes [SiH, SiH₂, SiH₃, or (SiH₂)_n] was suggested to explain this luminescence. Furthermore, tight-binding models¹⁰ show that the presence of monohydrides leads to new bonding states which are formed deep within the silicon valence bands. With higher H content, such as SiH₃, even deeper states occur, expanding the gap even more. These calculations¹⁰ have shown that a large gap increase occurs as a function of increasing hydrogen content, and for 30% hydrogen, the band gap increases to 1.8 eV. Thus, in the hydride model, the peak energy of the

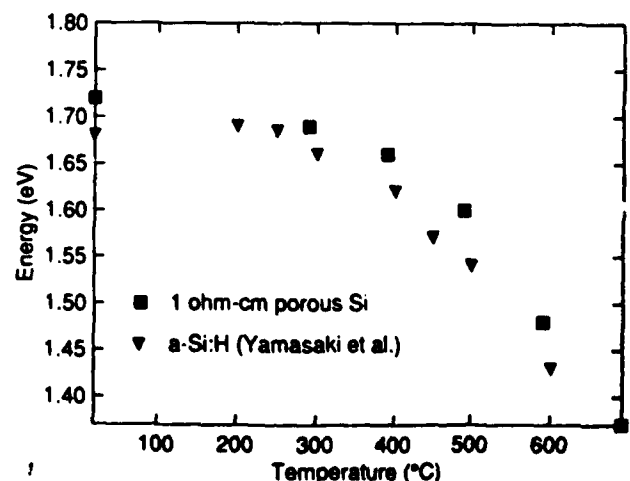


FIG. 4. Shift in the PL energy of the sample in Fig. 1 as a function of annealing temperature (squares) and shrinking of the optical gap of *a*-Si:H as a function of heating due to hydrogen loss (triangle); see Ref. 8.

luminescence in porous silicon can be related to the type of hydride present, and the intensity is a function of surface area (number of hydrides).

The redshifting of the PL as a function of heating (and thus hydrogen desorption) shown in Fig. 4 is continuous and very closely resembles the shrinking of the optical gap of *a*-Si:H as a function of annealing, which relates directly to a decrease of bonded hydrogen from 28% to 8% in this temperature range.⁸ The loss of hydrogen in the temperature range of 200–800 °C for porous silicon has been reported previously.⁴ These results are very indicative of a hydride-related luminescence process.

We have observed fatiguing of the PL for the 1 Ω cm sample of 90% porosity using the 488 and the 514 nm lines of the laser, and it is very similar to results obtained in chalcogenide glasses.¹¹ However, the reverse behavior was noted in a 1 Ω cm sample of 40% porosity (PL peak position at 710 nm). In this case, continuous laser light exposure leads to a long time (10 min) luminescence intensity increase. This may indicate the presence of metastable states similar to those seen in the chalcogenide system.¹¹ These results will be discussed elsewhere.

In conclusion, it has been shown that for a 1 Ω cm 70 μm porous silicon sample, the PL peak energy is constant as a function of depth. Upon heat treatments to 390 °C, the whole sample exhibits a PL band redshift and intensity drop, but the new PL peak position is independent of depth. If the samples are inhomogeneous as a function of depth, as has been reported,⁶ then it is very difficult to explain these results in terms of the quantum confinement

model. Furthermore, the redshifts of the PL in porous Si upon heating are very similar to those observed for optical band gap shrinking of *a*-Si:H as a function hydrogen loss during annealing. These results suggest that a silicon hydride-type luminescence is active in the porous silicon structures.

The authors would like to thank O. J. Glembocki for help with the photoluminescence and for helpful discussions.

- ¹L. E. Canham, *Appl. Phys. Lett.* **88**, 1046 (1990).
- ²A. Bsiessy, J. C. Vial, F. Gaspard, R. Herino, M. Ligeon, F. Muller, R. Romestein, A. Wasiela, A. Halimaoui, and G. Bomchil, *Surf. Sci.* **284**, 198 (1991).
- ³S. Gardelis, J. S. Rimmer, P. Dawson, and B. Hamilton, *Appl. Phys. Lett.* **89**, 2118 (1991).
- ⁴S. M. Prokes, O. J. Glembocki, V. M. Bermudez, R. Kaplan, L. E. Friedersdorf, and P. C. Searson, *Proc. Mater. Res. Soc.* **256**, 107 (1992).
- ⁵J. A. Freitas, Jr., U. Strom, J. E. Butler, and K. A. Snail, *Proceedings of the 2nd International Conference on New Diamond Science and Technology* (Materials Research Society, Pittsburgh, PA, 1991), p. 823.
- ⁶M. A. Tischler, R. T. Collins, J. H. Stathis, and J. C. Tsang, *Appl. Phys. Lett.* **60**, 639 (1992).
- ⁷L. E. Friedersdorf, P. C. Searson, S. M. Prokes, O. J. Glembocki, and J. M. Macaulay, *Appl. Phys. Lett.* **60**, 2285 (1992).
- ⁸S. Yamasaki, N. Hata, T. Yoshida, H. Oheda, A. Matsuda, H. Okushi, and K. Tanaka, *J. de Phys. (Paris) Colloq.* **42**, C4-298 (1981).
- ⁹D. J. Wolford, B. A. Scott, J. A. Reimer, and J. A. Bradley, *Physica B* **117/118**, 920 (1983).
- ¹⁰D. A. Papaconstantopoulos and E. N. Economou, *Phys. Rev. B* **24**, 8233 (1981), and references therein.
- ¹¹J. Cernogora, F. Mollot, and C. Benoit a la Guillaume, *Phys. Status Solidi A* **18**, 401 (1983).

Photoluminescence studies of polycrystalline diamond films

J. A. Freitas, Jr.

Sachs/Freeman Associates, Landover, Maryland 20785-5396

J. E. Butler and U. Strom

Naval Research Laboratory, Washington, DC 20375-5000

(Received 10 April 1990; accepted 17 July 1990)

The photoluminescence spectra of polycrystalline diamond films prepared by filament assisted chemical vapor deposition are dominated by a defect band with a strong zero phonon line near 1.68 eV and weak phonon replicas at lower energies. The 1.68 eV line is blueshifted from the 1.675 eV zero phonon line associated with the neutral vacancy in bulk diamond. The line shape and position of the 1.68 eV line are shown to depend on substrate material (Si, Mo, Ni). The 1.68 eV emission for Ni and Mo substrates is interpreted in terms of the stress shifted and broadened neutral vacancy emission. The broader 1.68 eV line observed for Si substrates may indicate the additional effects of Si absorption by the diamond films. Films prepared by an oxygen-acetylene flame technique exhibit two additional luminescence bands with zero phonon lines at 1.95 and 2.16 eV. These lines have been tentatively assigned to nitrogen-vacancy complexes. The temperature dependence (6 K–300 K) of the luminescence of a free-standing diamond film, which had been deposited on a molybdenum substrate, is comparable to similar observations reported for bulk diamond. We have also observed a strong dependence of the PL spectra radially across a given combustion film and associated this with details of the flame chemistry.

I. INTRODUCTION

It has recently been possible to grow relatively thick, large area polycrystalline diamond films. In order to realize potential opto-electronic applications of these films it is essential to understand the nature of the extrinsic and intrinsic defects in such films. One important aspect of such studies is to relate the defect structures to the film preparation technique and substrate type. A recent report¹ described defect signatures using cathodoluminescence (CL) measurements on diamond films prepared by hot-filament chemical vapor deposition (FACVD) onto Si substrates. We report here preliminary photoluminescence (PL) studies of diamond films prepared by FACVD and an oxygen-acetylene torch (combustion) process using Ni, Mo, as well as Si substrates. Whenever possible, the defects in the films are identified by comparing their luminescence spectra with well-known defect spectra in natural diamond.²⁻⁵

II. EXPERIMENTAL DETAILS

A. Film deposition techniques

The FACVD deposition of diamond was performed in a vertical 4.45 cm i.d. fused silica tube. A tungsten or rhenium filament was suspended 5 mm above the substrate, which was supported on a 2.54 cm o.d. molybdenum encased heater. The filament temperature was maintained at 2200 ± 50 °C and the substrate at

875 °C. The gas flow (ca. 100 sccm of 0.5% methane in hydrogen) was introduced at the top of the vessel and the pressure was maintained at 40 Torr during the course of the deposition. The chamber was pumped by a two-stage mechanical pump and the base pressure was 0.03 Torr.

The combustion deposition of diamond⁶ was performed in ambient air using a commercial oxygen-acetylene brazing torch with a 0.89 mm i.d. orifice. The gas flow rates were controlled by mass controllers, with the total flow rate of ca. 3 slm and an oxygen/acetylene mass flow ratio of ca. 0.95. The flame was directed down onto a substrate supported on a water cooled copper block. The substrate temperature, 800 ± 100 °C, was adjusted by varying the thermal conductivity to the copper block.

B. Substrates

FACVD diamond was grown simultaneously on a polycrystalline Ni disk and a Si wafer [(100), *n*-type] substrate. Neither substrate had been intentionally pretreated (e.g., the usual diamond scratching). While isolated crystals of diamond were observed on both substrates, the density was several orders of magnitude higher on the Ni disk compared with the Si where most crystals seemed to be associated with unintentional scratches. X-ray diffraction confirmed the presence of diamond on both samples. The 1332 cm^{-1} diamond phonon was observed by Raman scattering on both

samples, with the Si sample yielding a significantly broader Raman line width (20 vs 10 cm^{-1}).

One combustion deposited sample was grown on a portion of a Si wafer [(100), *n*-type] which had been intentionally scratched with $6 \mu\text{m}$ diamond polishing powder and then cleaned with solvents. The deposition time was several hours. An annular pattern of isolated diamond crystals was observed with a low density of crystals in the center (directly under the inner flame cone), increasing to a maximum density 3 mm radially outward from the center, and decreasing to a low and eventually zero density at 5 to 6 mm from the center.

The other combustion deposited sample was grown in air for 30 min on the end of a molybdenum screw which had been polished with $6 \mu\text{m}$ diamond powder and then cleaned. Upon cooling to room temperature, a continuous diamond film (ca. $15 \mu\text{m}$ thick and 8 mm diameter) delaminated from the substrate. This film was nearly transparent in the center degrading to a grey-brown color on the edges. The average facet size observed on the polycrystalline films was roughly $1 \mu\text{m}$ in dimension.

C. Optical measurement technique

The PL experiments were carried out at temperatures between 6 and 300 K in a Janis supervaritemp cryostat. The temperature was measured and controlled by a sensor located in the copper-sample holder. This system was modified, allowing vertical positioning steps smaller than $2 \mu\text{m}$. Most spectra were excited by either a krypton (476.2 nm-2.6036 eV) or an argon (476.5 nm-2.6020 eV, 457.9 nm-2.7077 eV) ion laser. The laser spot size was approximately $50\text{--}100 \mu\text{m}$ and the nominal laser power varied between 10 and 50 mW. The excited PL was analyzed by a single or double grating monochromator and detected by a GaAs photomultiplier tube, operated in a photon counting mode. We used colored glass filters to reduce the laser intensity background in the PL spectra when using the single spectrometer.

III. RESULTS AND DISCUSSION

A. Substrate and deposition dependence

In Fig. 1, PL spectra obtained at 6 K (using a double spectrometer) are shown for two FACVD films deposited on Si (top spectrum) and on Ni (bottom spectrum) substrates. The sample and substrate preparation and characteristics were described in the previous section. Both spectra are dominated by a relatively sharp zero phonon line (ZPL) PL band, at about 1.68 eV (P_1), and its weak phonon replicas. The strong, broad luminescence background observed in the top spectrum has been reported by many research groups and its origin is not yet well understood. However, its intensity relative to the Raman peak at about 1332 cm^{-1} decreases with increasing film thickness and quality.⁷

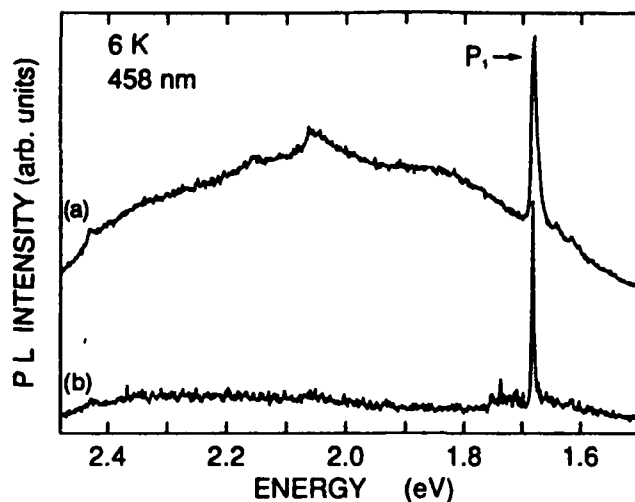


FIG. 1. Photoluminescence spectra obtained at 6 K from an FACVD polycrystalline film deposited on Si (top spectrum) and polycrystalline Ni (bottom spectrum) substrates. The dominant feature is the sharp ZPL (P_1) at 1.68 eV.

Figure 2 shows PL spectra of two diamond films, deposited by the combustion technique (oxygen-acetylene torch) on Si and molybdenum substrates, top and bottom spectra, respectively. The measurements were carried out at a temperature of 6 K. The luminescence emitted by the samples was dispersed by a single grating spectrometer and the exciting laser light was excluded by an appropriate color glass filter. The Si substrate film consists of individual crystallites with size varying from 10 to $200 \mu\text{m}$, while the molybdenum substrate film is a free-standing film made up of crystallites with average grain size of a few microns, as described previously. As observed in the spectrum of

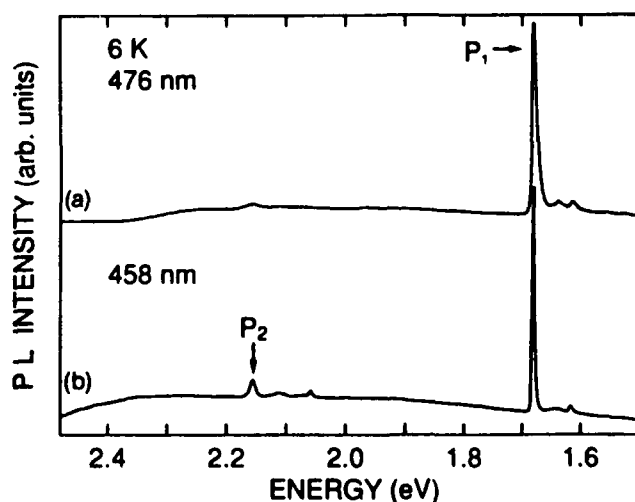


FIG. 2. Photoluminescence spectra (6 K) of diamond films deposited by the combustion technique onto Si [spectrum (a)] and molybdenum [spectrum (b)] substrates, respectively. Both spectra show the 1.68 eV (P_1) and 2.16 eV (P_2) defect bands.

FACVD films (Fig. 1), the 1.68 eV (P_1) ZPL band and phonon replicas are the dominant spectral features in Fig. 2. The phonon replicas are easier to observe in Fig. 2 than in Fig. 1 due to the better signal to noise, resulting from the larger crystallite sizes and film uniformity. The new feature observed in Fig. 2 is the PL band with the ZPL around 2.16 eV (P_2) and associated phonon replicas.

In natural and synthetic diamond the 2.16 eV center is induced by irradiation followed by annealing. The temperature annealing behavior of this system suggests a divacancy as a possible structure⁴; however, results of isotope studies of nitrogen doped synthetic diamond⁸ may imply the direct or indirect participation of nitrogen in this center. The 1.68 eV center, a common feature observed in PL spectra of CVD diamond films, has been assigned to the neutral vacancy center (V° , whose ZPL is at 1.673 eV), and which is induced in all natural and synthetic diamond by irradiation.

A comparison of the 1.682 eV center with V° shows that the former is blueshifted by 5 to 8 meV and has a linewidth 4 to 10 times broader than the latter. These characteristics may suggest that the 1.68 eV ZPL is associated with another center such as the defect with the ZPL at 1.685 observed in homo- and hetero-epitaxial CVD films intentionally doped with Si,⁹ or in Si-implanted and annealed natural diamond.¹⁰ However, it is important to note that the 1.68 eV system observed for the undoped diamond films is about 5 meV redshifted from the Si-center. In addition, the energy position and linewidth of the Si-center seems to be independent of the substrate, deposition technique, or crystallite grain size, which contrasts the behavior of the 1.68 eV center. Clearly, careful experiments must be carried out on well-controlled samples to achieve a definite identification of the 1.68 eV center.

If one assumes that the 1.68 eV system is the neutral vacancy, the line shift can be explained in terms of residual stress existent in the individual crystallites, since stress of 1 to 2 GPa parallel to $\langle 100 \rangle$ is enough to induce a 6 to 7 meV blueshift.³ As a result of this residual stress (not expected to be uniaxial), the linewidth will broaden, masking the observation of the ZPL doublet character, and leading to the observed sample dependent peak position.

Recently, Collins and coworkers reported CL and absorption studies of microcrystals and polycrystalline diamond films grown by microwave assisted CVD technique.^{11,12} The defects incorporated during the sample growth and induced by electron irradiation in their CVD samples were compared with centers observed in unirradiated and electron irradiated natural diamond. In their work they suggested that the assignment of the 1.68 eV band with the neutral vacancy (GR1) is incorrect because of the large blueshift observed in com-

parison with natural diamond. They also point out that the GR1 center is completely quenched in electron irradiated natural diamond which has been annealed at 900 °C, which is the substrate temperature of most CVD techniques.

Using the same approximation described by Collins and Robertson¹³ in their CL studies of the 2.156 eV center in sintered diamond, Robins and coworkers¹ estimated a residual stress of the order of 3 GPa in their CVD-grown films. If we assume the same order of magnitude for the residual stress in our films, then we can account for the width of the ZPL in our spectra. A residual stress of about 3 GPa will be enough to cause the broadening and line shift observed in the V° ZPL in our films. The smaller line shift (1 or 2 meV) observed in the 2.156 eV center in comparison with the V° may be understood in terms of the complexity of this center and its different symmetry (trigonal instead of tetrahedral). We also would like to point out that the procedure which creates and quenches the GR1 center in natural diamond is quite a different process from that observed in CVD films. In CVD films during the deposition, impurities and vacancies are mobile and coexist in a thermal-equilibrium phase which has not been investigated.

In Fig. 3 we show only the ZPL at 1.68 eV with the associated phonon replica for the various samples represented in Figs. 1 and 2. It is apparent from these data that the ZPL linewidth for films deposited on Si substrates is approximately 2.5 broader than for the films deposited on Ni or molybdenum substrates. In addition, the ZPL peak positions are redshifted for the Si substrates. One possible explanation is that the films on Si are stressed to a greater extent than the films on the metal substrates. Alternatively, Si atoms can be absorbed in the diamond film which can lead to a new defect center with slightly lower ZPL energy.^{9,10}

B. Spatial dependence

To verify the homogeneity of the combustion films we have carried out PL measurements in a film deposited on a Si substrate with average crystallite size varying from 50 to 200 μm . Attempting to probe individual crystallites of the film, which exhibit the typical annular pattern of isolated diamond, we reduced the laser spot size to about 30 μm . The sample was moved inside the dewar allowing us to probe crystallites from the outside part to the central part of the film. Some results are shown in Fig. 4, where the spectrum (a) was obtained by aiming the laser beam at a crystal at the external part of the annular film. This spectrum is dominated by a broad luminescence band with phonon replicas and ZPL at 1.95 eV (P_3). This system is the dominant luminescence band observed by annealing preirradiated diamond which contains isolated substi-

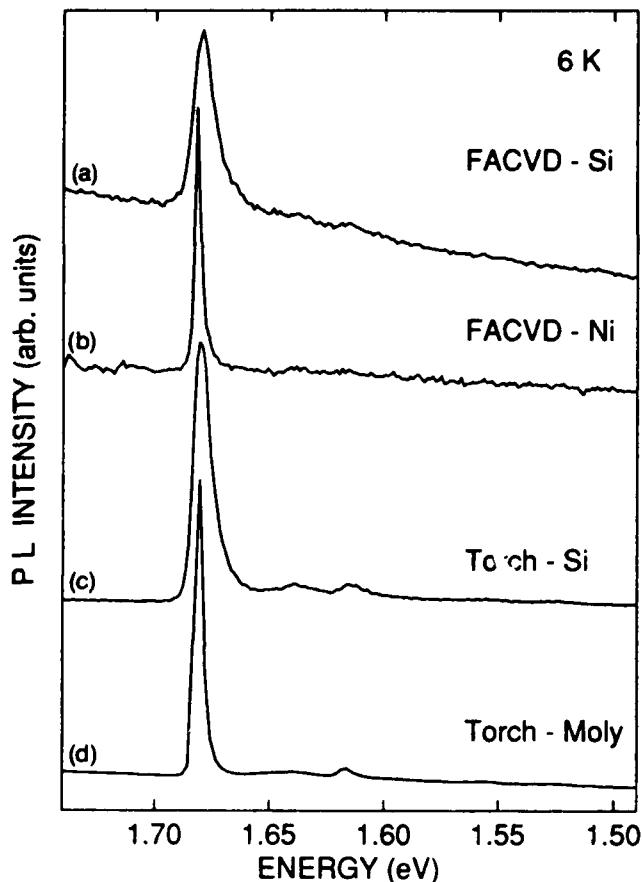


FIG. 3. Low temperature (6 K) PL spectra of the films presented in Figs. 1 and 2. The linewidth of the 1.68 eV (P_1) band is broader and peak shifted to low energy for films deposited on Si substrates.

tutional nitrogen impurities. Detailed studies carried out by Davies and Hamer¹⁴ strongly suggest that the 1.95 eV system is a nitrogen-vacancy pair (N-V). By moving the laser spot slightly toward the center of the film we observe, as shown in spectrum (b), a new luminescence band, the 2.16 eV (P_2) system discussed previously. For a crystal located closer to the center of the film we observe a sizable reduction of the 1.95 eV center PL intensity, so the luminescence spectrum is dominated by the 2.16 eV center, as shown in spectrum (c). For crystallites at the central part of the film, represented by the spectrum (d), the luminescence spectrum is dominated by the 2.16 eV (P_2) and 1.68 eV (P_1) centers. Since the combustion film is deposited in an open atmosphere, one can expect the incorporation of nitrogen in this film, as observed in Fig. 4, spectra (a) and (b), which shows the dominant presence of the 1.95 eV center associated with the N-V pair. However, for crystallites deposited more toward the center of the annular film, we observe a sizable reduction of the 1.95 eV center, spectra (c) and (d), suggesting that the higher pressure in the flame at this part of the film may exclude the nitrogen, reducing its incorporation. This

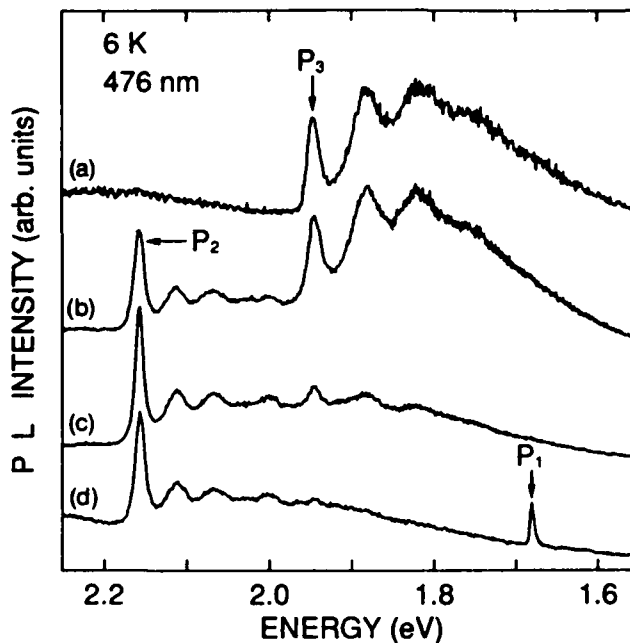


FIG. 4. PL spectra obtained at 6 K from an oxyacetylene film deposited on a Si substrate. The curves (a) to (d) were obtained by focusing the laser into four crystallites positioned from the top toward the center of the sample, respectively. These spectra show the 1.68 eV (P_1), 1.95 eV (P_3), and 2.16 eV (P_2) systems.

seems to be a plausible assumption; with a lack of nitrogen we can expect that the dominant defects should be isolated vacancies and vacancy complexes, as observed in spectra (c) and (d). This observation is in agreement with CL studies of intentionally nitrogen-doped films reported by Yokota *et al.*¹⁵

C. Temperature dependence

The temperature dependence of the PL spectra measured for the polycrystalline, free-standing diamond film, which was deposited on a molybdenum substrate, is shown in Fig. 5. The measuring temperatures for the three films were 6 K, 100 K, and 300 K for spectra (a), (b), and (c), respectively. It should be noted that the line shape and PL intensity are not changed significantly between 6 K and 100 K. On the other hand, the spectral features, in particular the associated phonon replica, are very much reduced for the 300 K measurement. Similar observations were reported¹⁶ for natural diamond. An accurate identification of the defect center may require a precise determination of the phonon sidebands. It is therefore essential that PL measurements be carried out at or below 100 K.

IV. CONCLUSION

Photoluminescence measurements carried out for polycrystalline diamond films have revealed strong PL emissions near 1.68, 1.95, and 2.16 eV. These de-

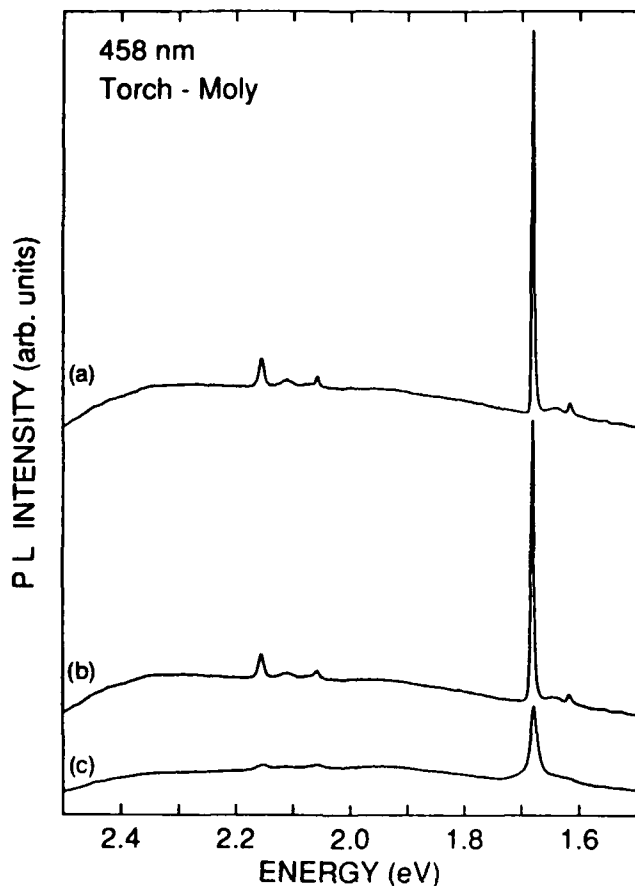


FIG. 5. Temperature dependence of the 1.68 eV (P_1) and 2.16 eV (P_2) bands of a diamond film deposited by the combustion technique onto a molybdenum substrate. Measurement temperatures: curves (a) 6 K, (b) 100 K, and (c) 300 K, respectively.

fects have been interpreted in terms of similar defect lines observed for natural diamond. In particular, the 1.95 eV and 2.16 eV bands are very close to similar PL emissions of natural diamond which are known to involve nitrogen complexes, although an unambiguous identification of the natural diamond spectra is yet to be made. The 1.68 eV PL observed for films deposited on Ni and Mo was interpreted in terms of a stress shifted and broadened neutral vacancy emission. This observation is in accord with the interpretation of the CL measurements by Robins and coworkers.¹ The broader 1.68 eV PL line observed for Si substrates, independent of diamond film growth technique, may

indicate the contribution of the well-known Si defect emission at 1.685 eV, which is likely induced in our films deposited on Si due to the interdiffusion of Si into the diamond lattice during the growth process. The temperature dependence of the PL intensity experiment shows a strong quenching and broadening of the ZPL and associated phonon replicas for temperatures above 100 K, as observed in natural diamond.¹⁶

ACKNOWLEDGMENTS

We thank W. A. Carrington for supplying the torch deposited films. Helpful discussions with S. G. Bishop are gratefully acknowledged. This work was supported in part by the Office of Naval Research.

REFERENCES

- ¹L. H. Robins, L. P. Cook, E. N. Farabaugh, and A. Feldman, *Phys. Rev. B* **39**, 13367 (1989).
- ²G. Davies, *Chemistry and Physics of Carbon*, edited by P. L. Walker, Jr. and P. A. Thrower (M. Dekker, New York, 1977), pp. 1-143.
- ³C. D. Clark, E. W. J. Mitchell, and B. J. Parsons, *The Properties of Diamond*, edited by J. E. Field (Academic Press, New York, 1979), pp. 23-77.
- ⁴J. Walker, *Rep. Prog. Phys.* **42**, 1605 (1979).
- ⁵G. Davies, *Rep. Prog. Phys.* **44**, 787 (1981).
- ⁶L. M. Hansen, W. A. Carrington, J. E. Butler, and K. A. Snail, *Mater. Lett.* **7**, 289 (1988).
- ⁷J. E. Butler, F. G. Celli, D. B. Oakes, L. M. Hansen, W. A. Carrington, and K. A. Snail, *High Temp. Mater. Chem.* (in press).
- ⁸G. Davies, *J. Phys. C: Solid State* **12**, 2551 (1979).
- ⁹V. S. Vavilov, A. A. Gippius, A. M. Zaitsev, B. V. Deryagin, B. V. Spitsyn, and A. E. Alesenko, *Sov. Phys. Semicond.* **14**, 1078 (1980).
- ¹⁰A. M. Zaitsev, V. S. Vavilov, and A. A. Gippius, *Sov. Phys. Leb. Inst.* **10**, 15 (1981).
- ¹¹A. T. Collins, M. Kamo, and Y. Sato, *J. Phys. D: Appl. Phys.* **22**, 1402 (1989).
- ¹²A. T. Collins, M. Kamo, and Y. Sato, in *Diamond, Boron Nitride, Silicon Carbide and Related Wide Bandgap Semiconductors*, edited by J. T. Glass, R. F. Messier, and N. Fujimori (Mater. Res. Soc. Symp. Proc. **162**, Pittsburgh, PA, 1990).
- ¹³A. T. Collins and S. H. Robertson, *J. Mater. Sci. Lett.* **4**, 681 (1985).
- ¹⁴G. Davies and M. F. Hamer, *Proc. R. Soc. London A* **348**, 285 (1976).
- ¹⁵Y. Yokota, H. Kawarada, and A. Hiraki, in *Diamond, Boron Nitride, Silicon Carbide and Related Wide Bandgap Semiconductors*, edited by J. T. Glass, R. F. Messier, and N. Fujimori (Mater. Res. Soc. Symp. Proc. **162**, Pittsburgh, PA, 1990).
- ¹⁶C. D. Clark and C. A. Norris, *J. Phys. C: Solid State Phys.* **4**, 2223 (1971).

PHOTOLUMINESCENCE SPECTROSCOPY OF DIAMOND FILMS

J.A. Freitas, Jr.^{*}, J.E. Butler, S.G. Bishop^{**}, W.A. Carrington^{***}, and U. Strom
 Naval Research Laboratory, Washington, DC 20375-5000
^{*}Sachs/Freeman Associates, Landover, MD 20785-5396
^{**}University of Illinois, Urbana-Champaign, Urbana, IL 61801
^{***}University of South Florida, Tampa, FL 33620

ABSTRACT

Photoluminescence spectroscopy has been used to characterize polycrystalline diamond films prepared by filament assisted chemical deposition and by combustion (in an oxygen-acetylene flame) techniques. The luminescence spectra of the chemical vapor deposited films are dominated by a defect band possibly associated with a neutral vacancy with a strong zero phonon line at 1.68 eV and weak phonon replicas at lower energies. The combustion films exhibit two additional luminescence bands with zero phonon lines at 1.95 and 2.16 eV. The 1.95 eV band has been tentatively assigned to a nitrogen-vacancy pair. We have also observed a strong dependence of the PL spectra radially across a given combustion film and associated this with details of the flame chemistry.

INTRODUCTION

The electronic, optical and mechanical properties of diamond have made this material unique for many technological applications. However, cost (of natural and synthetic diamond) and difficulties in tailoring this crystal to specific applications have limited its utilization.

The recent discovery that diamond films can be deposited on nondiamond substrates by a chemical transport reaction method stimulated an international race to discover new ways of growing synthetic diamond from gases. Diamond films grown by this process are suitable for many optical and electronic applications because of the possibility of fabricating large area and doping/impurity controlled films. However, at the present stage, the film morphology is polycrystalline with crystallite sizes varying from submicron to a few hundred microns, depending upon the growth process, substrate type/preparation and temperature, gas mixture, and growth time. Also observed are graphitic/amorphous carbon components which vary with the film preparation conditions. These film characteristics establish properties quite different from bulk diamond, and limit the number of immediate applications.

Despite of the large volume of work recently reported on polycrystalline diamond films, only a small fraction deal with the investigation of the formation of intrinsic and extrinsic defects in these films [1]. Bulk diamond has been the subject of studies for many years, therefore there are many relevant reviews [2,3,4] of the characterization of diamond by optical absorption, photoluminescence (PL), photoconductivity and cathodoluminescence (CL). These earlier studies provide a baseline for the characterization of polycrystalline diamond.

We report here a preliminary PL investigation of radiative defects in polycrystalline diamond films prepared by filament assisted chemical vapor deposition (FACVD) and combustion deposition (oxygen-acetylene torch) processes. Whenever possible, the defects in the films are identified by comparing their luminescence spectra with well known defect spectra in natural diamond [2,3,4,5].

EXPERIMENTAL TECHNIQUE

We have examined films deposited on different substrates by FACVD and combustion processes. The FACVD deposition of diamond was performed in a vertical 4.45 cm i.d. fused silica tube. A tungsten or rhenium filament was suspended 5 mm above the substrate, which was supported on a 2.54 cm o.d. molybdenum encased heater. The filament temperature was

maintained at $2200 \pm 50^\circ\text{C}$ and the substrate at 875°C . The gas flow (ca. 100 sccm of 0.5% methane in hydrogen) was introduced at the top of the vessel and the pressure was maintained at 40 torr during the course of the deposition. The chamber was pumped by a two stage mechanical pump and the base pressure was 0.03 torr.

The combustion deposition of diamond [6] was performed in ambient air using a commercial oxygen-acetylene brazing torch with a 0.89 mm i.d. orifice. The gas flow rates were controlled by mass controllers, with the total flow rate of ca. 3 slm and an oxygen/acetylene mass flow ratio of ca. 0.95. The flame was directed down onto a substrate supported on a water cooled copper block. The substrate temperature, $800 \pm 100^\circ\text{C}$, was adjusted by varying the thermal conductivity to the copper block.

FACVD diamond was grown simultaneously on a polycrystalline Ni disk and a Si wafer ((100), n-type) substrate. Neither substrate had been intentionally pretreated (e.g. the usual diamond scratching). While isolated crystals of diamond were observed on both substrates, the density was several orders of magnitude higher on the Ni disk compared with the Si where most crystals seemed to be associated with unintentional scratches. X-ray diffraction confirmed the presence of diamond on both samples. The 1332 cm^{-1} diamond phonon was observed by Raman scattering on both samples, with the Si sample yielding a significantly broader Raman line width (20 vs 10 cm^{-1}). A sharp 1580 cm^{-1} band of graphite was also observed on the Ni disk.

One combustion deposited sample was grown on a portion of a Si wafer ((100), n-type) which had been intentionally scratched with $6\text{ }\mu\text{m}$ diamond polishing powder and then cleaned with solvents. The deposition time was several hours. An annular pattern of isolated diamond crystals was observed with a low density of crystals in the center (directly under the inner flame cone), increasing to a maximum density 3 mm radially outward from the center, and decreasing to a low and eventually zero density at 5 to 6 mm from the center.

The other combustion deposited sample was grown in air for 30 minutes on the end of a molybdenum screw which had been polished with $6\text{ }\mu\text{m}$ diamond powder and then cleaned. Upon cooling to room temperature, a continuous diamond film (ca. $15\text{ }\mu\text{m}$ thick and 8 mm dia.) delaminated from the substrate. This film was nearly transparent in the center degrading to a grey-brown color on the edges. The average facet size observed on the polycrystalline films was roughly $1\text{ }\mu\text{m}$ in dimension.

The PL experiments were carried out at temperature between 6 and 300 K in a Janis super-vari-temper cryostat. The temperature was measured and controlled by a sensor located in the copper-sample holder. This system was modified allowing vertical positioning steps smaller than $2\text{ }\mu\text{m}$. Most spectra were excited by either a krypton ($476.2\text{ nm} - 2.6036\text{ eV}$) or an argon ($476.5\text{ nm} - 2.6020\text{ eV}$, $457.9\text{ nm} - 2.7077\text{ eV}$) ion laser. The laser spot size was approximately $50 - 100\text{ }\mu\text{m}$ and the nominal laser power varied between 10 to 50 mW. The excited PL was analyzed by a single or double grating monochromator and detected by a GaAs photomultiplier tube, operated in a photon counting mode.

RESULTS AND DISCUSSION

In Fig. 1, PL spectra obtained at 6K (using a double spectrometer) are shown for two FACVD films deposited on Si (top spectrum) and on Ni (bottom spectrum) substrates. The sample and substrate preparation and characteristics were described in the previous section. Both spectra are dominated by a relatively sharp zero phonon line (ZPL) PL band, at about 1.68 eV, and its weak phonon replicas. The strong broad luminescence background observed in the top spectrum has been reported by many research groups and its origin is not yet well understood. However, its intensity relative to the Raman peak at about 1332 cm^{-1} decreases with increasing film thickness and quality [7].

Fig. 2 shows PL spectra of two diamond films, deposited by the combustion technique (oxygen-acetylene torch) on Si and molybdenum substrates, top and bottom spectra respectively. The measurements were carried out at a temperature of 6K. The luminescence emitted by the samples was dispersed by a single grating spectrometer and the exciting laser light was excluded

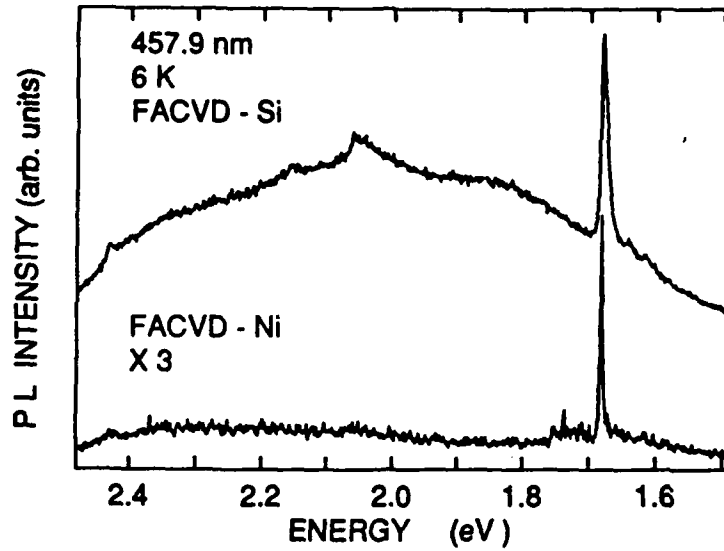


Fig. 1. Photoluminescence spectra obtained at 6K from FACVD polycrystalline film deposited on Si (top spectrum) and polycrystalline Ni (bottom spectrum) substrates. The dominant feature is the sharp ZPL at about 1.68 eV.

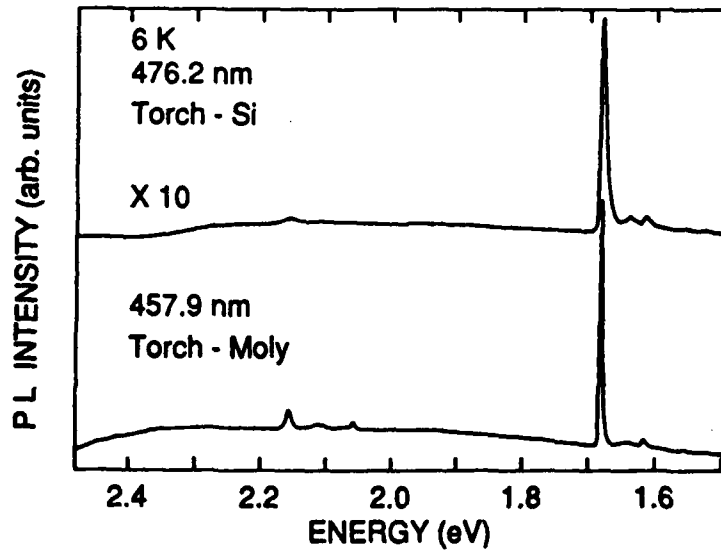


Fig. 2. Low temperature (6K) photoluminescence spectra of two diamond films deposited by combustion technique on Si and molybdenum substrates, top and bottom spectra respectively. The exciting laser wavelength is indicated with the spectrum. Both spectra show the ZPL and associated phonon replicas of the 1.68 eV and 2.16 eV defect bands.

by an appropriated color glass filter. The Si substrate film consists of individual crystallites with size varying from 10 to 200 μm , while the molybdenum substrate film is a free-standing film made up of crystallites with average grain size of a few microns as described previously. As observed in the spectrum of FACVD films (Fig. 1), the 1.68 eV ZPL band and phonon replicas are the dominant spectral features in Fig. 2. The phonon replicas are easier to observe in Fig. 2 than in Fig. 1 due to the better signal to noise, resulting from the larger crystallite sizes or film uniformity. The new feature observed in Fig. 2, is the PL band with the ZPL around 2.16 eV and associated phonon replicas.

In natural and synthetic diamonds the 2.16 eV center is induced by irradiation followed by annealing. The temperature annealing behavior of this system suggests a divacancy as a possible structure [4], however results of isotope studies of nitrogen doped synthetic diamond [8] may imply the direct or indirect participation of nitrogen in this center. The 1.68 eV center, a common feature observed in PL spectra of CVD diamond films, has been assigned to the neutral vacancy center (V^0 , whose ZPL is at 1.673 eV), and which is induced in all natural and synthetic diamond by irradiation.

A comparison of the 1.68 eV center with V^0 , shows that the former is blue shifted by 5 to 8 meV and has a linewidth 4 to 10 times broader than the latter. These characteristics may suggest that the 1.68 eV ZPL is associated with another defect center like the system with the ZPL at 1.685 observed in homo- and hetero-epitaxial CVD films intentionally doped with Si [9], or in Si-implanted and annealed natural diamond [10]. However, it is important to note that the 1.68 eV system is about 5 meV red shifted from the Si-center, and the energy position and linewidth of the Si-center seems to be independent of the substrate, deposition technique or crystallite grain size, which contrast the behavior of the 1.68 eV center. Clearly careful experiments must be carried out on well controlled samples to achieve a definite identification of the 1.68 eV center.

If one assumes that the 1.68 eV system is the neutral vacancy, the lineshift can be explained in terms of residual stress existent in the individual crystallites, since stress of 1 to 2 GPa parallel to $\langle 100 \rangle$ is enough to induce a 6 to 7 meV blue shift [3]. As a result of this residual stress (not expected to be uniaxial), the line width will broaden, masking the observation of the ZPL doublet character, and leading to the observed sample dependent peak position.

Using the same approximation described by Collins and Robertson [11] in their CL studies of the 2.156 eV center in sintered diamonds, Robins and coworkers [1] estimated a residual stress of the order of 3 GPa in their CVD-grown films. If we assume the same order of magnitude for the residual stress in our films then we can account for the width of the ZPL in our spectra. A residual stress of about 3 GPa will be enough to cause the broadening and lineshift observed in the V^0 ZPL in our films. The smaller lineshift (1 or 2 meV) observed in the 2.156 eV center in comparison with the V^0 may be understood in terms of the complexity of this center and its different symmetry (trigonal instead of tetrahedral).

To verify the homogeneity of the combustion films we have carried out PL measurements in a film deposited on a Si substrate with average crystallite size varying from 50 to 200 μm . Attempting to probe individual crystallites of the film, which exhibits the typical annular pattern of isolated diamond, we reduced the laser spot size to about 30 μm . The sample was moved inside the dewar allowing to probe crystallites from the outside part to the bottom part of the film. Some results are shown in Fig. 3.

In Fig. 3, the spectrum a) was obtained by aiming the laser beam at a crystal at the external part of the annular film. This spectrum is dominated by a broad luminescence band with phonon replicas and ZPL at 1.95 eV. This system is the dominant defect luminescence band observed by annealing pre-irradiated diamond which contains isolated substitutional nitrogen impurities. Detailed studies carried out by Davies and Hamer [12] strongly suggest that the 1.95 eV system is a nitrogen-vacancy pair (N-V). By moving the laser spot slightly toward the center of the film we observe, as shown in spectrum b), a new luminescence band, the 2.16 eV system discussed previously. For a crystal located closer to the center of the film we observe a sizable reduction of the 1.95 eV center PL intensity, so the luminescence spectrum is dominated by the 2.16 eV center as shown in spectrum c). For crystallites at the central part of the film, represented by the spectrum d), the luminescence spectrum is dominated by the 2.16 eV and 1.68 eV centers. Since the

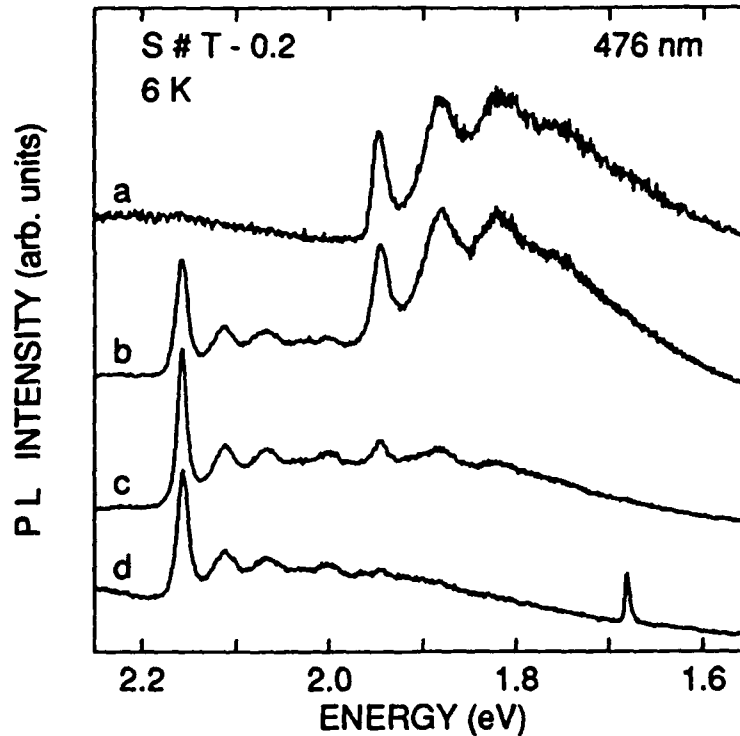


Fig. 3. PL spectra obtained at 6K from an oxyacetylene film deposited on a Si substrate. The curves a) to d) were obtained by focusing the laser into four crystallites positioned from the top toward the center of the sample respectively. These spectra show the 1.68 eV, 1.95 eV and 2.16 eV systems.

combustion film is deposited in an open atmosphere, one can expect the incorporation of nitrogen in this film, as observed in Fig. 3, spectrum a) and b), which shows the dominant presence of the 1.95 eV center associated with the N-V pair. However for crystallites deposited more toward the center of the annular film, we observe a sizable reduction of the 1.95 eV center, spectrum c) and d), suggesting that the higher pressure in the flame at this part of the film may exclude the nitrogen, reducing its incorporation. This seems to be a plausible assumption, with a lack of nitrogen we can expect that the dominant defects should be isolated vacancies and vacancy complexes, as observed in spectra c) and d).

CONCLUDING REMARKS

PL experiments carried out on FACVD and combustion deposited films exhibit the presence of luminescence bands associated with defects probably originating from mobile vacancies created during the film deposition. In situations where the nitrogen was expected to be present we observe the formation of N-V pairs, however, the isolated vacancy and vacancy complexes are the most common centers observed in our films. The lineshape and linewidth observed in the ZPL of the defect bands suggested a residual stress of 2 to 3 GPa in the individual crystallites, in agreement with Robins and coworkers [1]. Our temperature dependence of the PL intensity experiment show a strong quenching and broadening of the ZPL and associated phonon replicas, for temperatures above 100K, as observed in natural diamond [13].

ACKNOWLEDGEMENTS

This work was supported in part by the Office of Naval Research.

REFERENCES

1. L.H. Robins, L.P. Cook, E.N. Farabaugh, and A. Feldman, P.R. B., 39, 13367 (1989)
2. G. Davies, "Chemistry and Physics of Carbon", ed. P.L. Walker, Jr., and P.A. Thrower, 1977 (M. Dekker, N.Y.), pp 1-143
3. C.D. Clark, E.W.J. Mitchell and B.J. Parsons, "The Properties of Diamond", ed. J.E. Field, 1979 (Academic Press, N.Y.), pp 23-77
4. J. Walker, Rep. Prog. Phys., 42, 1605 (1979)
5. G. Davies, Rep. Prog. Phys., 44, 787 (1981)
6. L.M. Hansen, W.A. Carrington, J.E. Butler, and K.A. Snail, Mat. Lett., 7, 289 (1988)
7. J.E. Butler, F.G. Celli, D.B. Oakes, L.M. Hansen, W.A. Carrington and K.A. Snail, High Temp. Mat. Chem. (in press)
8. G. Davies, J. Phys. C: Sol. St., 12, 2551 (1979)
9. V.S. Vavilov, A.A. Gippins, A.M. Zaitsev, B.V. Deryagin, B.V. Spitsyn, and A.E. Alesenko, Sov. Phys. Semicond., 14, 1078 (1980)
10. A.M. Zaitsev, V.S. Vavilov and A.A. Gippius, Sov. Phys. Leb. Inst., 10, 15 (1981)
11. A.T. Collins and S.H. Robertson, J. Mat. Sc. Lett., 4, 681 (1985)
12. G. Davies and M.F. Hamer, Proc. R. Soc. Lond., A348, 285 (1976)
13. C.D. Clark and C.A. Norris, J. Phys. C: Sol. St. Phys., 4, 2223 (1971)